MOLECULAR INVESTIGATION OF PTZ-INDUCED EPILEPTIC
ACTIVITIES IN RAT BRAIN CELL MEMBRANES AND THE EFFECTS OF
VIGABATRIN

A THESIS SUBMITTED TO
THE GRADUATE SCHOOL OF NATURAL AND APPLIED SCIENCES
OF
MIDDLE EAST TECHNICAL UNIVERSITY

BY

SEVGİ TÜRKER GÖRGÜLÜ

IN PARTIAL FULFILLMENT OF THE REQUIREMENTS
FOR
THE DEGREE OF DOCTOR OF PHILOSOPHY
IN
BIOLOGY

AUGUST 2009

Approval of the Thesis

**MOLECULAR INVESTIGATION OF PTZ-INDUCED EPILEPTIC
ACTIVITIES IN RAT BRAIN CELL MEMBRANES AND
THE EFFECTS OF VIGABATRIN**

submitted by **SEVGİ TÜRKER GÖRGÜLÜ** in partial fulfillment of the
requirements for the degree of **Doctor of Philosophy of in Biological Sciences
Department, Middle East Technical University** by,

Prof. Dr. Canan Özgen   _____
Dean, Graduate School of **Natural and Applied Sciences**

Prof. Dr. Zeki Kaya   _____
Head of Department, **Biological Sciences**

Prof. Dr. Feride SEVERCAN   _____
Supervisor, **Biological Sciences Dept., METU**

Examining Committee Members:

Prof. Dr. Rüştü Onur   _____
Medical School of Pharmacology Dept., HU

Prof. Dr. Feride Severcan   _____
Biological Sciences Dept., METU

Assoc. Prof. Dr. Ewa Doğru   _____
Biological Sciences Dept., METU

Assoc. Prof. Dr. Yıldırım Sara   _____
Medical School of Pharmacology Dept., HU

Assist. Prof. Dr. Tülin Yanık   _____
Biological Sciences Dept., METU

Date:

I hereby declare that all information in this document has been obtained and presented in accordance with academic rules and ethical conduct. I also declare that, as required by these rules and conduct, I have fully cited and referenced all material and results that are not original to this work.

Name, Last name:

Signature   :

ABSTRACT

MOLECULAR INVESTIGATION OF PTZ-INDUCED EPILEPTIC ACTIVITIES IN RAT BRAIN CELL MEMBRANES AND THE EFFECTS OF VIGABATRIN

GÖRGÜLÜ TÜRKER, Sevgi

Ph.D., Department of Biological Sciences
Supervisor: Prof. Dr. Feride SEVERCAN

August 2009, 195 pages

The epilepsies are a heterogenous group of symptom complexes, whose common features is the recurrence of seizures. There is no certain therapy for epilepsy. In order to promote new advances for the prevention of epilepsy the molecular mechanism of epileptic activities should be clarified.

In the present study the goal is to obtain information for molecular mechanism of epilepsy. To achieve this, molecular alterations from pentylenetetrazol (PTZ)-induced epileptic activities on rat brain tissue and cell membranes were investigated by Fourier Transform Infrared (FTIR) spectroscopy, Fourier Transform Infrared Microscopy and Atomic Force Microscopy (AFM). Moreover, the therapeutic role of an antiepileptic agent vigabatrin (VGB) on epileptic rat brain membranes were examined at molecular level.

For better understanding of the action mechanism of PTZ and an antiepileptic drug VGB in cell membranes we firstly studied at model level using multilamellar liposomes (MLVs). We investigated PTZ-DPPC MLVs interactions

in terms of lipid phase behavior, order and dynamics and nature of hydrogen bonding around its polar part, using Fourier Transform Infrared (FTIR) spectroscopy, Differential Scanning Calorimetry (DSC), Electronspin Resonans Spectroscopy (ESR) and Steady State Fluorescence Spectroscopy. According to our data, PTZ has no ability to interact with membrane lipids. On the other hand, the results of VGB-DPPC interactions showed that VGB strongly interact with the head group and/or the region near the head of membrane phospholipids.

The molecular investigation of PTZ-induced epileptic activities revealed that PTZ-induced seizures cause a decrease in the lipid and protein content, membrane fluidity and glycogen level. They stimulate alterations in membrane packing and the secondary structure of proteins as well as lipid peroxidation. In addition, our results show the transcription of early genes following high dose PTZ administration. All these molecular alterations variatins are only resulted from the consequences of epileptic activities not from convulsant agent PTZ itself.

The important finding is that, VGB restored some of the alterations by PTZ-induced epileptic activities on brain cell membrane. For instance, it restored membrane fluidity, lipid peroxidation, phospholipid degradation and changes in membrane organization. However, it was found that VGB has no significant effects on the changes in protein secondary structure.

ÖZ

SIÇAN BEYİN HÜCRE MEMBRANLARINDA PTZ İLE İNDÜKLENMİŞ EPİLEPTİK AKTİVİTELERİN MOLEKÜLER DÜZEYDE İNCELENMESİ VE VİGABATRİNİN ETKİLERİ

GÖRGÜLÜ TÜRKER, Sevgi

Ph.D., Biyolojik Bilimler Bölümü
Tez Danışmanı: Prof. Dr. Feride SEVERCAN

Ağustos 2009, 195 sayfa

Epilepsi nöronlarda meydana gelen ani anormal elektrik deşarj sonucu tekrarlayan nöbetler, ve sonucunda ortaya çıkan sendromlar grubuna verilen isimdir. Bugüne kadar mevcut olan yöntemlerle epilepsinin henüz kesin bir yoktur. Epilepsi oluşumunu engellemek için epileptik aktivitelerin moleküler mekanizması tam olarak açıklığa kavuşturulmalıdır.

Bu çalışmada, amacımız epilepsinin moleküler mekanizmasını açıklamaya yönelik bilgiler elde etmektir. Bunun için PTZ ile oluşturulmuş epileptik aktivitenin sıçan beyin doku ve hücre membranı üzerindeki etkileri Fourier Kızılötesi Spektroskopisi (FTIR), Fourier Kızılötesi Mikroskopisi ve Atomik Kuvvet Mikroskopisi ile incelendi. Ayrıca antiepileptik ilaç olan vigabatrinin epileptik hücre membranı üzerindeki tedavi edici edici etkileri moleküler düzeyde araştırıldı.

Çalışmamızın ilk aşamasında PTZ'nin DPPC MLVs ile etkileşimi yani PTZ'nin lipid faz özellikleri, lipid düzeni ve akışkanlığı üzerine etkileri FTIR,

DSC, ESR ve Steady State Floresans Spektroskopisi ile incelendi. Sonuçlara göre, PTZ'nin membrane lipidleri ile etkileşime girmediği tespit edildi. Diğer taraftan, VGB'nin DPPC MLVs ile etkileşimi aynı teknikler ile çalışıldı. Sonuçlar, VGB'nin membran lipidlerinin kafa grupları ve kafa gruplarına yakın kısımları ile güçlü hidrojen bağı yaptığını ortaya çıkardı.

PTZ ile indüklenmiş epileptik aktivitelerin moleküler düzeyde incelenmesi sonucunda PTZ ile indüklenerek oluşturulmuş epileptik nöbetlerin lipid ve protein miktarında, membran akışkanlığında ve glikojen miktarında azalmaya neden olduğu bulundu. Ayrıca nöbetlerin membran organizasyonunda farklılaşmaya, lipid peroksidasyonuna ve protein ikincil yapılarında anlamlı değişikliklere neden oldukları tespit edildi. Bunun yanısıra, yüksek doz PTZ uygulmasının erken safha gen transkripsiyonuna sebep olduğu saptandı.

Bu çalışmanın önemli bulgularından biri vigabatrinin PTZ ile indüklenerek oluşturulmuş epileptik aktivite sonucu sıçan beyin hücre membranında meydana gelmiş bazı değişiklikleri kontrol değerine yaklaştırarak epileptik aktivitenin zararlı etkilerini engellemesidir. Örneğin VGB membran dinamiğindeki azalmayı, membran organizasyonundaki farklılaşmayı, lipit peroksidasyonu ve fosfolipit yıkımını bir ölçüde gidererek kontrol değerlerine doğru yaklaştırdı. Diğer taraftan ise VGB'nin ve protein ikincil yapılarındaki değişimler gibi patolojiler üzerinde olumlu bir etkisi olmadığı tespit edildi.

To my mother Rabia Türker

ACKNOWLEDGEMENT

TABLE OF CONTENS

LIST OF TABLES

LIST OF FIGURES

FIGURES

xv

xvii

LIST OF ABBREVATIONS

AFM   Atomic force microscopy
DPPC MLVs   Dipalmitoylphosphatidylcholine multilamelar vesicles
DSC   Differantial scanning calorimetry
ESR   Electronspin resonance spectroscopy
FTIR   Fourier transform infrared spectroscopy
ILAE   International League Agaist Epilepsy
MDA   Malonydialdehyde
NN   Neural network
PTZ   Pentylenetetrazol
ROS   Reactive oxygen species
VGB   Vigabatrin

CHAPTER I

INTRODUCTION

1.1 Epilepsy
1.1.1 Definition

Epilepsy was one of the first brain disorders to be described about 3000 years ago in Mesopotamia. The word epilepsy is derived from the Greek word for "attack." (Chollet, 2002).

An epileptic seizure (from the Latin *sacire*—to take possession of) is a sudden onset of symptoms and clinical manifestations caused by an abnormal, excessive, hypersynchronous burst of electrical activity that disrupt brain functions. This abnormal neuronal activity can cause strange sensations, emotions, and behavior, or sometimes convulsions, muscle spasms, and loss of consciousness (Lothman et al., 1991; McNamara, 1994; De Lorenzo et al, 2005; de Sousa et al., 2006; Commission on Epidemiology and Prognosis of the International League Agaist Epilepsy (ILAE), 1993). When unprovoked seizures occur recurrently, characterizing a diverse collection of brain disorders, the condition is called epilepsy (Commission on Epidemiology and Prognosis of the International League Agaist Epilepsy (ILAE), 1993).

Epilepsy is a heterogeneous collection of neurological disorders that have in common a transient and recurrent hypersynchronous activation of large populations of neurons in distinct focal areas or in the entire brain. It covers a number of conditions that involve recurrent seizures unprovoked by an acute systemic or neurological insult (de Sousa et al., 2006).

In order to define epilepsy, the word disorder has a broader meaning than the strict definition of disease. While the adjectives ascribed to the term disease are "serious, active deepseated, prolonged or permanent", a disorder "is usually a physical or mental derangemeny, often slight, partial, and temporary". In this sense, the term disorder may be preferred by some as it reflects not only the medical aspects (disease) but also the many psychological aspects (illness) of epilepsy (Editorial, 2003).

1.1.2 Epileptogenetic Process

Epileptogenesis refers to the development of an epileptic disorder. It is well known from experimental studies with animal models (Mello et al., 1993), as well as from studies with patients (Weiss et al., 1986) that there is a latent period between induction of a localized cerebral insult, such as head trauma, and the appearance of a chronic epileptic condition. During the latent period, neuronal loss and abnormal synaptic reorganization occurs (Mello et al., 1993; Leite et al., 1996). This reorganization of the neuronal integration leads to abnormally increased excitability and synchronization, and eventually to the occurrence of spontaneous seizures (Isokawa and Mello, 1991). Once developed, epilepsy should not be viewed as a random succession of seizures, but as a dynamic process that results in both ictal phenomena and interictal functional and structural abnormalities in the brain (Engel et al., 1991). Patients who develop chronic intractable epilepsy demonstrate progression in both the number of seizures and in seizure-related neurological symptoms, such as cognitive and behavioral disorders (Williamson et al., 1993, Cockerell et al., 1997).

"A challenge arising from the existing data is trying to fill the gaps of the hypothesis of progression of epilepsy, however; new molecular approaches are needed (Pitkänen et al., 1999)".

1.1.3 Classification of Epilepsy and Epilepsy Syndromes

Epileptic syndromes are defined by many factors, including type of seizure, age of onset, cause, seizure types, family history, findings at physical examination, the pattern of electroencephalography (EEG), and neurological imaging (DeLorenzo 1991). This diversity of expression has led to the standard classification of epilepsy and the numerous different epilepsy syndromes (Frazen 2000). Each type of epilepsy shares the common feature of persistently increased neuronal excitability that manifests sporadically during seizure generation (Lothman *et al*., 1991; McNamara, 1999; 1994; Engel, 2001).

Classification of epilepsy syndromes in the ILAE system depends on two distinctions; location of the lesion (localized or generalized) and known or suspected cause (idiopathic, symptomatic, or cryptogenic) (Commission of Classification and Terminology of the International League Against Epilepsy, 1995). This classification can be summarized as follows;

Localized Epilepsies are caused by focal diseases, whereas generalized epilepsies are caused by diseases that affects the entire cortex. The cause may be an obvious structural lesion, eg, tumor or malformation, or it may be microscopic or merely a defect of neurotransmission.

Idiopathic Epilepsies usually are inherited and presumed to result from abnormalities in neurotransmission without associated structural abnormalities. These kinds of epilepsies were termed idiopathic because the cause was unknown. However, recent advances in molecular biology and genetics have demonstrated that most idiopathic epilepsies are due to genetically determined abnormalities of neurotransmission; therefore they are no longer idiopathic.

Symptomatic Epilepsies result from known structural disease or known cause. Structural disorder, e.g., malformation, tumor, and trauma, is usually apparent on neuroimaging. Known causes may result in visible structural disorders or less visible brain effects. Examples of symptomatic epilepsy without

structural abnormalities include some perinatal anoxia, metabolic abnormalities (eg, amino acidopathy, storage disease), and chromosomal defects.

Cryptogenic Epilepsies are presumed to have a structural basis, but there is no demonstrable structural disorder and the cause is unknown. In some cases a structural brain disorder is apparent because of the presence of neurological signs, such as mental retardation or hemiparesis. Most cryptogenic epilepsies are symptomatic, in which the disorder simply has not been demonstrated with contemporary diagnostic tools. The advent of high-resolution magnetic resonance imaging (MRI) has already shifted many diagnoses of cryptogenic epilepsy into the symptomatic epilepsy category, because lesions have been demonstrated on MRI's that were not evident on computed tomography scans.

1.1.4 Classification of Seizures and Associated Symptoms

There have been several efforts to classify seizures especially after the first recording of the human EEG in 1934. The classification of epileptic seizures by the Commission on Classification and Terminology of the ILAE (1981) is based on clinical events (seizure type) and characteristics of EEGs based on types of seizures, etiology and provoking factors (Dreifuss, 1990). A new classification is suggested within the recent years (Blume et al., 2001). Although there is some limitations, epileptic seizures are mainly categorized into three broad groups, each with several subgroups. This distinction is important because each seizure type responds differently to treatment (or medication) (Engel, 1992; Dam, 1996; 1986).

I. Partial Seizures arise from localised cortical regions and may spread to other cortical areas and to the opposite hemisphere involving the whole brain. They are characterized by the retention of consciousness since they begin in a limited brain region, therefore; consciousness is lost at onset of a seizure. The symptoms depend on which part of the brain is affected and what physical or mental activity that part of the brain controls.

There are three types of partial seizures:

- *Simple Partial Seizures* are not associated with alteration of consciousness, because they begin in a small, discrete area of the brain. The discharge is usually confined to a single hemisphere and the symptoms are specific to the affected brain region. Only one neurological modality is affected during the seizure, and the resulting symptoms, which depend on which region of the cortex is affected, may be motor, sensory, autonomic (sweating, gastric discomfort, vomiting), or psychic (anxiety, deja vu).

- *Complex Partial Seizures* are associated with alteration but not loss of consciousness. The patient is awake and stares blankly, but is not responsive to external stimuli. These attacks can arise from any region of the brain, but most commonly arise in the temporal lobe, followed by the frontal lobe. The seizure is often associated with automatism, e.g. repetitive hand movements, smacking, chewing etc. There is often a postseizure confusion period. This seizure type is often confused with the absence seizure type. It is the most common seizure type across all age groups.

- **Secondary Generalised Partial Seizures** are those attacks in which a partial seizure spreads to both hemispheres. The patient is unconscious and presents motor abnormalities with cramps.

II. Generalized Seizures start throughout the entire cortex at the same time. They cause loss of consciousness because cortical neurons that maintain consciousness are not able to perform their normal functions. Some generalized seizures e.g., myoclonic seizures, are so brief that it is difficult to determine whether there is any loss of consciousness; however, an EEG obtained during the seizures enables confirmation of generalized seizures. The types of generalized seizures are recognized in the ILAE classification, i.e., generalized tonic-clonic, tonic, clonic, and myoclonic seizures, or by lack of motor activity, i.e., absence, typical

absence, and atonic seizures. Infantile spasms are well-recognized identities, but they are not included in the ILAE classification.

- *Generalized Tonic-Clonic Seizures* begin with a tonic phase of whole-body stiffening, followed by a clonic phase of repetitive contractions. They cause unprotected falling if they occur while the patient is standing. These seizures last 2 to 3 minutes and are followed by a period of confusion or complete unresponsiveness for at least another few minutes (Futatsugi and Riviello 1998; Gloor et al., 1990).

- *Tonic Seizures* consist of only the tonic phase of generalized tonic-clonic seizures.

- *Clonic Seizures* consist of only the clonic phase of generalized tonic-clonic seizures.

- *Myoclonic Seizures* are brief and the most common signs are bilateral hand or arm jerks, although these seizures can affect any region of the body. Not all myoclonic movements are seizures, since myoclonus can arise in cortical, subcortical, or spinal cord structures. Only cortical myoclonic movements are considered seizures.

- *Absence Seizures* are manifested as brief (1-10 sec) episodes of staring and unresponsiveness. Most often there are no other manifestations, but episodes that last more than 7 to 10 seconds can be associated with eye blinking or with oral or manual automatisms. They are similar to complex partial seizures in that both are characterized by staring unresponsiveness, but the clinical situation in which they arise often enables differentiation.

- *Atypical Absence Seizures* present ictal symptoms similar to those of absence seizures, but last longer and often include more motor involvement. Atypical absence seizures are often associated with other types of seizures observed in severe forms of epilepsy.

- *Atonic Seizures* are manifested as sudden loss of muscle tone and subsequent unprotected falling or dropping to the ground. They are referred to as drop attacks, and often cause injury as part of multiple

seizure types resulting from severe epilepsy. These seizures must be differentiated from other causes of sudden falling.

- *Infantile Spasms* are manifested as forward flexion of the torso and extension of both arms. They occur in infants. EEG records show a characteristic pattern of hypsarrhythmia between seizures and an electrodecremental seizure pattern during a spasm.

- *Status Epilepticus* is a medical emergency, which occurs if the epileptic attack is prolonged, or if several seizures follow each another within a short period of time. Status epilepticus with tonic-clonic seizures is a severely dangerous condition, carrying a significantly increased health risk and requiring immediate treatment and often intensive care. Other epileptic seizures can appear as status epilepticus, e.g. complex partial status, which are also associated with a significant health risk.

III. Unclassified Seizures

Seizures that cannot be classified due to insufficient data are included in this group.

International Classification of Epileptic Seizures is given below: (1995)

I. Partial seizures
A. Simple partial seizures
    1. With motor signs
        a. Focal motor without march
        b. Focal motor with march (Jacksonian)
        c. Versive
        d. Postural
        e. Phonatory
    2. With somatosensory or special-sensory symptoms
        a. Somatosensory
        b. Visual
        c. Auditory
        d. Olfactory
        e. Gustatory
        f. Vertiginous
    3. With autonomic symptoms or signs
    4. With psychic symptoms
        a. Dysphasia
        b. Dysmnesic
        c. Cognitive
        d. Affective
        e. Illusions
        f. Structured hallucinations

B. Complex partial seizures
    1. Simple partial seizures at onset, followed by impairment of consciousness
        a. With simple partial features
        b. With automatisms
    2. With impairment of consciousness at onset
        a. With impairment of consciousness only
        b. With automatisms
C. Partial seizures evolving to secondarily generalized seizures
    1. Simple partial seizures evolving to generalized seizures
    2. Complex partial seizures evolving to generalized seizures
    3. Simple partial seizures evolving to complex partial seizures evolving to generalized seizures

II. Generalized seizures
A. Absence seizures
    1. Typical absence seizures
        a. Impairment of consciousness only
        b. With mild clonic components
        c. With atonic components
        d. With tonic components
        e. With automatisms
        f. With autonomic components
    2. Atypical absence seizures
B. Myoclonic seizures
C. Clonic seizures
D. Tonic seizures
E. Tonic-clonic seizures
F. Atonic seizures

III. Unclassified seizures

1.1.5 Etiology

Certain postnatal insults such as brain trauma, central nervous system (CNS) infections, cerebrovascular disease, and brain tumors greatly increase the incidence of epilepsy (Annegers, 1996). In a classical study covering 1935-1984, the presumed cause of epilepsy was vascular in 11% of all the incident cases of epilepsy, followed by congenital (8%), traumatic (5.5%), neoplastic (4.1%), degenerative (3.5%) and infective (2.5%) causes (Hauser et al., 1993). More recently, a population-based study in the UK reported that the etiology of epilepsy was vascular disease in 15%, cerebral tumor in 6%, alcohol-related in 6% and post-traumatic in 3% of the patients (Sander et al., 1990). The etiology of epilepsy varies considerably in different age groups. Notably, epidemiological studies have reported that in about 65% of cases the etiology of seizures was idiopathic/cryptogenic (Sander et al., 1990; Hauser et al., 1993).

It is evident that the more extensive the investigation, the more likely etiological factors are to be identified. Brain magnetic resonance imaging (MRI) identifies a high rate of positive causes in hospital-based surveys (Li et al., 1995).

The majority of epilepsies, both cryptogenic and symptomatic, lack an overt genetic determinant. However, genetics may contribute to susceptibility to epilepsy arising after a brain insult. The inherited pattern is prominent in many of the epilepsy syndromes. A single genetic locus controls more than 300 disorders, in which epileptic seizures are an important feature. However, they account for less than 1% of all epilepsies. Genetic determinants also contribute strongly to risk of idiopathic epilepsies, although most of them have complex inheritance in which the phenotypic variation within and between families is generally much greater than that observed in epilepsies with simple inheritance.

In short, there are many possible causes for seizures and epilepsy. Anything causing an alteration in the structure (macroscopic or microscopic) or function of cerebral neurons disrupts the electrical activity in the brain. These structural changes and provoking factors can lead to epilepsy (Hauser et al., 1996; Annegers et al., 1996; De Boer 2002; Fountain 2002).

1.1.6 Prevalence of Epilepsy

Epilepsy can affect anyone at any age, in any race or social class. Usually, seizures tend to start either in infancy, by late adolescence, or after 65. The majority of patients with epilepsy are infants below one year, or in the over-60 age group. The number of all cases of epilepsy is between 5 and 9 per 1000 population world over making it one of the most common neurological disorders. According to the studies of WHO, the incidence in developed countries is 6 per 1000 people a year, while it is 18,5 per 1000 people in developing nations. (Hauser et al., 1993; 1991; McNamara, 1999). It is evaluated that there are 300-600000 people suffering from epilepsy in Turkey (Aydın et al., 2002) .

1.1.7 Clinical Consequences of Epilepsy and Epileptic Seizures

There are limited number of studies, most of which are mainly at clinical level, reporting biochemical and functional alterations produced by single and repeated epileptic seizures (Thom et al., 2004). For example, in animals as well as in humans, seizures produce damage in two important subcortical brain structures of the limbic system which is responsible for memory, emotion and many other functions: the hippocampus and the amygdale (Holmes 1991; Ben-Ari 2001).

The alterations induced by epileptic seizures might be short-term and long-term. Some of the long-term alterations include temporary or permanent changes in synapses and brain circuits. For example, in temporal lobe epilepsy, seizures cause long-lasting changes in synaptic efficacy, called long-term potentiation. Even brief seizures produce changes in synaptic efficacy, which are followed several weeks later by aberrant formation of new synapses (Moshe 1998; Lynch 1996).

In addition to the effects of epilepsy, variations in distribution and depth of cortical sulci, cortical thickness, and boundaries between gray and white matter, and signal intensity that allow for the recognition of different malformation patterns have been reported (Guerrini and Carrozzo 2001; Walsh 1999; Guerrini et al., 1996; Friede 1989).

Brain damage caused by persistent and highly repetitive seizures (several times a day), a condition which is named status epilepticus, is associated with excitotoxic mechanisms in several brain regions. Excitotoxins are neuron-lesioning chemical mediators produced by excessive (pathologic) stimulation, such as those occurring in epileptic seizures (Wasterlain and Shirasaka 1994).

Epilepsy can cause reorganization of cognitive function, which is common in relatively young populations, can affect cortical areas involved in cognition, and may be associated with cognitive decline (Goldmann and Golby 2005).

"Although all these alterations have been described, epilepsy-induced molecular alterations at cellular level are not well known. In order to improve early diagnosis and appropriate treatment strategies for epilepsy, the correlation of epileptic seizure-induced molecular alterations with their pathology needs to be identified".

1.1.8 Oxidative stress and epilepsy

Oxidative stress is defined by the excessive production of free radicals, which act via peroxidation of membrane lipids, inactivation of enzymes, depolymerization of polysaccharides and disruption of nucleic acids (Dal-Pizzol et al., 2000). Enhanced oxidative stress, which contributes to the pathology of epilepsy, resulted from either enhanced reactive oxygen species (ROS) production or attenuated ROS scavenging capacity. This further leads to cell injury and, subsequently, cell death and tissue damage (Yatin et al., 2000). Lipid peroxidation is the most important effect of free radicals. Increased lipid peroxidation has been shown in both patients suffering from epilepsy and experimental animals (Bruce and Baudry, 1995; Singh et al., 2003; Tejada et al., 2007). This further leads to cell injury and, subsequently, cell death and tissue damage (Yatin et al., 2000). Lipid peroxidation is the most important effect of free radicals. Increased lipid peroxidation has been shown in both patients suffering from epilepsy and experimental animals (Bruce and Baudry, 1995; Singh et al., 2003; Tejada et al., 2007).

1.1.9 Animal models in epilepsy research

Epilepsy state can be characterized by some alterations in brain, therefore; the determination of these changes can provide early and accurate diagnostic information, which results in the improvement of theurapeutic strategies (Avanzini and Franceschetti, 2003; Patel, 2004; McCorry et al., 2004; Kelso and Cock, 2004). To achieve this, many different types of animal epileptic models have been developed. These animal models for epilepsy have played important role to understand the basic physiological and behavioral changes, which are directly associated with the pathological consequences found in human (Patel, 2004). Human epileptic syndromes and animal models are summarized as follows;

Table 1. Human condition related epileptic animal models

Human condition	Species studied/animal model
Neonatal and early childhood syndromes	
Severe epileptic encephalopthies	
Rasmussen`s syndrome	Rabbit / anti-GluR3 antibodies
Hypoxia- related	Rat / global hypoxia
Febrile convulsions	Rat / hyperthermia-induced
Late childhood and adolescence syndromes	
Absence epilepsies (including childhood, juvenile,myoclonic ,photo- and- pattern-induced)	Mice, rat / see Genetic Mutants
Non- age- related and other syndromes	
Temporal lobe epilepsy	Rat / kainic acid , pilocarpine , kindling
Epilepsy partialis continua	Baboon , cat / GABA withdrawal , tetanus toxin
Progressive myoclonus epilepsies	
Unverricht- lundborg disease	Mouse / cystatin B-deficient
Lafora`s disease	Beagle
Posttraumatic seizures	
Head injury-related	Rat / lateral fluid – percussion injury
Simple reflex epilepsies	
Photosensitivity	Baboon , chicken
Somatosensory + proprioceptive reflex (e.g., touch, tap, hot water	Rat / hot water
Audiogenic (startle)	Rat / mice/ GEPRs , DBA / 2 mice
Vestibular	Mouse / EL mouse
Cortical marformations associated with epilepsy	
Heterotopias	
Subcortical band (double cortex syndrome	Rat / rish mutation
Chromosomal anomolies associated with seizures or epilepsy	
Partial monosomy (15 Q) (Angelman syndrome)	Mouse / GABA receptor β 3 knockout
Metabolik disorders commonly associated with epilepsy	
Neonatal / infancy disorders	
Pyridoxine- dependent epilepsy	Mice / TNAP- deficient mice, BAL Be mice
Menkes` kinky hair disease	Mouse / macular mutant mouse
Childhood disorders	
Krabbe`s disease	Mouse / twitcher mouse
Epilepsy due to alcohol and drug abuse	
Alcohol	Mice / ethanol with drawal

1.1.9.1 Pentylenetetrazol (PTZ) epileptic models

Pentylenetetrazol (PTZ)-induced epileptic animal models such as PTZ threshold, kindling and acute convulsions have been widely used in both clinical and experimental studies in order to improve diagnosis and treatment strategies for epilepsy (Hansen et al., 2004; Pavlova et al., 2006). These models not only produce epileptic seizure activity, but also show seizure-induced changes similar to alterations observed in human epilepsy. Therefore, these models have been accepted as good models in epilepsy research (Sarkisian, 2001; Uribe-Escamilla et al., 2007).

1.1.9.2 Pentylenetetrazol (PTZ, metrazol)

Pentylenetetrazol (PTZ) which is a systemic convulsif agent can play facilitating role to spread out of epileptic seizures from thalamus, cortex and brain stem to diencephalon and cortex (Mirski and McKeon, 1986; Meldrum 1997; Mirski et al., 2003). After the injection of a single dose PTZ bilateral simetrik myoclonic jerks, tonic-clonic convulsions and tonic extansions appear within 1-2 minutes. (Ilhan *et al.,* 2005; Ping Li 2004; Eagles 2003; Fisher 1989).
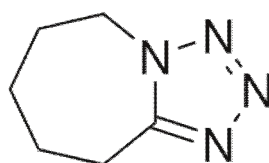
Figure 1. Chemical representation of PTZ

Even though several effects of the agent have been already described (Bloms et al., 1992; Bloms-Funke et al., 1996; Onozuka et al., 1996), its mechanism of action at the cellular level still is not fully understood (Sechi et al., 1997; Sejima et al., 1997).

One generally believed mechanism is that PTZ displays its activity by binding to the picrotoxin binding site at $GABA_A$ receptor complex (Ramanjaneyulu et al., 1984). Accordingly, some binding studies revealed that PTZ also affects the function of benzodiazepine receptor (Rocha et al., 1996), $GABA_A$ receptor (Follesa et al., 1999), both ionotropic and metabotropic glutamate receptors (Ekonomou et al., 2001). Moreover, it was also shown that PTZ is not effective when injected into the neuron (Hartung et al., 1987). All these studies indicated that epileptogenic agent PTZ acts at external site of cell membrane through binding on membrane channels and receptors. Despite these evidences there are also some reports stating that PTZ has the ability to penetrate and interact with the cell membrane through different mechanisms which may lead to the initiation of epileptic activity (Bloms et al., 1992; Madeja et al., 1996; Altrup et al., 2006). Previously, PTZ was suggested to be absorbed easily by membrane macromolecules (Chalazonitis, 1978). Altrup et al., (2006) recently reported that PTZ can incorporate with cell membrane and cause increased membrane pressure. Similarly, it was also shown that PTZ exerts its effect on potasium channel via interaction with cell membrane (Madeja et al., 1996). This corresponds to the fact that an increase of lipophilicity of PTZ elevates epileptogenic potency of the agent (Gross et al., 1972; Woodbury et al., 1980). Moreover, PTZ was also indicated to affect intracellularly GABAa receptor (Bloms-Funke et al., 1996) and $Na^+\backslash K^+$ pump (Dubberke et al., 1998) by penetrating into cell membrane. "*As a result, in spite of extensive use of PTZ for epileptogenic purposes, it is not clear that whether PTZ exerts its function through a direct interaction with membrane proteins or membrane lipids*".

1.1.10 Treatment of Epilepsy

The main treatment options for people with epilepsy are medications, surgery and vagus nerve stimulation. The ketogenic diet is an option for some children, and increasingly, for some adults. Investigational treatments may also be an option for eligible patients.

Overall, the prognosis for most epilepsy patients with antiepileptic treatment today is good in terms of seizure control. Evidence from population-based studies show that 70-80% of patients will ultimately become seizure-free (Cockerell et al., 1995; 1997). The long-term outcome of epilepsy is often predictable by observation of the early outcome of seizure control (Sillanpää, 2000). In 50-70% of the patients, seizures will be controlled with an initial antiepileptic drug, regardless of the specific drug used (Collaborative Group for the Study of Epilepsy, 1992). Switching to a second antiepileptic drug affords control in about one-third of initially uncontrolled patients (Smith et al., 1987). There are no clear differences in efficacy between first line monotherapy drugs such as carbamazepine, phenytoin, valproate, lamotrigine and oxcarbazepine (Mattson et al., 1985; 1992; Brodie et al., 1995; Bill et al., 1997), the newer antiepileptic drugs (gabapentin, levetiracetam, tiagabine, topiramate, *vigabatrin* and zonisamide) have been shown significant difference in efficacy or tolerability (Chadwick et al., 1996; Marson and Chadwick, 2001).

Up to 30% of all epilepsy patients will develop intractable epilepsy (Sander and Sillanpää, 1999). The epilepsy is considered intractable when a patient has epileptic seizures or other symptoms of epileptic syndrome despite optimal treatment and these symptoms restrict the patient's ability to lead a full and safe life (Hauser and Hesdorffer, 2001). In a prospective study of newly-referred epilepsy patients, the risk factors that predicted the development of intractable epilepsy were a large number of seizures before treatment, combined seizure types, early age at onset, and prolonged disease duration (Beghi and Tognoni, 1988). Moreover, the factors associated with intractable epilepsy include syndromes of secondarily generalized epilepsies (e.g., Lennox-Gastaut syndrome, West syndrome), certain seizure types such as atonic and tonic seizures, and certain etiologies such as sequlae of cerebral infections or trauma. Epilepsy patients with associated neurologic deficits and detectable structural brain damage have lower remission rates (Shorvon, 1990; Sander, 1993). Drug-resistant seizures and associated neurological disabilities are further related to poor social outcome and higher mortality rate (Hauser et al., 1980; Cockerell et al., 1997; Sillanpää, 2000).

Overall, patients with epilepsy have a mortality rate two to three times higher than expected (Annegers, 1999). The greatest increase in mortality occurs in the early years of diagnosis, in the symptomatic group and in patients with high frequency of tonic-clonic seizures (Hauser et al., 1980; Cockerell et al., 1997; Walczak et al., 2001).

1.1.10.1 Vigabatrin (VGB)

Vigabatrin (VGB, γ-vinyl-GABA, 4-amino-5-hexenoic acid, Sabril) is a newer (second generation) well-characterized antiepileptic drug (Mainardi et al., 2007). Taken orally, it suppresses seizure frequency by 50% or more in approximately half of the epileptic patients (Abbot et al., 2006). It is a structural analogue of gamma-aminobutyric acid (GABA) containing an alpha-vinyl group. The action mechanism of VGB is believed through a modification of GABAergic transmission due to its similarity to GABA. It replaces GABA as substrate and inhibits irreversibly gamma-aminobutyric acid transaminase (GABA-T), which is responsible for degradation of cytosolic GABA to succinate in the brain, by binding with high affinity, thus raising GABA concentrations (Manor et al., 1996; Petroff et al., 1999; Willmore et al., 2009).
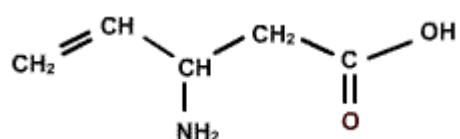
Figure 2. Chemical representation of VGB

The evaluation of theurapetic effects of antiepileptics like vigabatrin, which is a daily used drug, is very important since epilepsy treatment lasts for a long time period. It has been reported that the therapuetic effect of a drug depends on the biopharmaceutics (e.g. solubility, stability, permeability) and pharmacokinetics (e.g. extent of protein binding and volume of distribution) of the drug

(Panchagnula et al., 2001). Among these parameters biological permeability, which is based on the degree of incorporation and uniform distribution into lipid bilayer for a drug, has particular importance since it determines the biological profile and distribution of the drug in body, affecting its absorption, distribution and elimination (Saija et al., 1995; Malkia et al., 2001; Castelli et al., 2006).

As an orally delivered drug the interaction of VGB with cell membranes gains importance since it must cross several distinct barriers such as small intestine epithelium, BBB and neuronal cell membrane before reaching the target site of action in the brain. There are some studies stating that VGB interact with cell membranes and undergoes complete absorption (Frisk-Holberg et al., 1989), quickly enters the cerebrospinal fluid (Ben-Menachem et al., 1989) and effectively permeate the blood brain barrier (BBB) (Jung et al, 1977; Nanavati and Silverman, 1991; Tong, 2007). On the contrary to these studies, it has been reported that there are specific transporters for VGB on BBB (Wu et al., 2004; Berezowski et al., 2004), both neurones and glial cells (Eckstein-Ludwig et al., 1999). "*As a result, the corporation of VGB with cell membranes that affect its distribution in body are not identified very well* (Abbot et al., 2006)".

1.2 Spectroscopic and Calorimetric Techniques used in this study

1.2.1   Basis of Spectroscopy

Electromagnetic radiation is considered as two mutually perpendicular electric and magnetic fields, oscillating in single planes at right angles to each other. These fields are in phase and are propagated as a sine wave as shown in Figure 3, where E is the direction of the electric field while B is the direction of the magnetic field (Stuart, 1997).
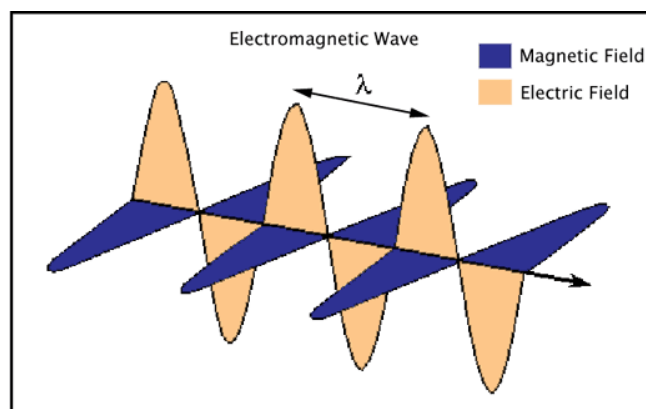
Figure 3. Electromagnetic wave

The interaction between electromagnetic radiation and matter can cause redirection of the radiation between energy levels of the atoms or molecules. In this phenomenon, the energy excites a molecule to a higher energy level. The type of excitation depends on the wavelength of the light (Freifelder *et al.,* 1982). The energy levels are usually described by an energy level diagram shown in Figure 4.

Distance between electrons and nucleus or between atoms in a molecule
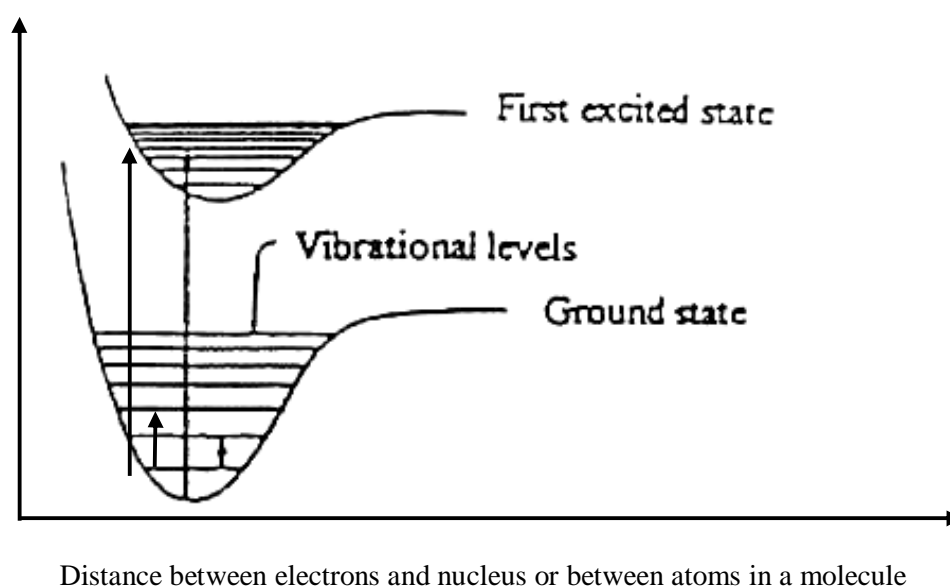
Figure 4. Energy level diagram illustrating the ground and first excited electronic energy level. Vibrational energy levels are represented as parallel lines superimposed on the electronic levels. The long arrows show a possible electronic transition from the ground state to the first excited state while the short arrow represents a vibrational transition within the ground electronic state (Freifelder, 1982).

18

The frequency dependence of absorption arises since energy is absorbed by transitions induced between different energy states of the molecules in the sample. The transitions occur only if there is a strong interaction between the incident radiation and the molecule. Absorption is most probable when the energy level separation matches the energy of the incident radiation as indicated below,

$$\Delta E = h\nu$$

where ΔE is the separation between the energy states of interest, ν is the frequency of the applied radiation and h is Planck's constant (h = 6.6×10^{-34} joule second).

$$c = \lambda \nu$$

where c is the speed of light in vacuum (3.0×10^8 ms^{-1}) and λ is the wavelength of light. These two equations can be used to identify a common spectroscopic unit called wavenumber, which is denoted by $\bar{\nu}$. Wavenumber is defined as the reciprocal of the wavelength as follows;

$$\bar{\nu} = \text{wavenumber} = (1/\lambda) \; [\text{ has a unit of cm}^{-1}]$$

Thus, $E = h\nu = h c \bar{\nu}$,

From these equations, it is clear that both wavenumber and frequency are directly proportional to energy

Spectroscopy is defined as the study of the interaction of electromagnetic radiation with matter. Spectroscopic techniques involve irradiation of a sample with some form of electromagnetic radiation, measurement of the scattering, absorption, or emission in terms of some measured parameters, and the interpretation of these measured parameters to give useful information. Figure 5 represents many of the important regions of the electromagnetic spectrum.
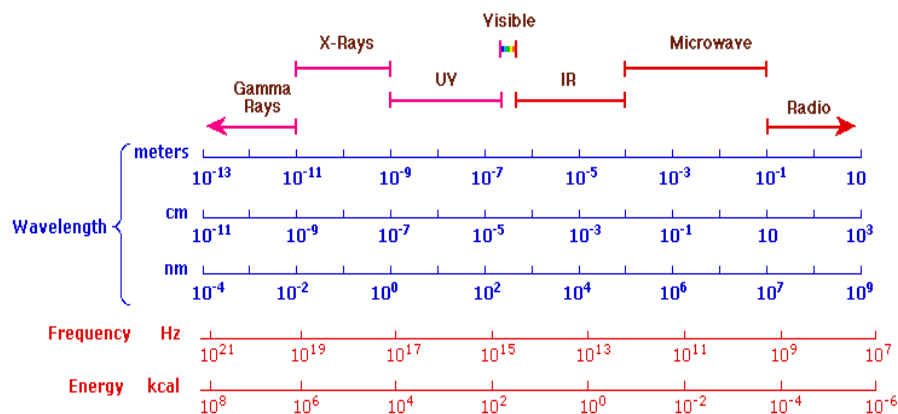
Figure 5. The Electromagnetic Spectrum

For most purposes it is convenient to treat a molecule as if it possesses several distinct reservoirs of energy. The total energy is given by the following equation (Campbell and Dwek *et al.,* 1984).

$$E_{total}=E_{translation}+E_{rotation}+E_{vibration}+E_{electronic}+E_{electronicspinorientation}+E_{nuclearspin\ orientation}$$

The contribution of $E_{translation}$, $E_{electron\ spin\ orientation}$ and $E_{nuclear\ spin\ orientation}$ are negligible since the separations between respective energy levels are very small. The separations between the neighboring energy levels corresponding to $E_{rotation}$, $E_{vibration}$ and $E_{electronic}$ are associated with the microwave, infrared and ultraviolet-visible regions of the electromagnetic spectrum, respectively (Campbell and Dwek, 1984).

1.2.2 Infrared Spectroscopy

The term "infrared" covers the range of the electromagnetic spectrum between 0.78 and 1000 µm. In the context of infrared spy, wavelength is measured in "wavenumber".

Infrared (IR) region is divided into three sub regions (Fig. 5) (Smith, 1999):

Region	Wavenumber range (cm^{-1})
Near	14000-4000
Middle	4000-400
Far	400-4

The atoms in a molecule are constantly oscillating around average positions. Bond lengths and bond angles are continuously changing due to this vibration. A molecule absorbs infrared radiation when the vibration of the atoms in the molecule produces an oscillating electric field with the same frequency as the frequency of the incident IR light. The molecule will only absorb radiation if the vibration is accompanied by a change in the dipole moment of the molecule. A dipole occurs when there is charge separation across bond. If the two oppositely charged molecules get closer or move further apart as the bond bends or stretches, the moment will change.

In a molecule, atoms vibrate and rotate relative to their center of mass. If the vibration energy is small, the motion can be approximated to Simple Harmonic Motion, SHM. These vibrational and rotational phenomena are used to determine the compounds of matter and its structure.

The vibrational frequency (ν_{vib}) of the spring-like bond is given by;

$$\nu_{vib} = \tfrac{1}{2} \left[\sqrt{(k / \mu)} \right]$$

where k is the force constant the stiffnes of the bond and μ is the molecular reduced mass of atom A (with mass m_A) and atom B (with mass m_B), and is defined as;

$$\mu = m_A\, m_B / (m_{A} + m_B)$$

All of the motions can be described in terms of two types of molecular vibrations.

21

One type of vibration, a stretch, produces a change of bond length. A stretch is a rhythmic movement along the line between the atoms so that the interatomic distance is either increasing or decreasing. The second type of vibration, a bend, results in a change in bond angle. These are also called scissoring, rocking or wigwag motions. Each of these two main types of vibration can have variations. A stretch can be symmetric or asymmetric. Bending can occur in the plane of the molecule or out of plane; it can be scissoring, like blades of a pair of scissors, or rocking, where two atoms move in the same directions (Volland, 1999). Figure 6 demonstrates the main types of variations schematically.
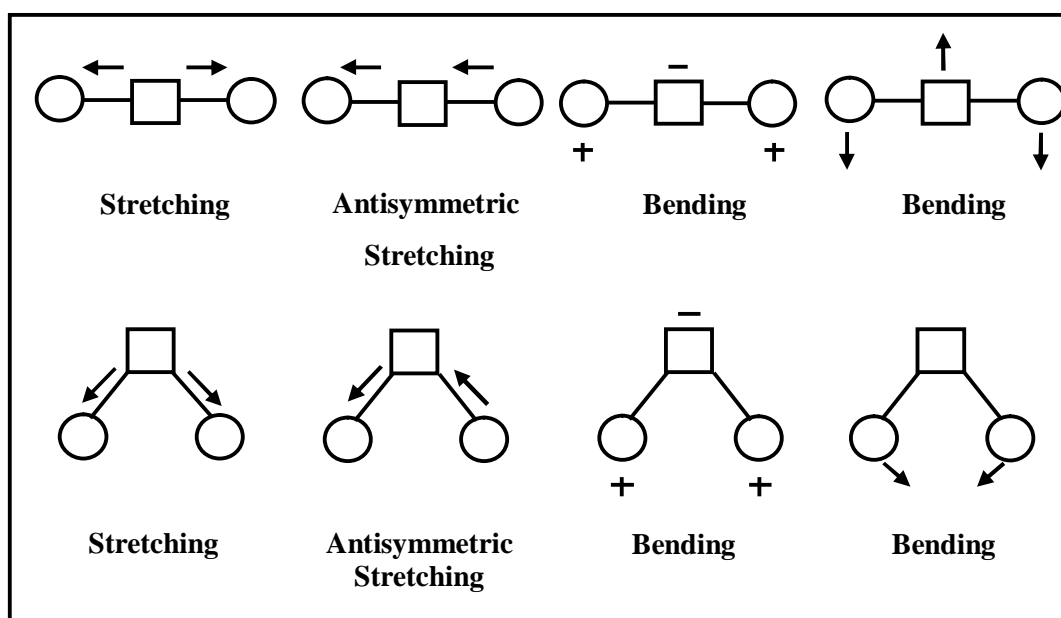
Figure 6. Types of normal vibration in a linear and non-linear triatomic molecule. Atomic displacements are represented by arrows (in plane of page) and by + and – symbols (out of page plane) (Arrondo *et al*., 1993).

An infrared spectrum usually consists of a plot of the absorption of radiation as a function of wavenumber. As each different material has a unique combination of atoms, no two compounds produce the exact same infrared spectrum. Therefore, an infrared spectrum can result in a positive identification of every different kind of material.

1.2.3 The Fourier Transform Infrared Spectroscopy (FTIR)

The pieces of FT-IR spectroscopy and their functions are listed below;

- A source generates light across the spectrum of interest.

- A monochromater (in IR this can be either a salt prism or a grating with finely spaced etched lines) separates the source radiation into its different wavelengths.

- A slit selects the collection of wavelengths that shine through the sample at any given time.

- In double beam operation, a beam splitter separates the incident beam in two; half goes to sample, and half to a reference.

- The sample absorbs light according to its chemical properties.

- A detector collects the radiation that passes through the sample, and in double-beam operation, compares its energy to that going through the reference.

- The detector outputs an electrical signal, which is normally sent directly to an analog recorder. A link between the monochromater and the recorder allows you to record energy as a function of frequency or wavelength, depending on how the recorder is calibrated.

- A moving mirror allows the determination of the precision of the position of an infrared band, which is the precision with which the scanning mirror position is known. To determine this position exactly, a helium-neon laser beam is incorporated in the beam of the source. This laser beam produces standard fringes by interference which can line-up successive scans accurately and can determine the position of the moving mirror at all times (George and Mclyntyre, 1987).
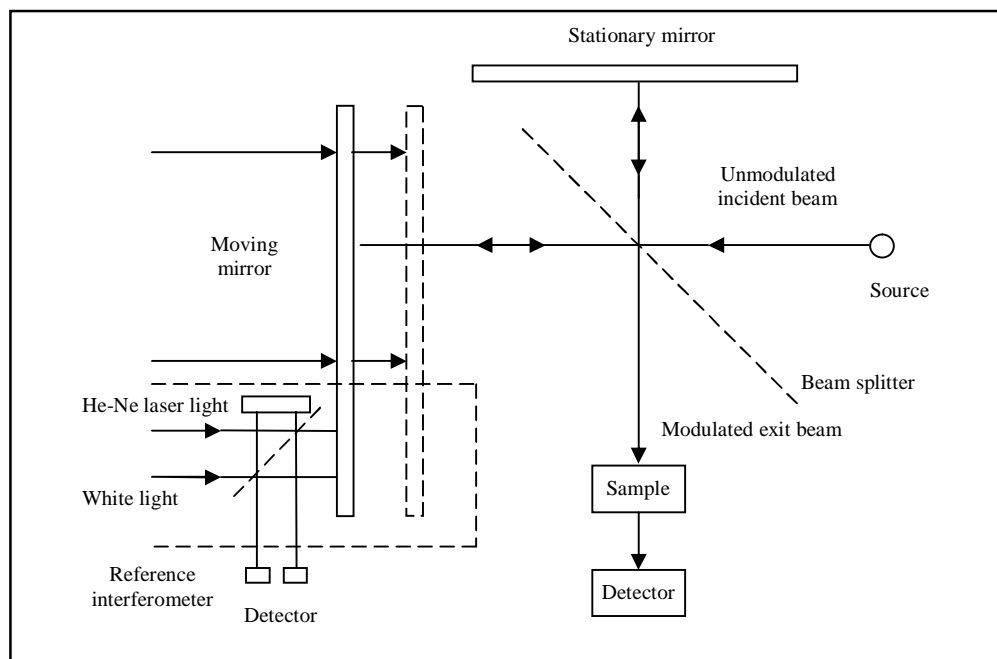
Figure 7. Instrumentation of FTIR spectrometer

The important parameter in the FT-IR spectrometer is the interferometer, which is commonly a Michelson Interferometer. This is a device that splits an electromagnetic beam in two directions to recombine them later so that the intensity variation can be determined as a function of the path difference between them. The interferometer contains two orthogonal mirrors: one movable and the other fixed. The light passes through a beam splitter, which sends the light in two directions at right angles. One beam goes to a stationary mirror then back to the beam splitter. The other beam goes to a moving mirror. The motion of the mirror makes the total path length variable versus that taken by the stationary-mirror beam. When the two meet up again at the beam splitter, they recombine, but the difference in path length creates constructive and destructive interference, which is called an interferogram.

The recombined beam passes through the sample. The sample absorbs all the different wavelength characteristics of its spectrum. The detector now reports variation in energy versus time for all wavelengths simultaneously. A laser beam is superimposed to provide a reference for the instrument operation.

Energy versus time is an odd way to record a spectrum until it is recognized the relationship between time and frequency was recognized: they are reciprocal. A mathematical function called Fourier transform allows us to convert an intensity-versus-time spectrum into an intensity-versus-frequency spectrum. The spectrometer computer is able to deconvolute (Fourier Transform) all the individual cosine waves that contribute to the interferogram, and so produce a plot of intensity against wavelength (cm), or more usually frequency cm^{-1}.

The main advantage of FTIR spectrometry lies in its ability to increase signal-to-noise ratio by signal averaging (Stuart, 1997). Moreover, in FTIR spectroscopy, it is possible to examine all wavelengths arriving at the detector simultaneously, compared to being able to sample only one spectral element at a time by the detector (Diem, 1993). The other strength of this technique is its speed and sensitivity. Moreover, it yields high quality infrared spectra from sample amounts as low as few micrograms (Dighton *et al.,* 2001). Furthermore, samples can be examined in a variety of physical states, such as solids, liquids and gases. In addition, the sample can be studies without the use any perturbing probe molecules. In other words, it is is a non-disturbing technique which provides structural and functional information about the sample (Liu et al., 1996; Toyran et al., 2004; Dogan et al., 2007). It gives valuable information about the biological samples by detecting changes in the functional groups belonging to the tissue components such as lipids, proteins, carbohydrates and nucleic acids, simultaneously (Kneipp et al., 2000; Bozkurt et al., 2007; Garip et al., 2007). The shift in peak position, bandwidth and peak area/intensity give valuable information, which can be used for rapid and proper identification of disease-states in a variety of biological samples such as tissues, membranes, cells and biofluids. Therefore, in recent years, this method has been widely used for diagnosis of several diseases by others (Liu et al., 1996; Yano et al., 1996; Schultz et al., 1998; Ci et al., 1999; Dicko et al., 1999; Severcan et al., 2000; Toyran et al., 2004; Petibois et al., 2006; Dogan et al., 2007; Bozkurt et al., 2007; Akkas et al., 2007a; Akkas et al., 2007b; Szczerbowska-Boruchowska et al., 2007).

1.2.4 Fourier Transform Infrared Microspectroscopy (FTIR microscopy)

Fourier transform infrared microspectroscopy is a powerful technique which is the combination of an infrared spectroscopy with a microscope. It allows the detection of chemical species from a spatial region. Combining spatial specificity with information on its chemical constitution, a chemical map can be constructed for the whole spatial area. This typically involves collecting the IR spectrum of the sample at a point, moving the sample to another location and collecting the spectrum at the second point and so on. In this manner, the whole area is mapped point-by-point.

FTIR microspectroscopy is a efficient instrument that can be used to collect IR spectra from microscopic regions of the tissue sections or tissue homogenates. The infrared spectra are evaluated to chemically characterize the absorbing molecules. This technique is applied to normal or diseased tissues. In this latter case, FTIR microscopy can reveal chemical changes that are associated with disease conditions, which can provide insights into the chemical mechanism of disease processes (Le Vine et al., 1999).

The value of infrared microscopy is two fold. Firstly, it allows the analysis of very small samples. The practical advantage of this sensitivity is that it allows the analysis of trace deposists of biological materials in situ, without extraction. Secondly, infrared microsopy equipped with computer controlled stages allow the distrubiton materials within tissue sections to be mapped with a high spatial resolution. This approach termed funcitonal group mapping, can provide a valuable aid for understanding spectral data as the distribution of a number of chromophores within tissues can be analyzed. It may be expected that functional groups arising from the same molecule will show a similar distribution within a tissue, and therefore; a comparison of the distribution of assigned and unassigned absorptions can be used to aid assigments (Jackson et al., 1998).
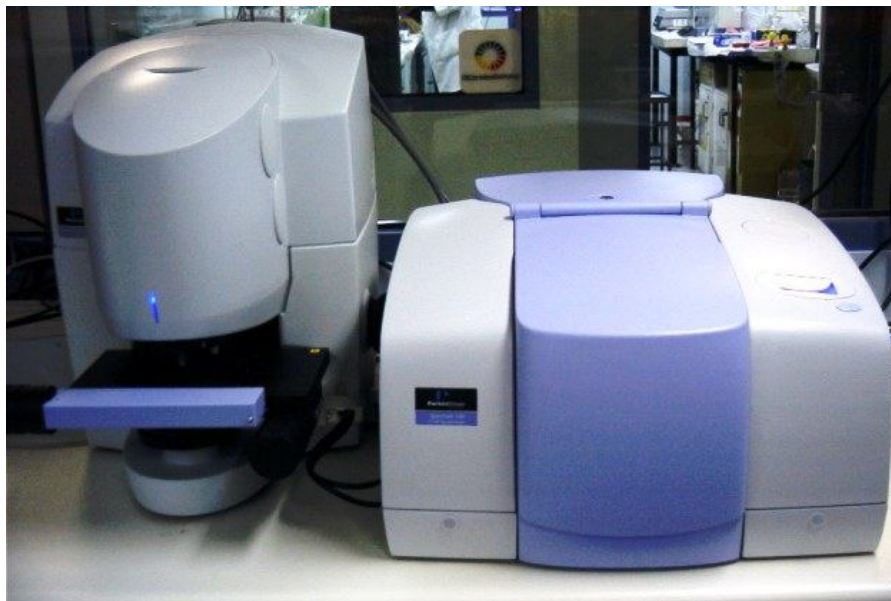
Figure 8. Perkin Elmer Spectrum Spotlight 400 imaging FTIR microscope

1.2.5 Electron spin resonance spectroscopy (ESR)

ESR measures the absorption of microwave radiation corresponding to the energy splitting of an unpaired electron when it is placed in a strong magnetic field. This spectroscopic technique detects the unpaired electrons in a chemical system. This can yield structural and dynamic information, even from ongoing chemical or physical processes without influencing the process itself. This make ESR spectroscopy an ideal technique to complement other analytical methods in wide range of application areas.

Since the molecules of interest in the current study do not contain free radical, we used spil label ESR method. This method consists in placing stable NO group in the system of interest either by attaching it onto a molecule of the system under study, or by introducing in this system a spin probe which is dissolved in the system without permeanent bonding to any of its molecule (Cannistraro et al., 1976).

Analysis of line positions and line shapes, either in liquid solutions or liquid crystals, membranes, solids can yield information about the rate of motion of the label, the structure, order, viscosity, polarity of the system.

The theory of ESR spectroscopy begins with a quantum analysis of the energy associated with the magnetic dipole moments of electrons in a molecule. Magnetic dipoles have two components - one that is due to spin angular momentum (arising from the electron spinning about its axis), and one due to orbital momentum. In the vast majority of cases, the spin angular momentum accounts for about 99% of the total magnetic dipole.

The strength of the magnetic dipole is characterized by the magnetic dipole moment, which is defined in terms of the interaction of the magnetic dipole with a magnetic field, H. The energy, E, of the magnetic moment is given by:

$$E = -\mu . H$$
$$= -\mu H \cos(\theta)$$
$$= -\mu_z H$$

Electrons also have an intrinsic spin angular momentum, P, which is an internal property of the particle. The dipole moment is proportional to P, and can be written:

$$\mu = \gamma P$$

A proportionality constant, called the magnetogyric ratio, contains an important factor, g. Inserting the magnetogyric ratio into the equation above, the dipole moment becomes:

$$\mu = -g\frac{e}{2mc}P$$

Since the quantum mechanical angular momentum is quantized, it is helpful to analyze the properties of an electron by considering the behavior of a particle restricted to motion about a ring. There is a de Broglie wavelength associated with the momentum, P. In order for the probability to be time-independent, the wave function must be single-valued, which limits the circumference of the ring to be an integral number times the de Broglie wavelength. That is:

$$2\pi r = M\lambda = M\frac{h}{P}$$

Therefore:

$$Pr = P_\phi = M\frac{h}{2\pi} = M\hbar$$

Where P (theta) is the magnitude of the *angular* momentum of the particle in the theta direction, and M is an integer (M = 0, 1, 2, 3, ...). This quantization of angular momentum allows electron orbitals to be designated by the following notation:

for M = 0, the electrons are said to be in a sigma orbital, and for M = 1, they are in a pi orbital. This derivation assumes that the potential energy is constant.

The spin angular momentum of a particle is characterized by the spin quantum number, where the allowed values of M_S range in unit increments from -S up to +S giving 2S + 1 components. For a system with a single electron, S=½, so the allowed values for m_S are +/-½.

The quantized angular momentum in the direction of the external magnetic field (the Z direction) can be written in terms of the spin quantum number:

$$P_Z = M_S \hbar$$

The dipole moment becomes:

$$\mu_Z = -g\frac{e}{2mc}M_S\hbar = -g\beta M_S$$

where beta is the Bohr magneton. The energy becomes:

$$E = \pm\tfrac{1}{2}g\beta H$$

These two possible values for energy are called Zeeman energies. These transitions are shown schematically in Figure 9.

$$E_\alpha = \tfrac{1}{2}g\beta H$$

$$\Delta E = g\beta H_r$$

$$E_\beta = -\tfrac{1}{2}g\beta H$$
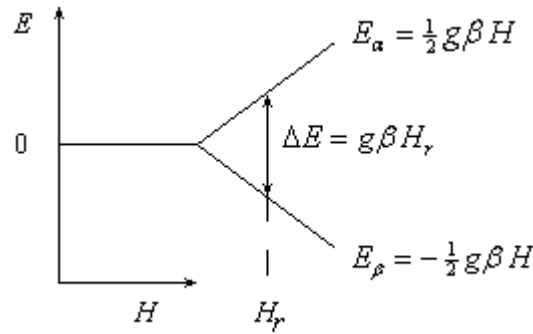
Figure 9. The transitions occur in ESR

Figure 10 is a pictoral representation of the sample cavity. In the presence of an external magnetic field, dipoles will align themselves either parallel or opposed to (antiparallel) the external field. Since parallel alignment is a lower and more stable energy condition, the population of electrons in this state is greater than in the antiparallel state. Energy transitions are initiated by supplying an electromagnetic field with high frequency (usually in the microwave range). If the energy of the microwave field corresponds to delta E, then the field is said to be at resonant frequency and transitions occur.
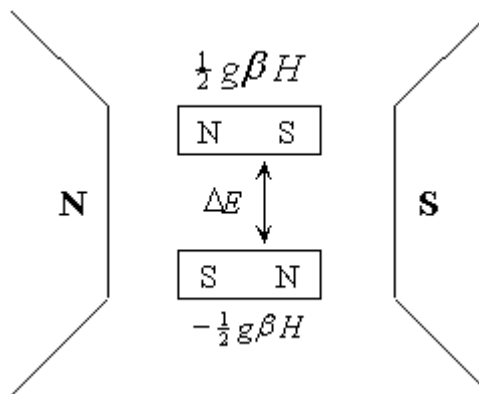
Figure 10. Schematic presentation of sample cavity

Dipoles in parallel alignment to the magnetic field absorb energy from the microwave field, sending them to higher energy states. Similarly, antiparallel dipoles release the same amount of energy to the electromagnetic field. Since there are slightly more parallel dipoles when resonance occurs, there will be a net absorption of energy by the dipoles. The energy from the electromagnetic field that is lost to the dipoles is detected and amplified yielding the ESR signal for the sample being analyzed.

The g value is a universal constant and is a characteristic of electrons (g_e = 2.00232). Whenever an external magnetic field is applied to a sample, an internal orbital magnetic moment can be introduced. This internal magnetic moment is caused by mixing in of excited states into the ground state, which is brought about by a coupling of the electron spin and orbital angular momenta. This phenomenon is characterized by the atomic spin-orbit coupling constant gamma.

The internal magnetic field may add to or subtract from the external field. Since H_r is defined to be the external magnetic field at resonance, g must be allowed to vary to account for any local magnetic fields.

1.2.5.1 ESR spectrometer

A typical ESR spectrometer have four essential components;

- A monochromatic microwave source
- A waveguide for guiding the microwave power to the sample
- A cavity designed to ensure a proper coupling between the sample and incoming wave
- A detector for microwave power to detect the response of the sample to microwave irradiation.
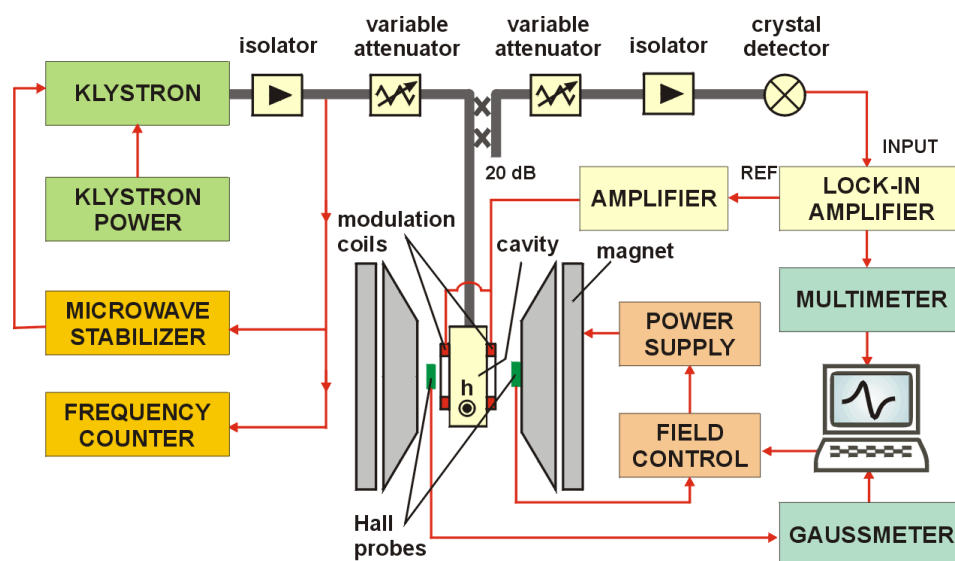
Figure 11. Schematic representation of ESR spectrometer

1.2.5.2 ESR in membrane research

Insight into the behavior of membranes has been obtained from ESR studies. As the membrane itself is not paramagnetic, it is necessary to make the membrane with a suitable paramagnetic probe. Stable nitroxide radicals have been widely used as spin probes in studies of biological membranes and model membrane systems (Dalton, 1984). The spin labels are specifically incorporated into membranes, therefore; the properties of the different region of the membrane can be studied.

It is used to investigate membrane properties and drug-membrane interactions. It is especially useful for the determination of membrane orderness, fluidity and localization of the drug molecules into membrane. An advantage of this study is its sensitivity, which allows the study of such effects at molecular or submolecular levels. Various membrane parameters have succesfully been studied by ESR spectroscopy of stable nitroxide radicals. Membrane order and dynamics have been evaluated as well as drug effects on membranes, including phase behaviour and permeability (Severcan and Cannistraro, 1990; Carton et al., 1992).

1.2.6 Differential Scanning Spectroscopy (DSC)

Differential scanning calorimetry (DSC) is a technique commonly used for determining the thermal properties of a variety of materials including biologically relevant systems. The main applications of DSC include determination of the effect of composition, hydration, pH, and solvent, on the phase-transition temperatures and enthalpies of model and biological membranes and pharmaceuticals (Severcan et al. 2005, Korkmaz and Severcan, 2005); thermal characterization of complex processes, such as the denaturation of proteins; and specific heat measurements in the glass-transition of polymers (Ceckler and Cunningham, 1997).

DSC consists of measuring the temperature difference between a sample solution and a reference solution as a function of temperature. To achieve this, the sample and reference material are subjected to variable temperature. Once a transition occurs in the sample, thermal energy is added to reference containers in order to maintain both sample and the reference at the same temperature. Since this energy input is precisely equivalent in magnitude to the energy absorbed in the particular transition, a recording of this balancing energy yields a direct calorimetric measurement of the transition energy (Bradrick *et al*., 1989; Castelli *et al*., 2003). This temperature difference, which is expressed in units of a power difference, is converted to a difference in the heat capacity between the sample solution and the reference solution as a function of temperature. The heat capacity versus temperature curve is analyzed to determine the transition temperature, T_m, and calorimetric enthalpy of transition ΔH_{cal} (Ohline et al., 2001).

For first order phase transitions such as the bilayer gel to liquid-crystalline transition, the transition temperature, T_m , is where the heat capacity, C_p, reaches its maximum value. The value of the calorimetric enthalpy (ΔH_{cal}) for the phase transition is determined by integrating the area under the peak.

From these values, the entropy of the phase transition is determined:

$\Delta S = \Delta H_{cal} / T_m$

Comparison of ΔH_{cal}, ΔS and T_m shows the effect of a structural modification (e.g. chain length) on the thermodynamics of the phase transition. However, the phase transition in bilayers involves more than just the initial and final states. In fact, intermediate "states" are formed during the transition, and a "non-two-state" model is necessary for phospolipids in liposomes (Mason, 1998; Sturtevant et al., 1987) . These intermediate states result from the formation of domains (e.g. disordered, mobile areas within the gel phase) before the phase transition temperature, and are due to lateral movement of the phospholipids within the bilayer. The asymmetric shape of the DSC peak reflects the fact that a non-two-state transition is occurring (Ohline et al., 2001).

Differential scanning calorimetry is a classic method, but application to biological systems is a recent event. DSC has been used to characterize phase transitions with respect to thermodynamic parameters such as transition temperature, enthalpy of transition, and entropy of transition (Koyama et al., 1999). This thermotropic properties can be correlated with changes in biological properties (Tien and Ottova, 2000).

The gel to liquid-crystalline phase transition is highly "cooperative." In cooperative transitions, the molecules cooperate with each other in gaining new motional freedom; when one molecule picks up motional energy then other nearby molecules find it easier to add motional energy. As the temperature approaches the transition temperature, T_m , the distance range of this cooperation increases. Near the phase transition temperature, you can picture islands of lipids in a more mobile phase intermixed with the less mobile gel phase. The number of molecules on average in these disordered "islands" is called the cooperative unit. In these islands the motions of the molecules are highly correlated. These correlated interactions aid in the sudden change of order at the phase transition temperature. The larger the cooperative unit, the narrower the phase transition temperature range. The gel to liquid-crystalline phase transition is first-order with some of the characteristics of second-order transitions. First-order phase transitions have a change in enthalpy and volume at the phase transition temperature. In other words, in first-order transitions there is an abrupt change in the properties of the

system at the phase transition temperature. In this respect, a first order phase transition is "completely correlated," that is completely cooperative. In a first order phase transition all the molecules undergo the phase transition together, subject only to the availability of thermal energy. A pure first-order transition has an infinitely sharp transition. Second-order transitions do not have enthalpy and volume changes at the transition temperature. For second order phase transitions, the formation of cooperative, correlated motions with limited range broadens the transition by pre-transition effects (i.e. the domains anticipate the transition or "start the transition" early). In the DSC of synthetic phospholipids the limited cooperativity of the transition results in a small peak at a lower temperature than the main melting peak, called the pre-transition, as well as a broadening of the main melting transition (Chapman, 1975; Szoka and Papahadjopoulos, 1980; Koyama et al., 1999; Ohline et al., 2001).

1.2.6.1 Instrumentation of DSC

During the determination, the instrument detects differences in the heat flow between the sample and reference. This information is sent to an output device, most often a computer, resulting in a plot of the differential heat flow between the reference and sample cell as a function of temperature. Since no thermodynamic physical or chemical processes occurs, the heat flow difference between the sample and reference varies only slightly with temperature, and shows up as a flat, or very shallow base line on the plot. However, an exothermic or endothermic process within the sample results in a significant deviation in the difference between the two heat flows. The result is a peak in the DSC curve. Generally, the differential heat flow is calculated by subtracting the sample heat flow from the reference heat flow. When following this convention, exothermic processes will show up as positive peaks (above the baseline) while peaks resulting from endothermic processes are negative (below the baseline) (Dean, 1995). Figure 12 shows instrumentation of a DSC.
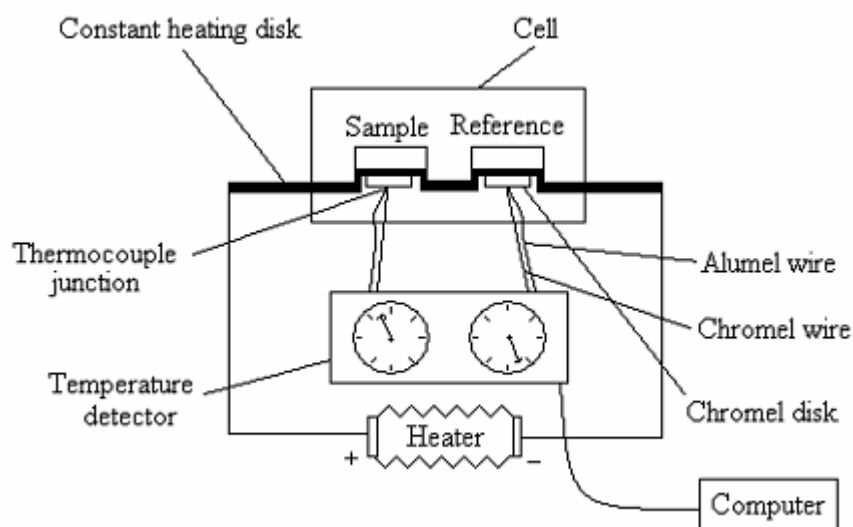
Figure 12. Schematic representation of DSC instrumentation

1.2.7 Steady State Fluorescence Spectroscopy

The initial step in a fluorescence measurement is electronic excitation of an analyte molecule via absorption of a photon (Figure 13). Once formed, an excited molecule has available a variety of decay processes by which it can rid itself of the energy imparted to it by absorption. In addition to fluorescence (the desired decay route), there are nonradiative decay processes, leading to release of energy in the form of heat rather than light. Other sample constituents may interact with an excited analyte molecule in such a way as to prevent it from fluorescing; such processes are called quenching. Also, an electronically excited molecule may undergo chemical reaction (photodecomposition).
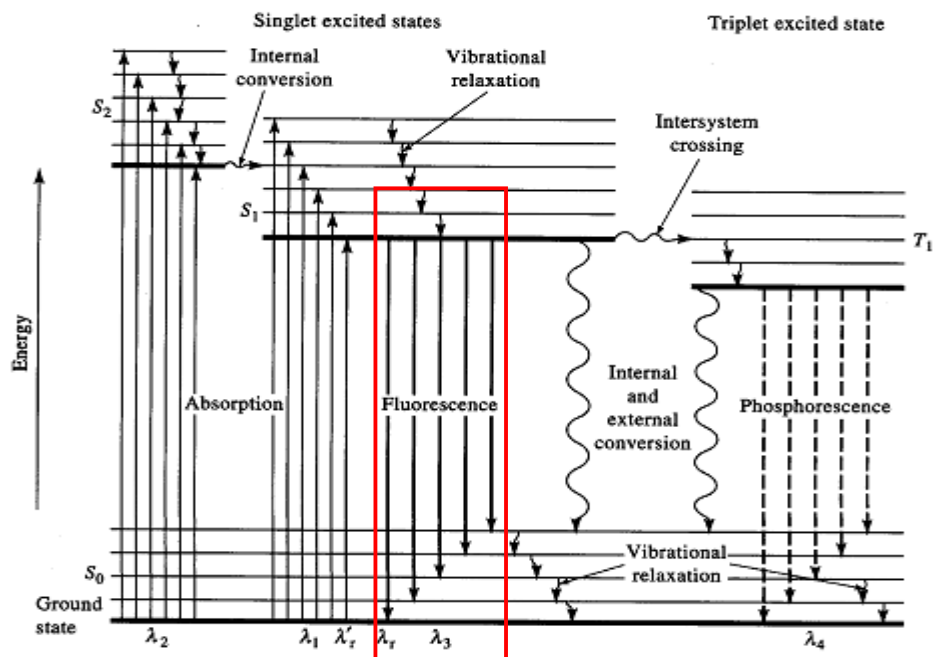
Figure 13. Representation of energy level diagram for fluorescence spectroscopy

Excitation of a molecule does not automatically produce fluorescence; many molecules exhibit very weak fluorescence. Most intensely fluorescent organic molecules contain large conjugated p-electron systems (Treton et al., 1999). For example, most polycyclic aromatic hydrocarbons are intensely fluorescent. Very few saturated organic molecules, and relatively few inorganic molecules, exhibit intense fluorescence. To extend the applicability of fluorometry to the many compounds that do not exhibit intense native fluorescence, chemical reactions can be used to convert (derivatize) nonfluorescent molecules to fluorescent derivatives, or a nonfluorescent molecule may have chemically attached to it a fluorescent tag or label (Zeemans et al., 1998).

Fluorophores are divided into two general classes-intrinsic and extrinsic. Intrinsic fluorophores are those that occur naturally. Extrinsic fluorophores are those added to a sample that does not display the desired spectral properties.

The key characteristic of fluorescence spectrometry is its high sensitivity. Fluorometry may achieve limits of detection several orders of magnitude lower than those of most other techniques. This is known as the fluorescence advantage. Limits of detection of 10^{-10} M or lower are possible for intensely fluorescent

molecules; in favorable cases under stringently controlled conditions, the ultimate limit of detection (a single molecule) may be reached. Because of the low detection limits, fluorescence is widely used for quantification of trace constituents of biological and environmental samples. Figure 14 shows total fluorescence measurements.
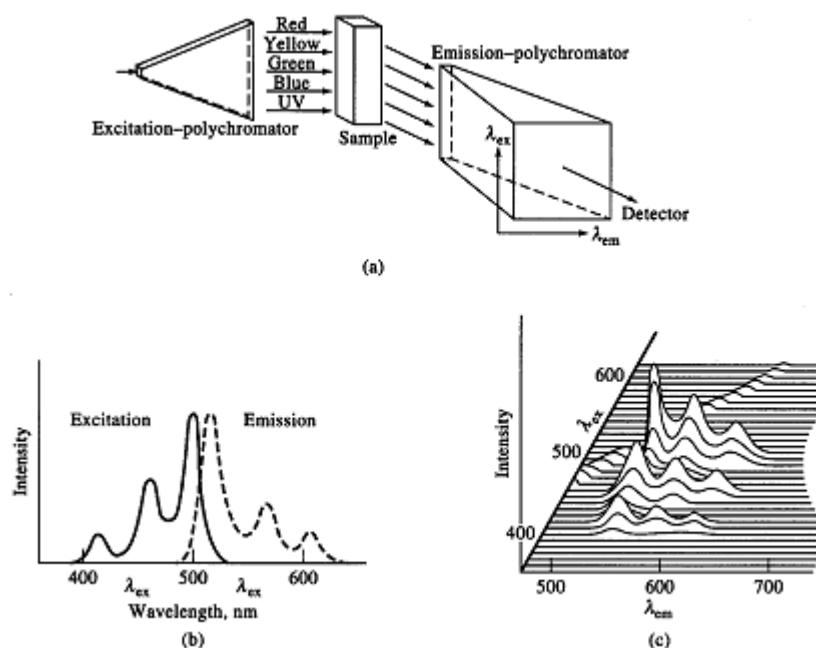
Figure 14. Total fluorescence measurements

The spectral range for most molecular fluorescence measurements is 200 to 1000 nm (10,000 to 50,000 cm^{-1}). Hence, optical materials used in UV/Vis absorption spectrometry are suitable for molecular fluorescence. Instrumentation for molecular fluorescence spectrometry is available from numerous manufacturers. Although commercial fluorescence spectrometers are useful in many situations, there are several important specialized applications (such as atmospheric remote sensing).
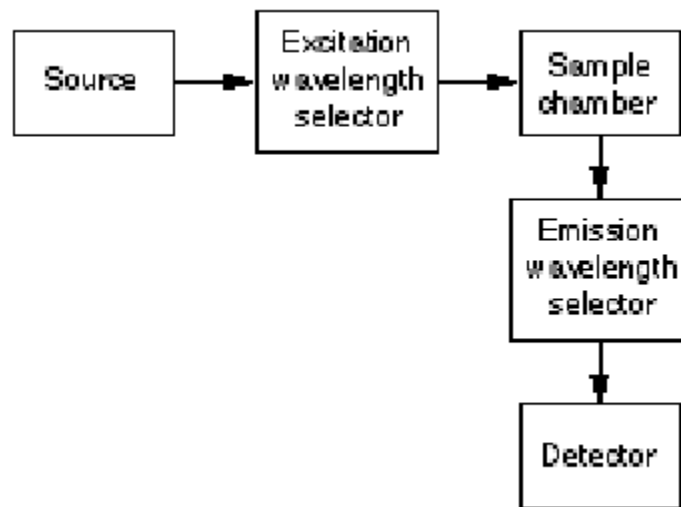
Figure 15. Schematic representaiton of steady state fluorescen spectroscopy

1.2.7.1 Steady state fluorescence spectroscopy in membrane research

This technique is one of the most widely used spectroscopic techniques in the fields of biochemistry and molecular biophysics. Although fluorescence measurements do not provide detailed structural information, the technique has become popular because of its sensitivity for detecting structural and dynamical properties of biomembranes.

Membrane typically do not display intrinsic fluorescence. For this reason, it is common to label membranes with probes which spontaneously partition into the nonpolar side chain region of the membrane. One of the most commonly used one is DPH. Because of its low solubility and quenched emission in water. DPH emisssion is only seen from membrane bound DPH.

Fluorophores absorbs light along a particular direction with respect to the molecular axes. For example, DPH only absorbs light polarized along its long axis. When a molecule is excited by polarized light, its fluorescence may be partially or fully polarized. A fluorometer can be used to measure fluorescence polarization by placing polarizing prisms or sheets in the excitation and emission beams.

The extent to which a fluorophore rotates during the excited state lifetime determines its polarization. Fluorescence polarization measurements have been used to determine the apparent viscosity of the side chain region of membranes, which is directly related to the membrane fluidity. Such measurements of membrane fluidity are typically performed using hydrophobic probe like DPH, which partitions into the membrane.

1.2.8 Atomic Force Microscopy (AFM)

The atomic force microscope (AFM), also known as the scanning force microscope(SFM), is an instrument which probes the interaction forces between sharp tip and the surface of a sample. The ability of this microscope to achieve high resolution (subnanometer) in liquids and to probe the mechanical properties of the sample at a nanometric scale. This makes the instrument increasingly interesting for the study of biological specimens.

The principle of the AFM ; a sharp tip fixed at the end of a flexible cantilever is raster-scanned over the surface of a sample. As the tip interacts with the surface, the cantilever deflects and its deflections are monitored and used to reonstruct the topography of the sample. Surfaces can be imaged nondestructively. The cantilever is a macroscopic spring that has a lower spring constant, meaning the applied force can be kept well below the force which would disturb the atoms from their sites, while still achieving measurable cantilever deflections. If the microscope is operated in liquids or in vacuum, high resolution is more readily achieved (Kasas et al., 1997).
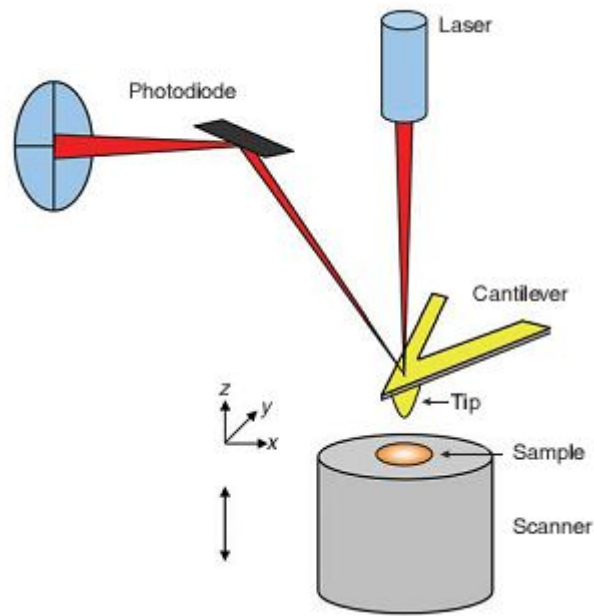
Figure 16. Schematic representation of a typical AFM. The sample sits on top of a piezoelectric tube in contact with the tip. The tip is fixed at the end of the cantilever, which is the triangular structure reflecting the laser beam. During the scan, the sample moves below the tip and small deformations of the lever are detected by deflection of the laser beam at the level of the two-segment photodiode.

There are three primary modes of AFM:

- Contact AFM, where the probe tip is in constant contact with the surface during scanning. The deflection of the probe cantilever is used to monitor the surface height. The obvious drawback to this mode is possible damage to the surface. A less obvious drawback is capillary forces from the meniscus of water that forms between the tip and the surface because of ambient water vapor. These forces are not present when contact AFM is done in a fluid environment. Advantages are fast scan speeds and high resolution.

- Non-Contact AFM is where the probe tip is scanned just above the surface at short enough range for atomic interactions to be monitored by the device. This overcomes the drawbacks of Contact AFM, but needs to be done extremely slowly if the surface

topology has any significant features on it. Also, it is only really useful for extremely hydrophobic samples, because an adsorbed fluid layer will trap the tip.

- Tapping mode, the tip is tapped rapidly (on the order of 300 kHz) against the surface as it scans over the area to be imaged. The amplitude of the oscillation of the probe in response to surface interaction is monitored by the microscope to form the images. This is the most useful mode for biological samples.

1.3 Aim of the study

In order to improve new diagnosis and treatment strategies for epilepsy the understanding of cellular and molecular mechanisms of epilepsy should be the ultimate goal.

The animal models for epilepsy have played important role to understand the basic physiological and behavioral changes, which are directly associated with the pathological consequences found in human (White, 2002). Taking into consideration this, we have selected PTZ-induced epileptic animal models. However, it is extensively used (Hartung et al., 1987; Bloms et al., 1992; Bloms-Funke et al., 1996), it is not clear that whether PTZ exerts its function through a direct interaction with membrane proteins or membrane lipids. For this reason, we firstly tested whether PTZ interacts with membrane lipids, or not. Since cell membrane is difficult to be characterized due to its complexity, we used a simplified model membrane system. We investigated PTZ-DPPC MLVs interactions in terms of lipid phase behavior, order and dynamics and nature of hydrogen bonding around its polar part, using different calorimetric and spectroscopic techniques. Therefore, we aimed to bring an explanation for its action mechanism.

We have concluded from model membrane studies that the molecular alterations of PTZ-induced seizures on brain tissue and cell membranes are only resulted from the consequences of epileptic activity not from convulsant agent itself.

Consequently, in the current study, we have investigated the effects of PTZ-induced epileptic activity on quantity of biomolecules, membrane fluidity, and lipid structure of rat brain tissues and cell membrane. We have also determined PTZ-induced changes in the protein secondary structure using neural networks (NN) based on FTIR spectral data as we have used previously for other biological systems (Akkas et al., 2007; Ceylan et al, 2009). Furthermore, we have also measured lipid peroxidation level after PTZ-induced convulsions. All these variations can be used to monitor epilepsy-induced pathology.

One of our purposes is to study therapeutic effect of an antiepileptic agent VGB, which is widely used drug, on epilepsy treatment. To achieve this, we first aimed to evaluate the degree of incorporation into lipid bilayer, which determines biological profile of VGB (Saija et al., 1995; Malkia et al., 2001; Castelli et al., 2006). For this reason, we have investigated the interaction of VGB with model membrane system using different calorimetric and spectroscopic techniques as mentioned above. Later, we have investigated the molecular effects of VGB treatment on epileptic cell membranes. We have studied the effects of VGB on quantity of biomolecules, membrane fluidity, and lipid order of epileptic cell membrane. We have also determined the effects of VGB on altered protein secondary structure after PTZ-induced convulsions. Moreover, we have also measured lipid peroxidation after VGB treatment.

CHAPTER 2

MATERIALS AND METHODS

2.1. Model membrane studies

2.1.1 Reagents

PTZ (1,8,9,10-tetrazabicyclo [5.3.0] deca-7,9-diene) and VGB (4-amino-5-hexenoic acid) was purchased from Sigma (St. Louis, MO, USA). Avanti Polar Lipids (Alabaster, AL) was the source of DPPC. Spin labels 5-and 16-doxyl stearic acid and the fluorescent probe 1,6-diphenyl-1,3,5-hexatriene (DPH) were obtained from Aldrich (St. Louis, MO) and Molecular Probes (Eugene, OR), respectively. All chemicals were obtained from commercial sources at the highest grade of purity available.

2.1.2 Methods

2.1.2.1 FTIR studies

Phospholipid MLVs were prepared according to the procedure reported in Severcan et al., (2005). 5 mg DPPC was dissolved in chloroform and the solution was subjected to a stream of nitrogen to remove excess chloroform followed by the vacuum drying for 2 hours. The thin films of lipid were then hydrated by adding 25 µL of phosphate buffer, pH 7.4. MLVs were formed by vortexing the mixture for 30 min at least 15°C above transition temperature of DPPC. In order to prepare PTZ containing MLV, the required amount of PTZ from stock solution was initially placed inside the sample tube. The excess of methanol was removed

by a stream of nitrogen, DPPC in chloroform was added and the preparation of MLV was performed as described above. For FTIR measurement, 20 µL of liposomes were placed between CaF_2 windows with 12 µm sample thickness. The spectra were recorded using a Perkin Elmer Spectrum 100 FTIR spectrometer (Perkin Elmer Inc., Norwalk, CT, USA) equipped with a DTGS detector in the temperature range of 25-60°C. The temperature was controlled digitally by Graseby Specac controller unit. The samples were incubated for 5 min at each temperature before acquisition of a spectrum. The interferograms were averaged for 100 scans at 2 cm^{-1} resolution.

Since the OH stretching bands due to buffer appear in the regions of 3400-3200 cm^{-1} and 1800-1500 cm^{-1}, these bands overlap with the other bands of interest. To improve resolution of the infrared bands, spectrum of the buffer was taken at different temperatures and it was subtracted from the spectra of liposomes at corresponding temperatures. Subtraction process was done by using Perkin Elmer software program. Figure 16 represent the infrared spectra of DPPC before and after water subtraction. The band positions were measured from the center of weight. Furthermore, molecules in the air affect the spectra of samples. To overcome this, spectrum of the air was recorded as a background spectrum and subtracted automatically from the spectra of samples by using appropriate software. Figure 17 shows the infrared spectrum of air.
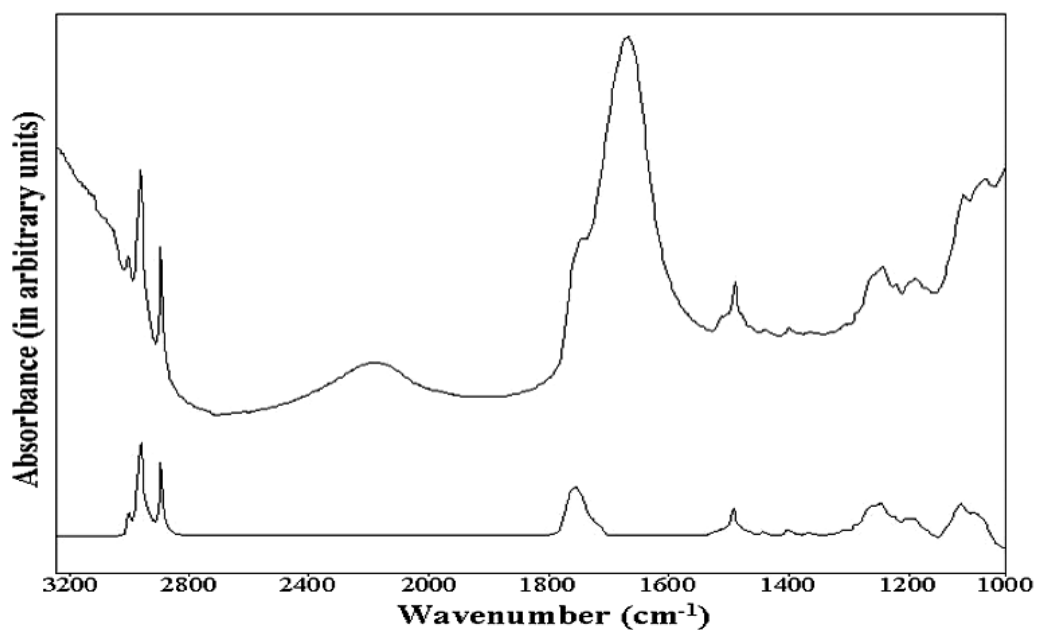
Figure 17. FTIR spectrum of DPPC liposomes. Upper spectrum shows the liposomes before water bands were subtracted and the spectrum below shows the liposomes after subtraction.
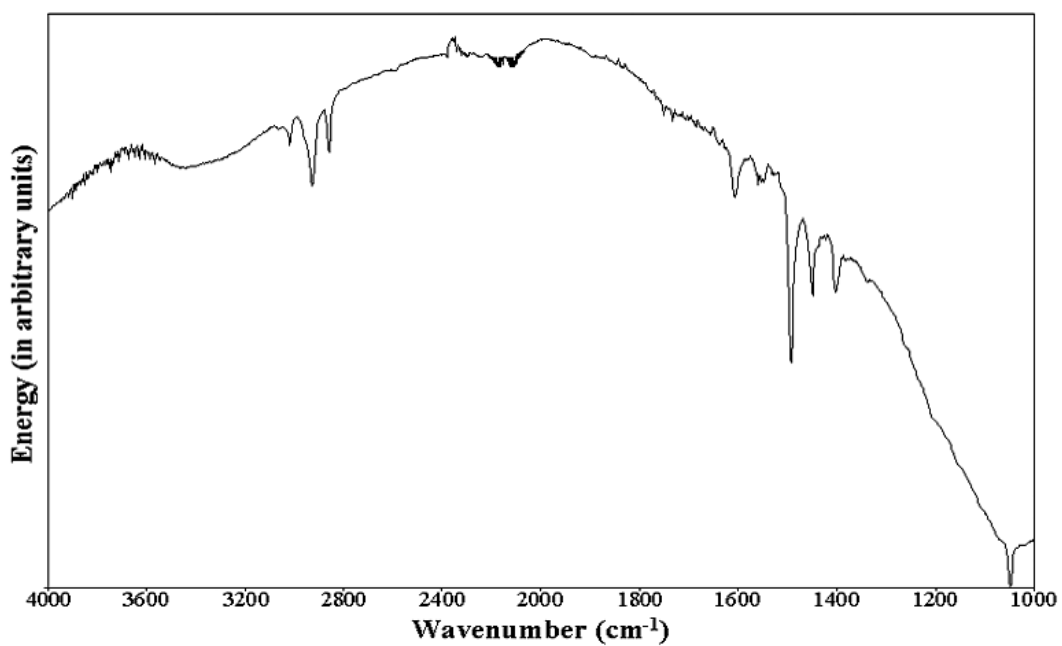
Figure 18. Infrared spectrum of air.

46

2.1.2.2 DSC studies

MLVs were prepared in the absence and the presence of 1, 12, and 24 mol % PTZ and VGB. For the preparation of MLVs, PTZ dissolved in organic solvent mixed with DPPC dissolved in chloroform. The organic solvents were then removed under a stream of nitrogen followed by vacuum pumping overnight. The MLVs were formed by hydrating the lipids (10 mg of lipid/ml) in 10 mM sodiumphosphate, pH 7.4 and vortex mixing at least 15°C above the gel to liquid crystalline phase transition temperature of the phospholipids. The MLVs were frozen in liquid nitrogen and thawed three times in a water bath and then degassed for 30 min under vacuum. A 500 µL aliquot of the MLV suspensions was added to each of the three chamber in a Calorimetry Sciences MCDSC multi-cell differential scanning calorimeter (Calorimetry Sciences, Lindin, UT). The scans were made at 0.08 ^{o}C/min. Only heating curves are presented. Cooling curves were essentially identical.

The cooperativity and enthalpy values were calculated by the equations written below:

$$\text{Cooperativity unit} = \Delta H^{o}_{vH} / \Delta H^{o} \text{ cal}$$

ΔH^{o} cal : area under main transition
ΔH^{o}_{vH} : van`t Hoff enthalpy

$$\Delta H^{o}_{vH} = 6.9 \, Tm^{2} / [(T_2 - T_1) / 2]$$

Tm: center point of phase transition (^{o}K)
T_1 ; start temperature for phase transition (^{o}K)
T_2 : end temperature for phase transition (^{o}K)

2.1.2.3 ESR studies

MLV containing (1 mol %) 5- or 16-doxyl streaic acid in DPPC with 0, 1, 12 and 24 mol % PTZ and VGB were prepared by the same procedure outlined above except that 20 mM sodium phoshate (pH 7.5) was used to hydrate the lipids. Spectra were recorded on a Bruker ESP 300 X-band ESR spectrometer operating at 9.2 GHz.

The following spectral parameters were used: microwave power, 200 mw; field strength, 3924 G; sweep width, 80-100G; sweep time, 160-200 s; time constant, 500 ms; modulation amplitude, 1.0-2.0 G; and dataset, 1000-2000 points. The temperature samples (25 µL) placed in a capillary glass tube was regulated 50^0C, corresponding to the liquid crystalline phase, by a Love Controls 1600 Series temperature controller (Michigan City, IN).

The order parameters, S, were calculated from spectra in the upper part of the acyl chain (5-doxyl) according to the equation

$$S = \frac{A_P - A_\perp - C}{A_P + 2A_\perp + 2C} 1.66$$

where A_P and $A_\perp$ are the apparent parallel and perpendicular hyperfine splittings, the constant $C = 1.4 - 0.053(A_P - A_\perp)$ is an empirical correction for the difference between the true and apparent values of $A_\perp$, and the factor 1.66 is a solvent polarity correction factor. The correlation time τ_c was calculated from spectra which monitor the lower part of the acyl chain using 16-doxyl stearic acid spin label by

$$\tau c = 6.5 \times 10^{-10} W_0 \left[\left(\frac{h_0}{h_{-1}} \right)^{1/2} - 1 \right]$$

where $K = 6.5 \times 10^{-10}$ sG^{-1} is a constant depending on microwave frequency and the magnetic anisotropy of the spin label, W_0 is the peak-to-peak width of the central line, and $\frac{h_0}{h_{-1}}$ is the ratio of the heights of the central and high field lines, respectively.

2.1.2.4 Steady state fluorescence spectroscopy studies

For steady-state fluorescence spectroscopy, DPH was chosen as a probe. 2.5 mM MLV of DPPC with DPH at the ratio of 1:200 and containing different concentration of convulsants were formed employing the procedure mentioned above. The spectra were recorded on a Perkin Elmer MPF-66 fluorecence spectrometer. The excitation and emission wavelenght for DPH was 351 nm. and 430 nm, respectively. The temperature range was varied in the range 10 $^{\circ}$C to 60 $^{\circ}$C and the samples were incubated for 5 min. at each temperature before scanning.

The polarization parameter was calculated by

$$P = \frac{I_P - GI_\perp}{I_P + GI_\perp}$$

where I_P and $I_\perp$ represent vertical and horizontal components of the intensity of emitted light,, respectively, when the excitation light is vertically polarized. The correction factor $G = \dfrac{I_P}{I_\perp}$ (horizontally polarized excitation beam) compensates for the differential in the monochromator's transmission efficiency for vertically and horizontally polarized light.

2.1.2.5 Statistical Analysis

In the figures and tables the mean of at least three experiments was plotted and calculated together with the standard error of mean. Statistical significance was assesed using Mann-Whitney nonparametric test. Significant differences was statistically considered at the level of p≤0.05.

2.2. Animal studies

2.2.1 Reagents

Pentylenetetrazol (PTZ), sucrose, trizma base, ethylene diamine tetra acetic acid (EDTA), phenylmethylsulfonylfluoride (PMSF), buthylatedhyroxytoluene, magnesium chloride, pepstatin, aprotonin, and thiobarbituric acid were purchased from Sigma (Sigma Chemical Co., St. Louis, MO,USA). Trichloroacetic acid and hydrochloric acid from Merck. All chemicals were used without further purification.

2.2.2 Animal Studies for PTZ-induced seizures

All procedures were conducted in accordance with wellfare guidelines and approved by Ethics committee (KOU-44543). Experiments were carried out on adult male Wistar rats weighing 200–250 g. All animals were allowed free access to standard rat food and tap water before the experiments. All rats were housed under standard conditions in a room under a constant 12-h light/dark cycle with humidity of 40-50 %. The animals were divided into three different groups as control (n=16), subconvulsant (n=16) and convulsant (n=16) group. Each group was used for homogenate and cell membrane preparation. While the control group was administrated by physiological saline, the treated groups were administrated by subconvulsant (25 mg/kg) and convulsant (60 mg/kg) dose of PTZ for two weeks. Subconvulsant dose reflects absence-myoclonic seizures while convulsant dose reflects tonic-clonic generalized seizures in humans (Eloqayli et al., 2003; Erakovic et al., 2001; Fisher, 1989). After each injection during two weeks, the rats were placed in plexi glass cages to record latency, duration and incidence of the seizures. The seizure severity were evaluated by using Racine (1999). In subconvulsant group (25 mg/kg) convulsions were not observed. Convulsant dose of PTZ (60 mg/kg) i.p produced tonic-clonic seizures without mortality.

The intensity of seizures was also scored according to Racine (1999) as follows:

Stage 1: myoclonic twitches

　　　　2: generalized tonic–clonic seizures

　　　　3: generalized tonic–clonic seizures

　　　　4:generalized tonic–clonic seizures

　　　　5:generalized tonic–clonic seizures

　　　　6: generalized tonic–clonic seizures

After the observation, the animals they were killed by decapitation and the brains were quickly dissected out. The dissected brain samples were used for homogenate tissue and cell membrane preparation.

2.2.3 Animal studies for vigabatrin application

All procedures were conducted in accordance with welfare guidelines and approved by Ethics committee (KOU-44543). Experiments were carried out on adult male Wistar rats (n = 21) weighing 200–250 g. All animals were allowed free access to standard rat food and tap water before the experiments. All rats were housed under standard conditions in a room under a constant 12-h light/dark cycle with humidity of 40-50 %. The animals were divided into three different groups as control (n=7), PTZ (epileptic) (n=7) and Epileptic_VGB (n=7) group. While the control group was administrated by physiological saline, epileptic group the twere administrated by PTZ (epileptic) (60 mg/kg). Epileptic_VGB group first received 100 mg/kg dose of VGB and then 60 mg/kg PTZ for two weeks. All these concentrations of the agent were administered to the animals were decided according to the literature (Saline et al., 1999). After two weeks, the animals they were killed by decapitation and the brains were quickly dissected out.

2.2.4 Sample preparation brain homogenate for FTIR study

The brains were chopped in buffer containing 0.25M sucrose, 10mM Tris–HCL, pH 7.4, 1mM EDTA and 1mmol PMSF. They were homogenized using a Potter Elvehjem type glass-Teflon homogenizer and then centrifuged at 100 000 g for 1h at 4^oC. The pellets containing plasma membrane, mitochondria, lysosome, endosplasmic reticulum and golgi apparatus were used for FTIR spectroscopic studies.

2.2.5 Sample preparation of plasma membrane for FTIR study

Stock solutions of the following were prepared in advance:

(A) 0.25 M sucrose, 10 mM Tris-HCl, 1 mM $MgCl_2$, pH 7.4, density 1.03 g/mL (1.3450)

(B) 0.25 M sucrose, density 1.03 g/mL (1.3450)

(C) 2.0 M sucrose, 10 mM Tris-HCl, 1 mM $MgCl_2$ pH 7.4, density 1.26 g/mL (1.4297)

The brains were chopped in reagent A and pepstatin, aprotonin and PMSF have been added. The sample was homogenized gently with 8-10 strokes of a tissue homogenizer using a loose-fitting teflon pestle in an ice bath. 4000 lbs pressure was applied to the homogenates three times and 10000 lbs pressure was applied once by using French pressure cell. To remove connective tissue, homogenate was filtered through three or four layers of cheesecloth premoistened with Reagent A. Then, the homogenate was diluted with an equal volume of Reagent A, and mixed gently. The homogenate was centrifuged for 10 min at $300 \times g$ and 0-2°C. The supernatant poured off and saved in a cold beaker. The pellet was resuspended in half the initial volume with Reagent A. And, the pellet was centrifuged again. The supernatans from two extractions were pooled and centrifuged 15 min at $1500 \times g$, 0-2°C. The final supernatant was poured off. The final pellet was resuspended in 50 mL of Reagent A and homogenized gently using two or three 10-second strokes of the loose-fitting pestle. The volume of the suspension was increased about two-fold using Reagent C.

The sample was transferred to 32-mL centrifuge tubes with 26-27 mL of the above suspension, and carefully overlaid the tubes with 4 mL of Reagent B. Later, the sample was centrifuged at 104,000 × g for max 75min at 2°C. Acceleration was set to 5 and deceleration was set 0-3. Plasma membrane sheets will form a layer at the interface. This layer was collected, resuspended an equal volume of Reagent B and homogenized as before with three or four strokes of the loose-fitting pestle. Finally, the plasma membrane fractions were centrifuged Centrifuge as before at 1500 × g for 20 min. The supernatant was drawn off and the pellet was resuspended in 2-5 mL of Reagent B. This plasma membrane sheet fraction was stored at -70°C till FTIR study (Hubbart et al., 1983; Scott et al., 1993).

2.2.6 FTIR spectroscopic study

FTIR spectra were recorded at 4000-400 cm^{-1}. 15 µL homogenate and cell membrane samples were placed between ZnSe windows with Teflon spacer to give 12 µm sample thickness. IR spectra were obtained using Perkin Elmer Spectrum One Spectrometer equipped with a deuterated triglycine sulfate (DTGS) detector. The atmospheric water vapor and carbondioxide interference were automatically substracted from the sample spectrum using spectrometer software. Interferograms were averaged for 200 scans at 2 cm^{-1} resolution. Three spectra from each sample were recorded and identical spectra were obtained. These were averaged for each sample using Perkin Elmer Spectrum One software program. The averages were then used for data evaluation and statistical analysis.

Water absorption bands at 3050–2800cm^{-1} and 1700–1500cm^{-1} strongly overlap with the bands of interest arising from functional groups belonging to proteins and lipids. To provide a better resolution of the infrared bands, the water absorption bands were subtracted in each spectrum using Perkin Elmer Spectrum One software program (Figure 18). For the determination of the variations in the peak area, peak positions and bandwidths, each original spectrum was analyzed by using the same software. The band positions were measured from the center of weight.

The same software was also used for other spectral analyses including baseline correction, normalization and deconvolution. The spectra were normalized with respect to specific bands just for visual demonstration of the spectral differences in the spectra.
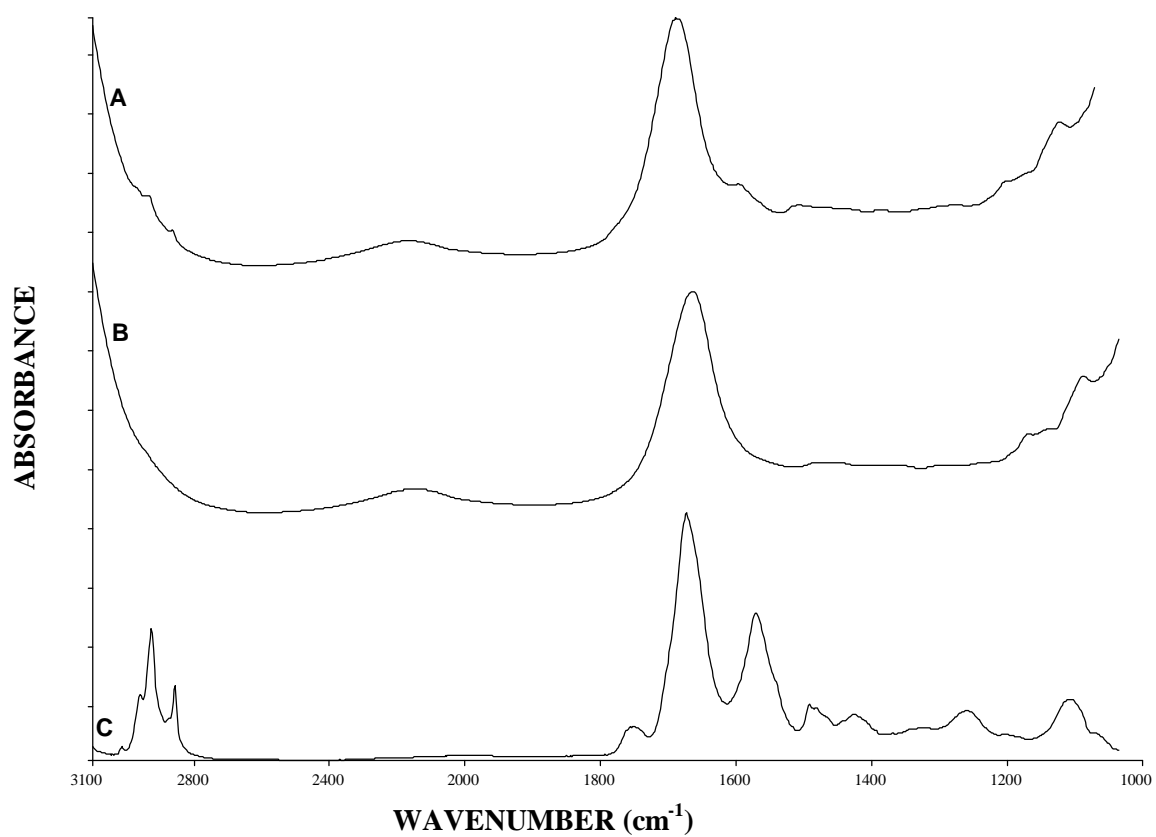
Figure 19. Rat brain homogenate and cell membrane spectra of before and after subtraction process.

2.2.7 Protein secondary structure determination

Amide I band between 1700 and 1600 cm^{-1} resulted from proteins was evaluated for the analysis of secondary structure of proteins. The neural networks were first trained using a data set, which contains FTIR spectra of 18 water soluble proteins recorded in water applying the method described in reference (Severcan, Severcan and Haris, 2004). The secondary structures of these proteins were known from X-ray crystallographic analysis. Amide I band was preprocessed before applying to the neural networks. Preprocessing involves normalization and discrete cosine transformation (DCT) of this band. To improve the training of the neural networks, the size of the training data set was increased by interpolating the available FTIR spectra. NNs were trained using Bayesian regularization. For each structure parameter, a separate NN was trained whose number of inputs, i.e. the number of DCT coefficients, and number of hidden neurons were optimized. The trained NNs have standard error of prediction values of 4.19 % for alpha-helix, 3.49 % for beta-sheet and 3.15 % for turns. The secondary structure parameters of the proteins were predicted by applying to the inputs of the trained NNs the preprocessed FTIR data. The details of the training and testing algorithm can be found in (Severcan, Severcan and Haris, 2004).

Amide I band was also analyzed by using the OPUS 5.5 (Bruker Optic, GmbH). The spectral comparisons of Amide I band (1700-1600 cm^{-1}) were carried out on vector normalized second derivatives. Since absorption maxima appear as minima in the second derivatives, minimum positions were used for the comparisons in the second derivative spectra (Ozek et al., 2009). Peak height is very sensitive to changes of FWHH (fullwidth at half height) of the FTIR bands in the second derivative spectra, therefore; concentration sensitive changes in the components of Amide I band were monitored by using these spectra. In this way, the identification of peak frequencies as well as detailed qualitative and quantitative evaluation of protein secondary structure components was attained.

2.2.8 FTIR microspectroscopic study

10 µL homogenate samples were placed on CaF2 windows. Then, the samples were kept in dry environment at room temperature for 10-20 min. An IR microscope Perkin Elmer Spotlight 400 coupled to Perkin Elmer FTIR spectrometer was used to map homogenate samples. The microscope was equipped with a computer controller x/y stage which permitted spectral mapping of the sample in a defined step within a rectangular area. A grid pixel coordinates within homogenate sample was defined and IR spectra were collected from each points in the grid. Spectra were taken in both x and y directions in the steps of 500 µm (using an aperture diameter of 6.25 µm). FTIR spectra were recorded at 4000-900 cm^{-1} with 100 numbers of scans.

The data evaluation was carried out using Perkin Elmer FTIR microscope Auto Image software. By selecting specific bands arisen from lipids and proteins chemical maps was constructed for each group.

2.2.9 Measurement of lipid peroxidation (TBAR assay)

As an index of lipid peroxidation, we performed TBARS test, which is well adopted for this measurement as described previously (Pothiwong et al., 2007). Briefly, the samples were homogenized by Teflon glass homogenizer in cold 0.02 M phosphate buffer (pH 7.4) at the concentration of 25 % (w/v). The homogenates were diluted to 5 % with the phosphate buffer containing 0.25 ml buthylatedhydroxytoluene (BHT), which prevents artificial increase of MDA. Then, the homogenates were incubated for 60 min at 37 $^{\circ}$C. After the incubation, 2 ml of trichloroacetic acid (TCA) solution (28 % w/v in 0.25 N HCl) was added. The samples were centrifuged at low speed and 4 ml of supernatants were mixed with 1 ml of thiobarbituric acid (TBA) (1 % w/v in 0.25 N HCl). Subsequently, the samples were kept in boiling water for 30 min to get chromophore development.

The samples were cooled to room temperature and the absorbance values were measured at 535 nm. MDA values were determined with the extinction coefficient (1.56×10^{-5} cm^{-1}/M) (Buege and Aust, 1978). TBA activity was expressed per milligram of protein. The protein content was measured by the method of Lowry et al (1951).

2.2.10 Cluster Analysis

For the comparison of control and PTZ treated groups, hierarchial cluster analysis were performed on spectra using thirteen smoothing point Savitzky-Golay algorithm. It was applied to find out spectral relationships among control and PTZ convulsions groups using frequency range between 1800-900 cm^{-1}. The spectra were first vector normalized over the investigated frequency range and then Ward's algorithm was used to construct dendograms by OPUS 5.5 (Bruker Optic, GmbH). Spectral distance was calculated between pairs of spectra as Pearson's product moment correlation coefficient. Cluster analysis offers the opportunity to evaluate experimental results and differentiate between control and treated samples without training spectral data. This analysis tests the interpoint distances between all samples and shows the information in the form of dendrogram based on their closeness.

2.2.11 Atomic Force Microscopic Study of Isolated Cell Membrane

AFM images of isolated cell membrane samples for control (n=5) and epileptic (n=5) were captured by NanoScopeIIIa Multimode, Digital Instruments AFM Microscopy. 20 microliters membrane samples in buffer solutions were attached to freshly cleaved mica and allowed to dry for several minutes. Images were acquired in tapping mode with silicon nitride V-shaped cantilevers of 160 micrometer length and nominal frequency of 300 kHz. The spring constant of the cantilever was 0.35 N/m. Two frames of 512 by 512 pixels were recorded simultaneously at scan frequencies below 2 Hz.

CHAPTER 3

RESULTS

3.1 Model Membrane Studies

This part of the study is precisely addressed to investigate the interaction of an epileptic agent PTZ and an antiepiletic agent VGB with DPPC MLVs by DSC, FTIR, ESR and steady state fluorescence spectroscopy.

3.1.1 The investigation of the Interaction of PTZ with DPPC MLVs

As mentioned in detail in the section 1.1.8.2, it is not clear that whether PTZ exerts its function through a direct interaction with membrane proteins or membrane lipids. Therefore, in the present study we aimed to clarify whether PTZ interact with lipid membranes or not.

The infrared spectra of DPPC MLVs, containing different concentrations of PTZ were obtained as a function of temperature in order to elaborate the effects of PTZ on both gel phase and liquid crystalline phases. In the absence of PTZ, multilamellar liposome of DPPC MLVs represents a pretransition from the gel phase to ripple phase at 35 ^{o}C and a main transition from the ripple phase to liquid crystalline phase at 41 ^{o}C. In the FTIR experiments, before the data analysis, the water bands were subtracted from the sample spectrum since water absorption bands at 3050-2800 cm^{-1} and 1700-1500 cm^{-1} strongly overlap with the bands arising from different functional groups belonging to lipids.

Figure 20 shows representative FTIR spectra of DPPC MLVs in the absence and presence of PTZ at low and high concentrations in the liquid crystalline phase (50 ^{0}C), in the region of 3050-2800 cm^{-1}. The spectra were normalized with respect to the CH_2 asymmetric stretching mode to demonstrate visually the comparative difference in the frequency and bandwidth values of the specific bands of lipid. However, the original spectra were used for the precise determination of variations in the frequency and bandwith values.
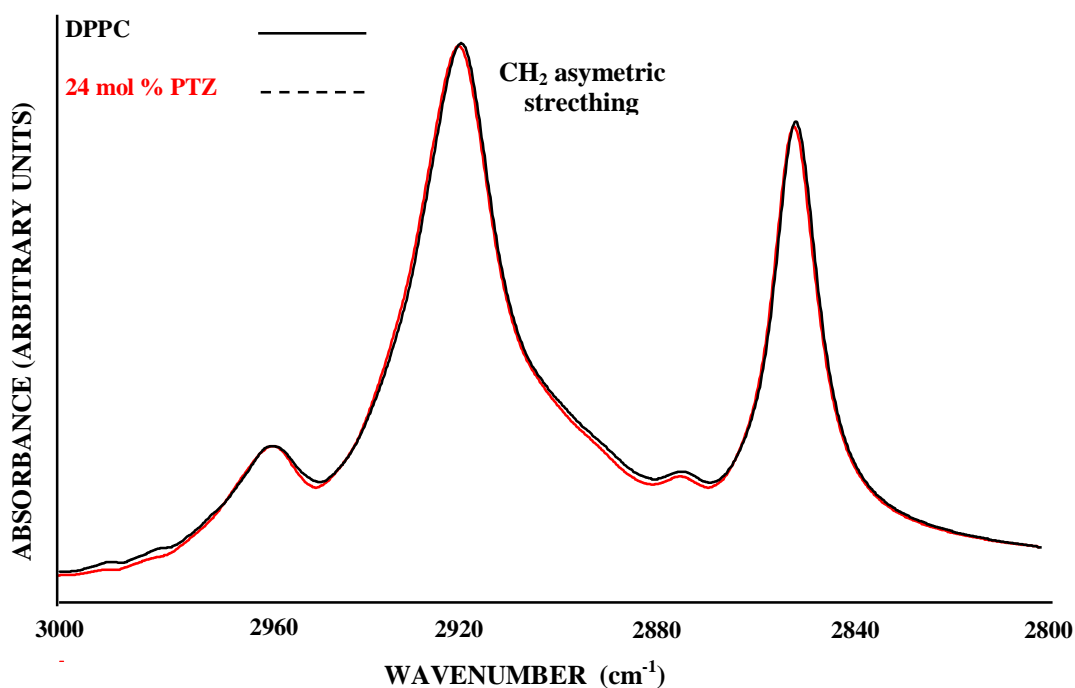
Figure 20. Infrared spectra of DPPC liposomes in the absence and the presence of PTZ at 50^{0}C in the region of 3050-2800 cm^{-1}. (The spectra were normalized with respect to the CH_2 asymmetric stretching mode at 2925 cm^{-1}).

The changes in acyl chain flexibility e.g. order-disorder state of DPPC MLVs due to the presence of different concentrations of PTZ were examined by analyzing of the CH_2 asymmetric stretching mode frequency.

As seen from the figure, the frequency values of this band did not vary significantly with the addition of PTZ in both the gel and liquid crystalline phases (Figure 21). This means that PTZ at even high concentration did not show significant change in the order of DPPC MLVs.
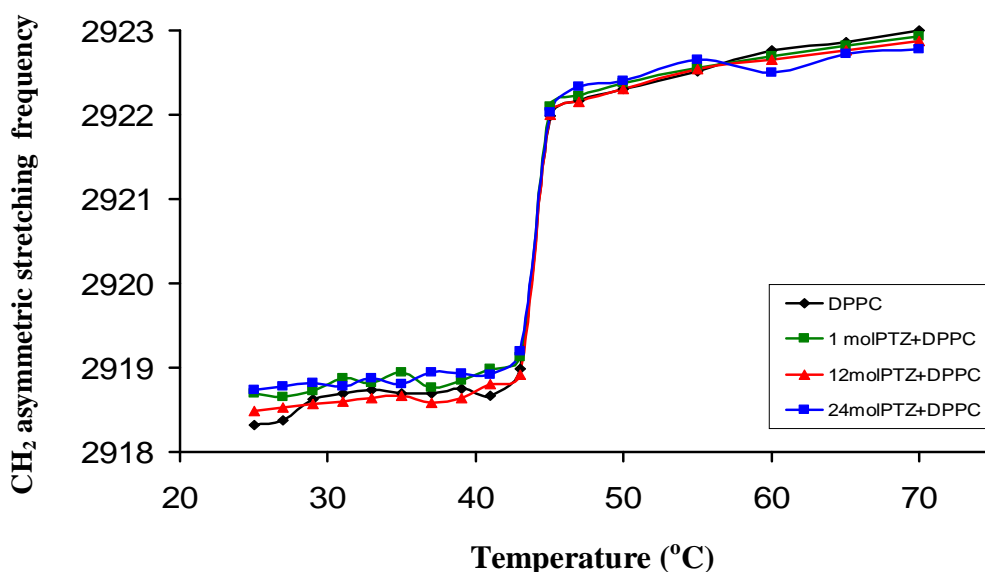
Figure 21. Temperature dependence of frequency changes of the CH_2 asymetric mode of DPPC MLVs in the absence and presence of PTZ.

The result obtained from FTIR experiments was further supported in the liquid crystalline phase by ESR spectroscopy using the spin label 5-doxyl stearic acid that gives information about membrane order in the upper part of the lipid chain. Figure 22 shows the ESR spectra of DPPC MLVs labeled with 1 mol% 5-doxyl stearic acid in the absence and presence of PTZ at 50 ^{0}C which monitors to the liquid crystalline phase of DPPC MLVs. The order parameters were calculated from the ESR spectra and were listed in Table 2. As seen from the table, order parameters did not alter with the presence of PTZ.
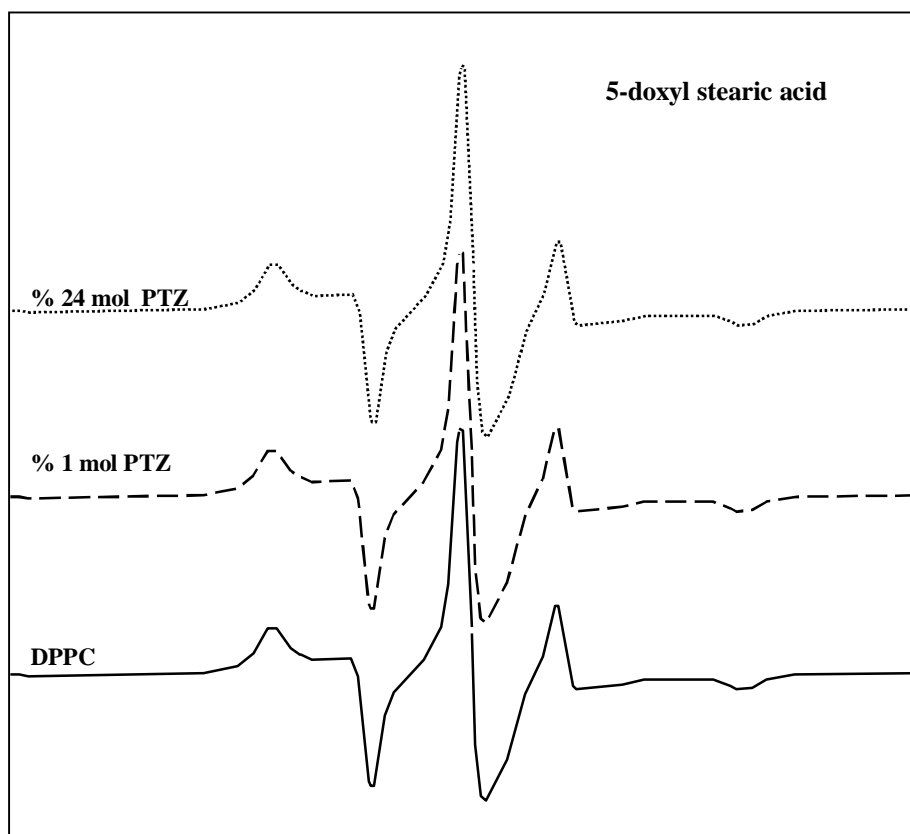
Figure 22. ESR spectra at 50 °C of spin labeled with 5-doxyl stearic acid in DPPC MLV containing different concentrations of PTZ.

Table 2. Order parameter for 5- doxyl stearic acid intercalated into DPPC MLVs containing different concentrations of PTZ at two different temperatures corresponding to the gel and liquid crystalline phase of DPPC MLVs. The values are the mean ± standart deviation for each sample. The degree of significance was denoted as ($p<0.05^*$), ($p<0.01^{**}$) and ($p<0.001^{***}$).

Sample	Membrane Order Parameter (S)	
	25 ^{O}C	50 ^{O}C
DPPC	0.525±0.021	0.523±0.033
1 mol % PTZ + DPPC	0.523±0.002	0.525±0.019
12 mol % PTZ +DPPC	0.526±0.008	0.526±0.021
24 mol % PTZ + DPPC	0.527±0.013	0.522±0.061

We have also investigated the effect of PTZ on dynamics (fluidity) of DPPC MLVs by FTIR, ESR and steady state fluorescence spectroscopy.

In the FTIR experiments, the bandwidth values of the CH_2 asymmetric stretching band were studied. The bandwidth values were measured at 80% of height of the peak. Table 3 represents the changes in the bandwidth values with the presence of PTZ at two different temperatures which correspond to gel and liquid crystalline phases of DPPC MLVs. As observed from the table, PTZ did not exert significant effect on the bandwidth values of CH_2 asymmetric stretching mode of DPPC MLVs in both gel and crystalline phases.

Table 3. The bandwidth values of the CH_2 asymmetric stretching mode of DPPC in the absence and presence of PTZ at 25oC and 50oC. The values are the mean ± standart deviation for each sample. The degree of significance was denoted as ($p<0.05^*$), ($p<0.01^{**}$) and ($p<0.001^{***}$).

Sample	CH_2 asymmetric stretching bandwidth	
	$25\,^{O}C$	$50\,^{O}C$
DPPC	22.43 ± 0.04 cm^{-1}	25.25 ± 1.02 cm^{-1}
1 mol % PTZ + DPPC	22.72 ± 0.07 cm^{-1}	25.24 ± 1.04 cm^{-1}
12 mol % PTZ +DPPC	22.22 ± 2.08 cm^{-1}	25.33 ± 0.09 cm^{-1}
24 mol % PTZ + DPPC	23.11 ± 0.03 cm^{-1}	25.38 ± 2.05 cm^{-1}

In ESR spectroscopic studies we used the spin label 16-doxyl stearic acid that provides information on the rate of acyl chain motion in the lower portion of the chain towards the center of the membrane. Figure 23 displays the ESR spectra for DPPC MLVs labeled with 16-doxyl stearic acid at 50 ^{0}C with different concentrations of PTZ. The correlation time calculated from the spectra is listed in Table 6. As can be observed from the table, membrane dynamics did not alter significantly in the presence of PTZ.
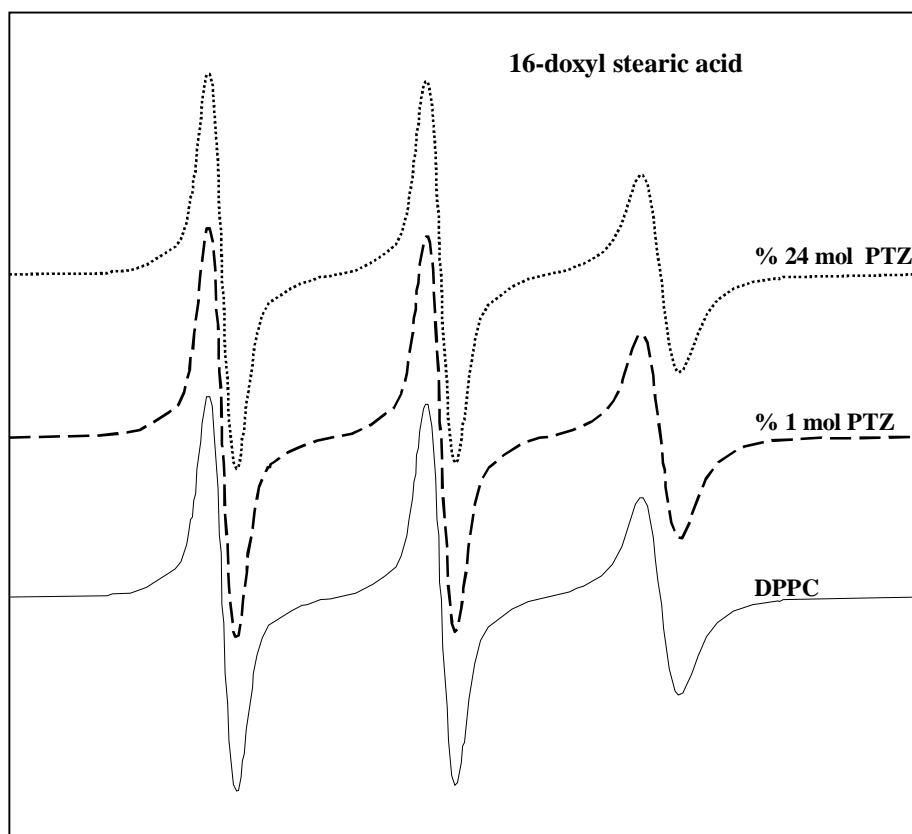
Figure 23. ESR spectra at 50 °C or spin labeled 16- doxyl stearic acid in DPPC MLVs containing different concentrations of PTZ.

Table 4. Correlation times for 16-doxyl stearic acid intercalated into DPPC MLVs containing different concentrations of PTZ at a temperature corresponding to the gel and liquid crystalline phase.

Sample	Correlation Time (τ_c)	
	25 $^\mathrm{O}$C	50 $^\mathrm{O}$C
DPPC	$4.81 \times 10^{-10} \, \mathrm{s}^{-1}$	$4.92 \times 10^{-10} \, \mathrm{s}^{-1}$
1 mol % PTZ + DPPC	$4.80 \times 10^{-10} \, \mathrm{s}^{-1}$	$4.91 \times 10^{-10} \, \mathrm{s}^{-1}$
12 mol % PTZ +DPPC	$4.74 \times 10^{-10} \, \mathrm{s}^{-1}$	$4.93 \times 10^{-10} \, \mathrm{s}^{-1}$
24 mol % PTZ + DPPC	$4.79 \times 10^{-10} \, \mathrm{s}^{-1}$	$4.94 \times 10^{-10} \, \mathrm{s}^{-1}$

Polarization values for DPH incorporated into DPPC MLV were also measured by steady state fluorescence spectroscopy. The polarization parameter for DPPC MLVs in the absence and presence of PTZ is plotted as a function of temperature in Figure 24. As can be observed from the figure, the polarization values of DPPC did not change significantly in the presence of PTZ.
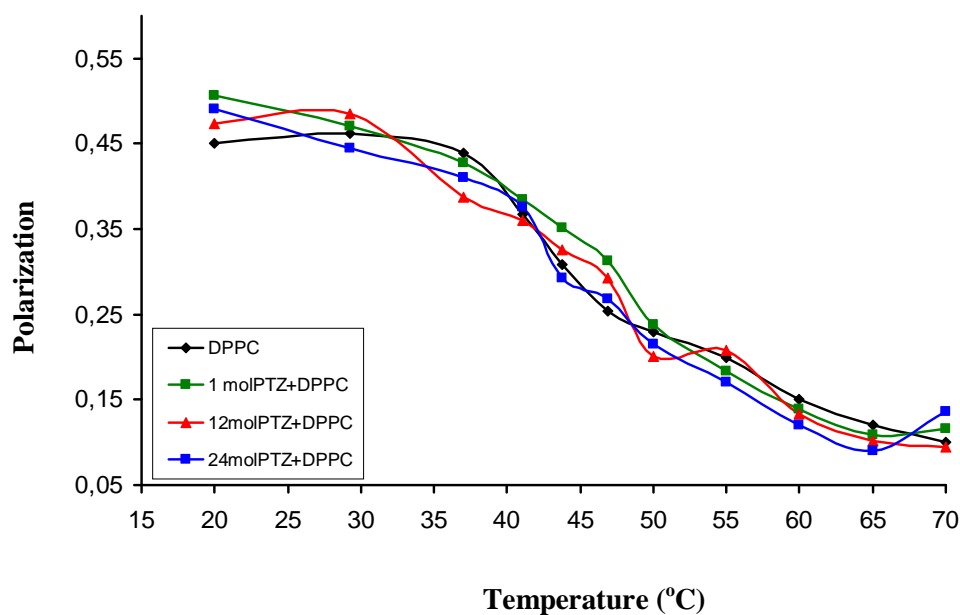
Figure 24. Polarization values for DPH in DPPC MLVs containing different concentrations of PTZ at variable temperature

The temperature dependent frequency change of the C=O ester stretching (1730 cm^{-1}) and the PO_2^- asymmetric double stretching modes (1230 cm^{-1}) of DPPC MLVs containing different mole fractions of PTZ are shown in Figures 25 and 26, respectively. As seen from the figures, both in the gel and liquid crystalline phases, the frequency values of these bands have not altered with the presence of PTZ. FTIR results revealed that the agent does not alter the frequency values of these bands even at high concentration.
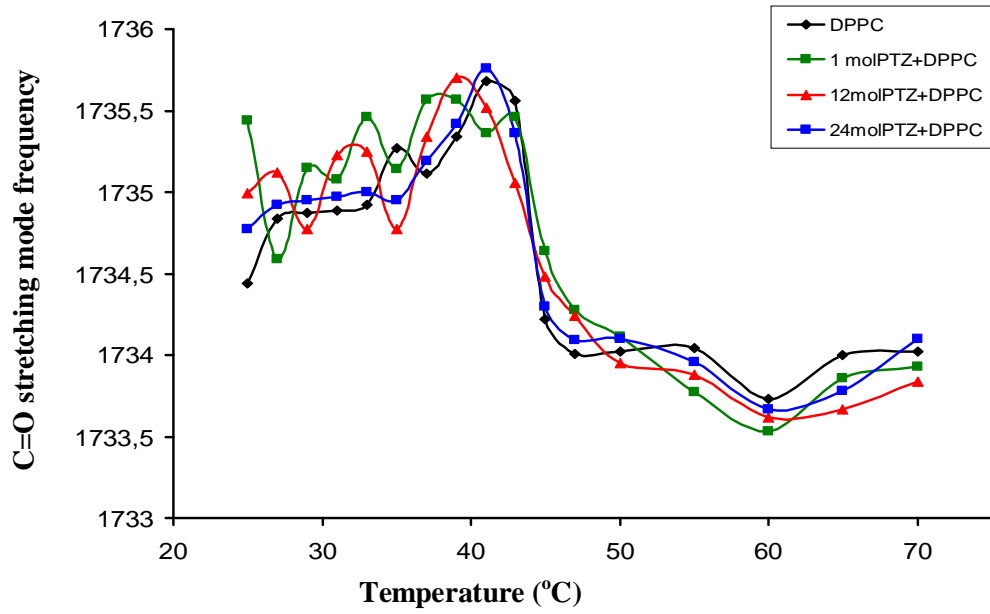
Figure 25. Temperature dependence of the frequency of the C=O stretching mode of DPPC MLVs in the absence and presence of PTZ.
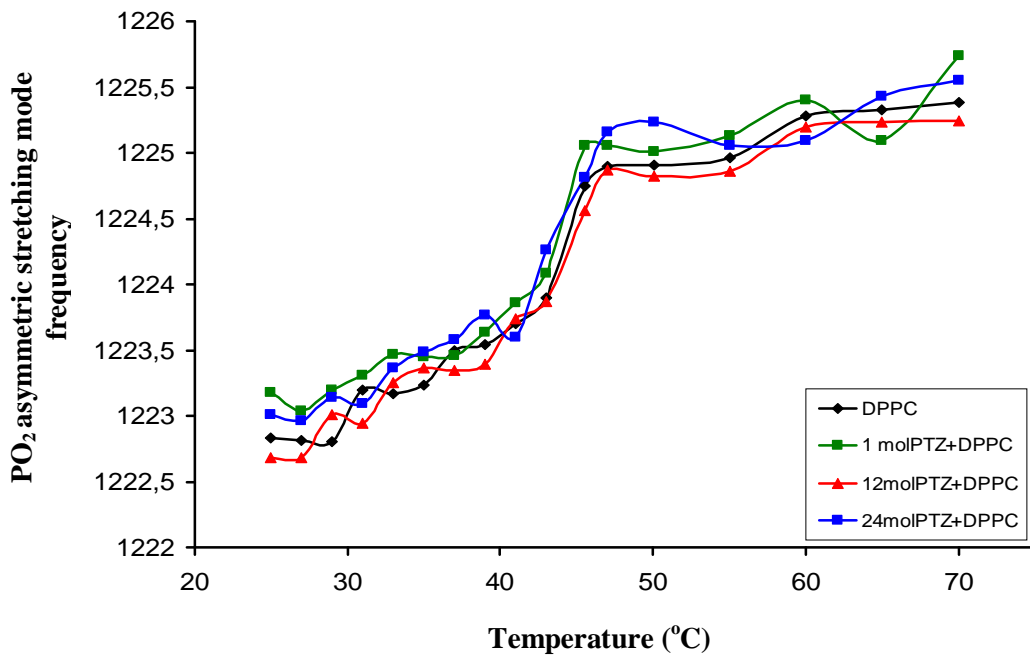
Figure 26. Temperature dependence of the frequency of the PO_2^- asymmetric double bond stretching mode of DPPC MLVs in the absence and presence of PTZ.

DSC was used to investigate the effect of PTZ on phase behavior of DPPC MLVs. Figure 27 shows the thermograms of DPPC MLVs in the absence and presence of different concentrations of PTZ. As can be seen from the figure, with the presence of the PTZ, the shape of transition curves and also the transition temperatures did not change except that a slight decrease in the intensity of the pretransition curve was observed. In order to further elaborate the effects of PTZ on DPPC, the thermograms were analyzed in detail to yield enthalpy and cooperativity.
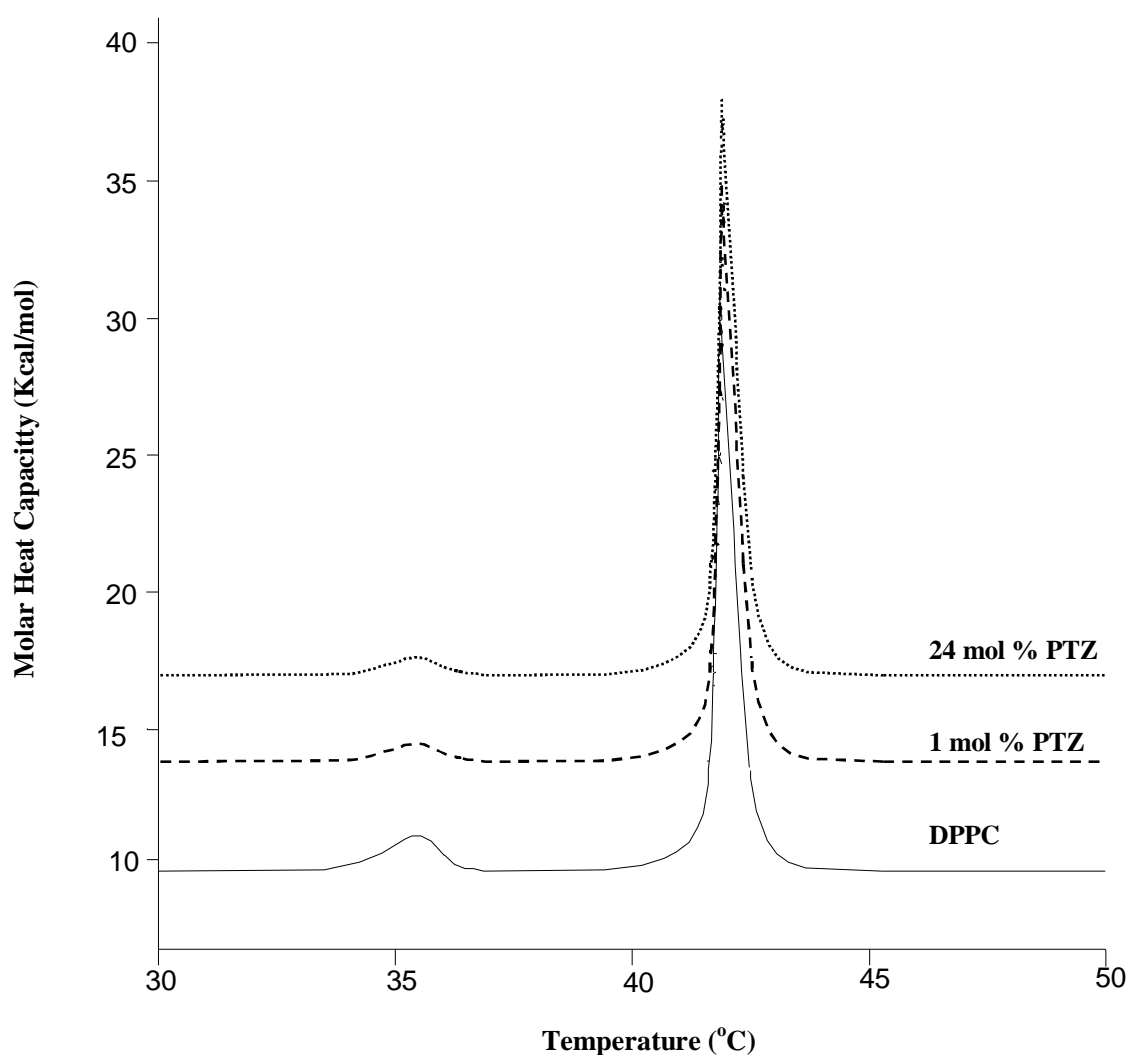
Figure 27. DSC thermograms of DPPC MLVs in the absence and presence of PTZ with different concentrations.

The values of qualitative assessments are plotted against different PTZ concentrations in Figures 28 and 29, respectively. As can be observed from both figures PTZ changed neither the enthalpy nor the cooperativity of the gel to liquid crystalline transition for DPPC MLVs.
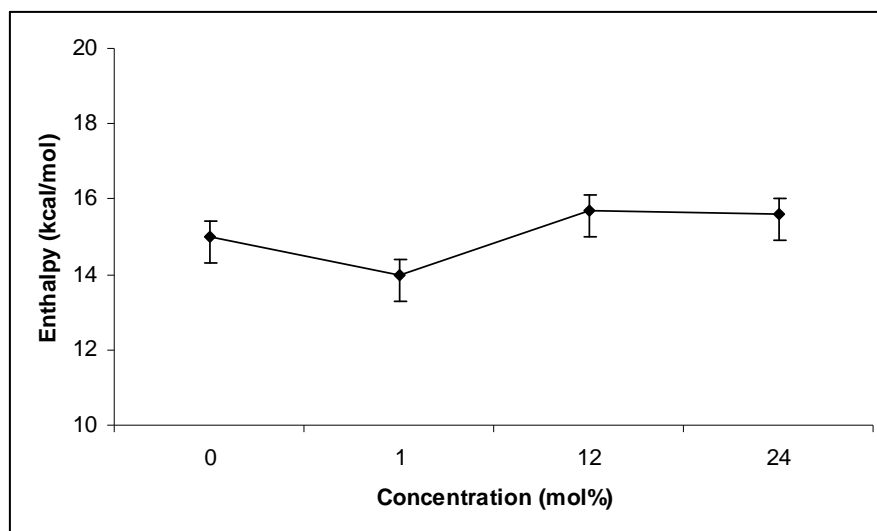
Figure 28. The variation with PTZ concentration of the enthalpy of the gel to liquid crystalline transition for DPPC.
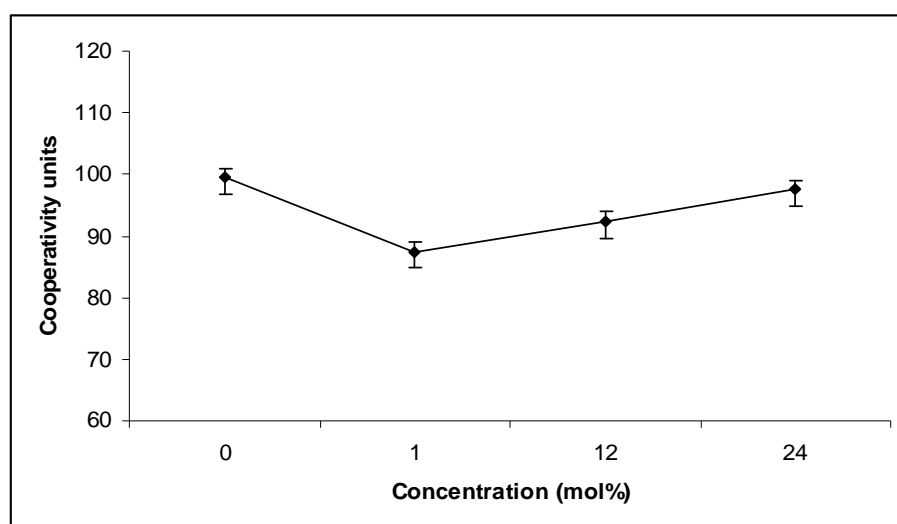
Figure 29. The variation with PTZ concentration of the cooperativity of gel to liquid crystalline transition for DPPC.

The information about the effect of PTZ on the phase transition behavior of DPPC MLVs was also obtained using FTIR spectroscopy by monitoring the frequency variations of the C-H stretching modes in Fig 21. The abrupt increase in the frequency values at 41 ^{o}C corresponds to main phase transition. As can be seen from the figure with the addition of PTZ, at even high concentrations, neither the shape of the phase transition curve nor the main phase transition temperature did not change, which are in agreement with DSC results.

3.1.2 The investigation of the interaction of VGB with DPPC MLVs

As mentioned before, it is not clear that the corporation of VGB with cell membranes that affect its distribution in body are not identified very well. Therefore, in the present study we aimed to clarify whether PTZ interact with lipid membranes or not.

The infrared spectra of DPPC MLVs, containing different concentrations of VGB were obtained as a function of temperature to see the effects of VGB on both the gel phase and liquid crystalline phases of the membrane. In the absence of VGB, multilamellar liposome of DPPC represents a pretransition from the gel phase to ripple phase at 35 ^{o}C and a main transition from the ripple phase to liquid crystalline phase at 41 ^{o}C, as mentioned before.

Figure 26 shows representative FTIR spectra of DPPC MLVs in the absence and presence of VGB in the liquid crystalline phase (50 ^{0}C), in the region of 3050-2800 cm^{-1}. The spectra were normalized with respect to the CH$_2$ asymmetric strecthing mode.
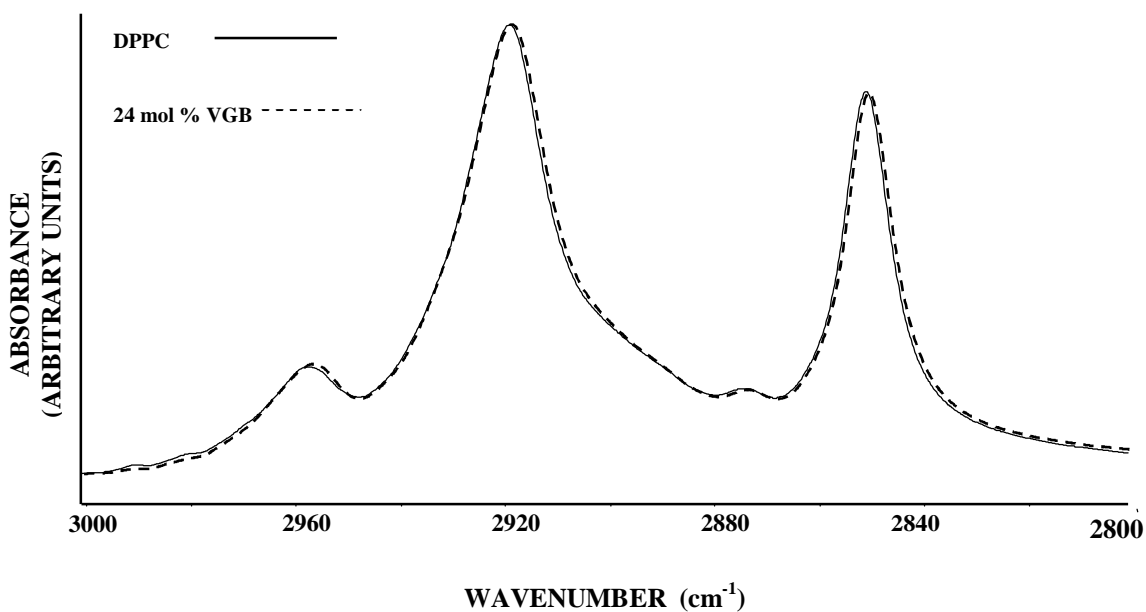
Figure 30. The infrared spectra of DPPC liposomes in the absence and the presence of VGB at 50^0C in the 3050-2800 cm^{-1}. (The spectra were normalized with respect to the CH_2 asymmetric stretching mode at 2925 cm^{-1}).

The changes in order of DPPC MLVs due to the presence of VGB were examined by analyzing of the CH_2 asymmetric strechting mode frequency (Figure 26). As seen from the figure, with the addition of VGB, in the gel phase, an increase in the frequency was observed implying a decrease in the order of the bilayer (Casal et al., 1984; Severcan et al., 1997; Villalain et al., 1986). On the other hand, in the liquid phase no significant change was observed in the frequency values of the CH_2 stretching band with the addition of VGB.
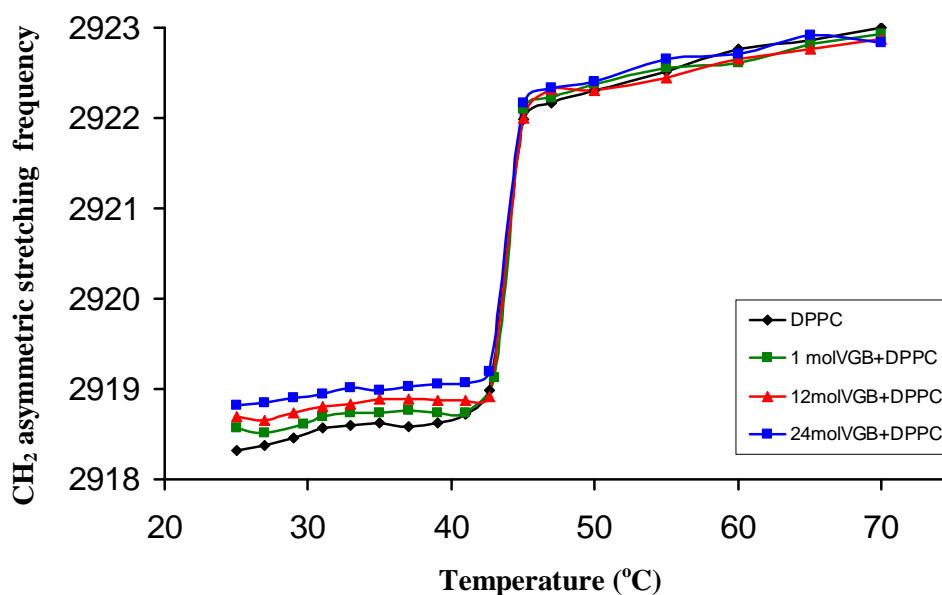
Figure 31. Temperature dependence of frequency changes of the CH_2 asymetric mode of DPPC MLVs in the absence and presence of VGB.

Figure 32 shows the ESR spectra of DPPC MLVs labeled with 1 mol% 5-doxyl stearic acid at 50 ^{0}C which monitors the liquid crystalline phase of DPPC MLVs in the absence and presence of VGB. Order parameters were calculated from the ESR spectra and were listed in Table 5. As seen from the table, VGB alters the order parameters in the gel phase by decreasing it. However, its effect on the parameter is negligible in the liquid crystalline phase as in agreement with FTIR findings.
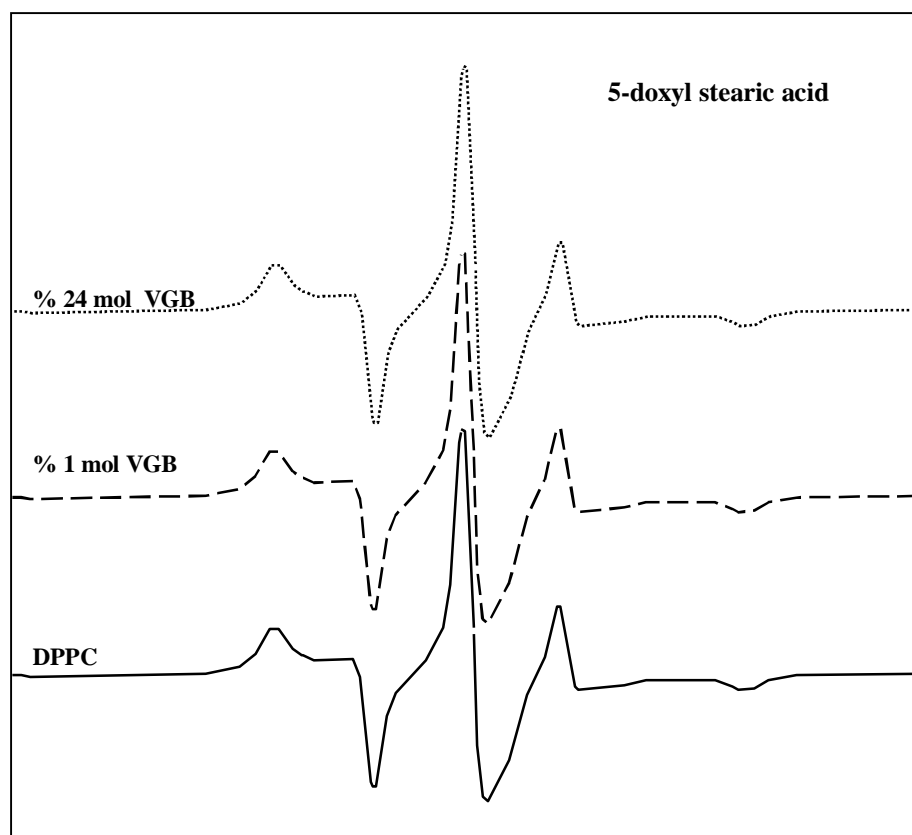
Figure 32. ESR spectra at 50 °C of spin labeled with 5-doxyl stearic acid in DPPC MLV containing different concentrations of VGB.

Table 5. Order parameter for 5- doxyl stearic acid intercalated into DPPC MLVs containing different concentrations of PTZ at a temperature corresponding to the gel and liquid crystalline phase of DPPC MLVs. The values are the mean ± standart deviation for each sample. The degree of significance was denoted as (p<0.05*), (p<0.01**) and (p<0.001***).

Sample	Membrane Order Parameter (S)	
	25 ^{O}C	50 ^{O}C
DPPC	0.533±0.021	0.522±0.001
1 mol % VGB + DPPC	0.530±0.012	0.524±0.009
12 mol % VGB +DPPC	0.528±0.002	0.525±0.020
24 mol % VGB + DPPC	0.529±0.003	0.523±0.060

Table 6 represents the changes in the bandwidth values with the presence of VGB at two different temperatures which correspond to gel and liquid crystalline phases of DPPC MLVs. As observed from the table, the bandwidth values of CH_2 stretching mode increases slightly but significantly both in the gel and liquid crystalline phases with the presence of VGB.

Table 6. The bandwidth values of the CH_2 asymmetric strecthing mode of DPPC in the absence and presence of VGB at 25^oC and 50^oC. The values are the mean ± standart deviation for each sample. The degree of significance was denoted as (p<0.05*), (p<0.01**) and (p<0.001***).

Sample	25^oC	50^oC
DPPC	22.43 ± 0.01 cm^{-1}	25.25 ± 0.03 cm^{-1}
1 % mol VGB + DPPC	22.72 ± 0.02 cm^{-1}	25.44 ± 0.04 cm^{-1}
12 % mol VGB + DPPC	$22.99\pm0.02*$ cm^{-1}	$26.24\pm0.03*$ cm^{-1}
24 % mol VGB + DPPC	$23.39\pm0.03*$ cm^{-1}	$26.96\pm0.02*$ cm^{-1}

Figure 33 displays the ESR spectra for DPPC MLVs labeled with 16-doxyl stearic acid at 50 ^0C with different concentrations of VGB. The correlation time calculated from the spectra is listed in Table 7. As can be observed from the table, membrane dynamics was altered with the addition of VGB, indicating fluidifying effect of VGB on DPPC MLVs.
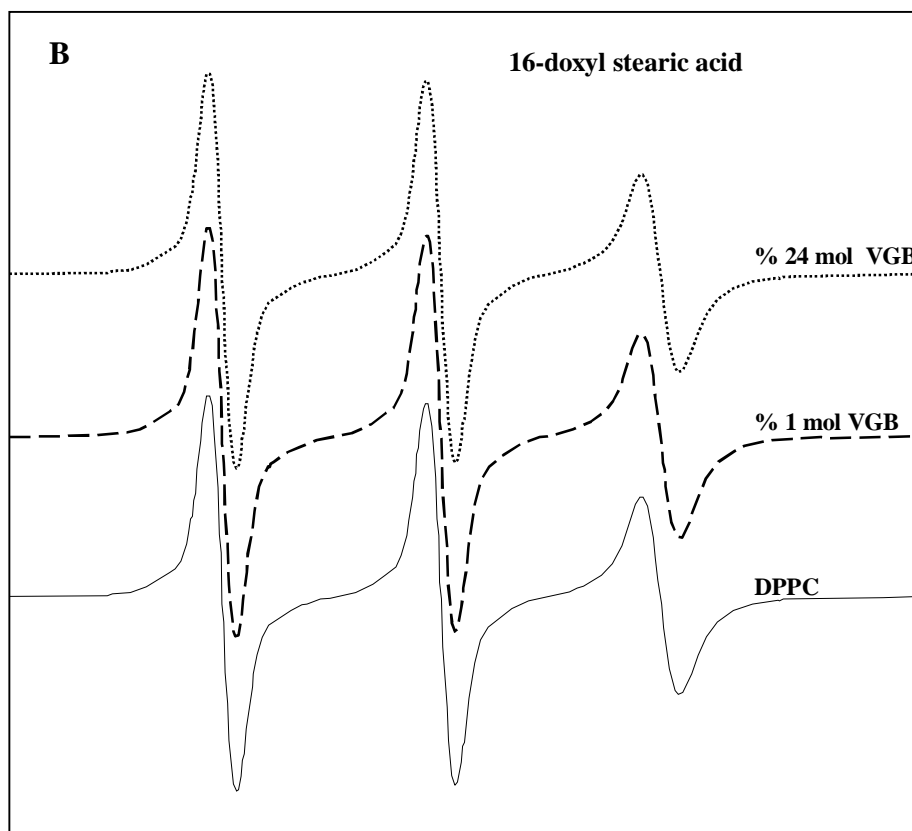
Figure 33. ESR spectra at 50 °C or spin labeled 16- doxyl stearic acid in DPPC MLVs containing different concentrations of VGB.

Table 7. Correlation times for 16-doxyl stearic acid intercalated into DPPC MLVs containing different concentrations of VGB at a temperature corresponding to the gel and liquid crystalline phase. The values are the mean ± standart deviation for each sample. The degree of significance was denoted as (p<0.05*), (p<0.01**) and (p<0.001***).

Sample	Correlation Time (τ_c)	
	25 °C	50 °C
DPPC	$4.90 \times 10^{-10} \, s^{-1}$	$4.91 \times 10^{-10} \, s^{-1}$
1 mol % VGB + DPPC	$4.81 \times 10^{-10} \, s^{-1}$	$4.82 \times 10^{-10} \, s^{-1}$
12 mol % VGB +DPPC	$4.76 \times 10^{-10} \, s^{-1}$	$4.75 \times 10^{-10} \, s^{-1}$
24 mol % VGB + DPPC	$4.79 \times 10^{-10} \, s^{-1}$	$4.80 \times 10^{-10} \, s^{-1}$

The polarization parameter for DPPC MLVs in the absence and presence of VGB is plotted as a function of temperature in Figure 34. As can be observed from the figure, the polarization values of DPPC changed in the presence of VGB.
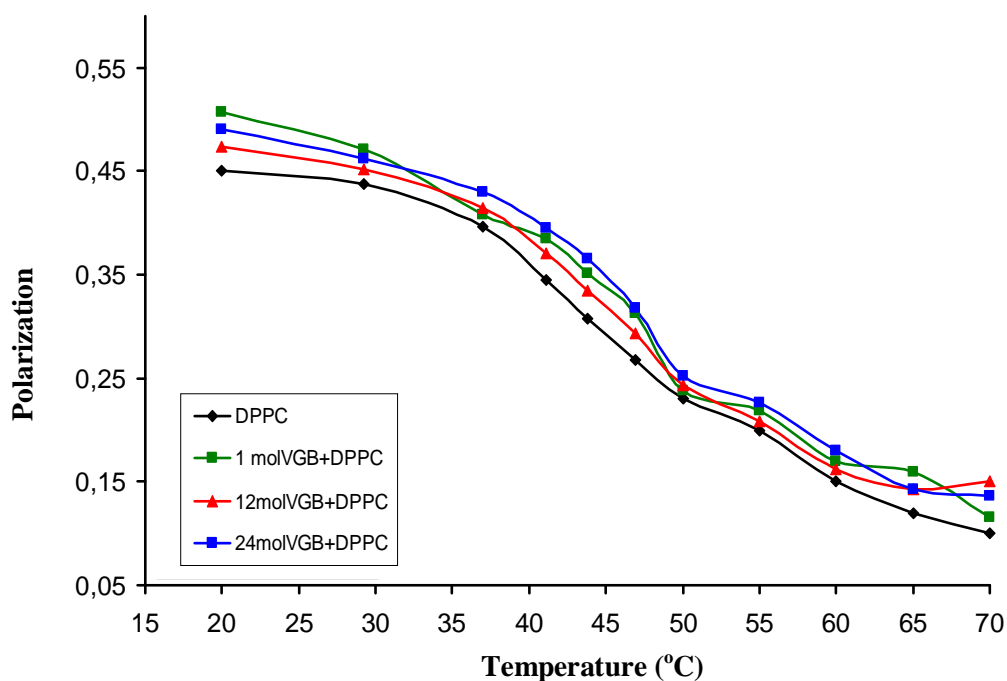
Figure 34. Polarization values for DPH in DPPC MLVs containing different concentrations of VGB at variable temperature.

The interaction of VGB with the glycerol backbone near the head group of phospholipids in interfacial region was monitored by analyzing the frequency changes of the C=O ester stretching (1730 cm^{-1}). The temperature dependence of the frequency of this band is shown in Fig.35. The decrease in the frequency was observed in the presence of VGB in both in gel and liquid crystalline phase implying an increase in the strength of hydrogen bonding (Korkmaz and Severcan, 2005).
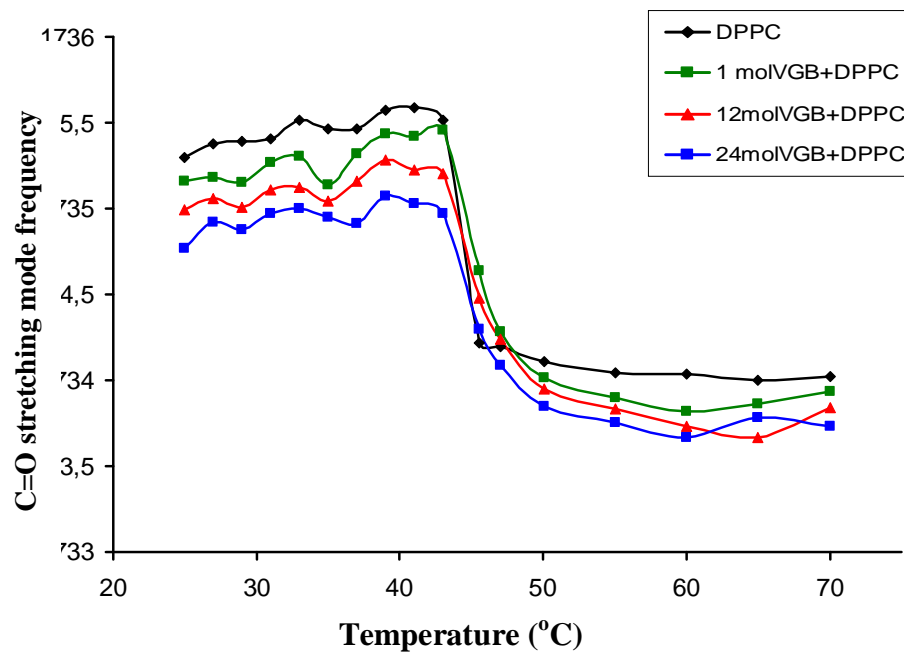
Figure 35. Temperature dependence of the frequency of the C=O stretching mode of DPPC MLVs in the absence and presence of VGB.

The other band located at 1230 cm^{-1} for probing the head group of DPPC is the PO$_2^-$ asymmetric double stretching modes. As can be observed from Figure 35, the frequency value of this band also shifted to lower values with the increasing concentration of VGB.
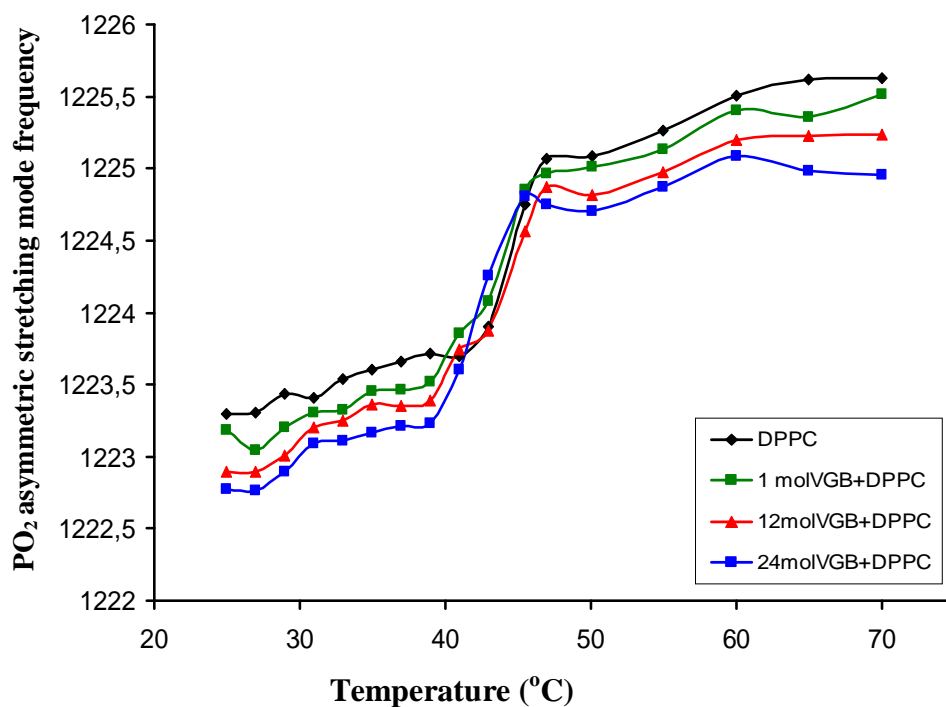
Figure 36. Temperature dependence of the frequency of the PO_2^- asymmetric double bond stretching mode of DPPC MLVs in the absence and presence of VGB.

Figure 37 shows the thermograms of DPPC MLVs in the absence and presence of different concentrations of VGB. As can be observed from the figure, with the presence of the VGB, the pretranstion was broadened which means that there is perturbation of the ripple phase. On the other hand, although the presence of VGB did not alter the shape of main transition curve and there was a slight change in the main transition temperature as observed in the figure. In order to further elaborate the effects of VGB on DPPC thermotrophic properties, the thermograms were further analyzed in detail to yield enthalpy and cooperativity. The values of qualitative assessments were plotted against different VGB concentrations in Figures 38 and 39, respectively. As can be observed from both figures, VGB slightly changed on both the enthalpy and the cooperativity of the gel to liquid crystalline transition for DPPC MLVs.
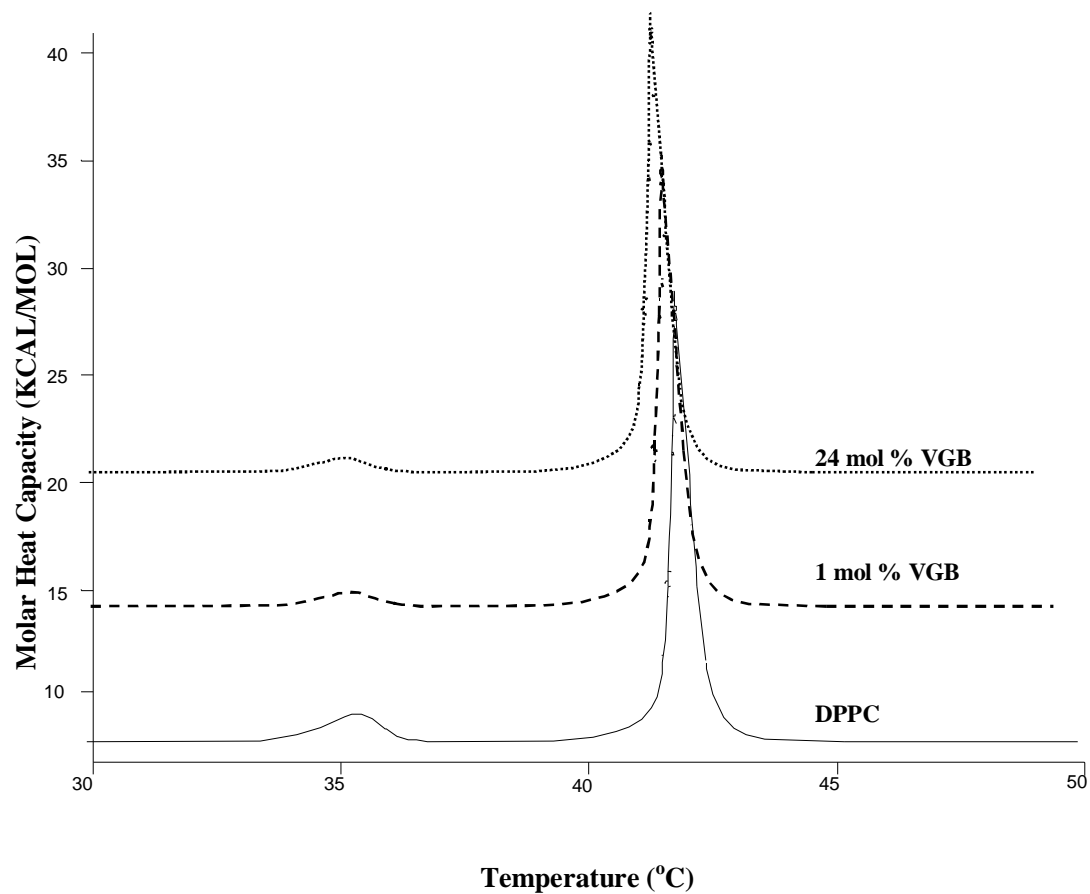
Figure 37. DSC thermograms of DPPC MLVs in the absence and presence of VGB with different concentrations.
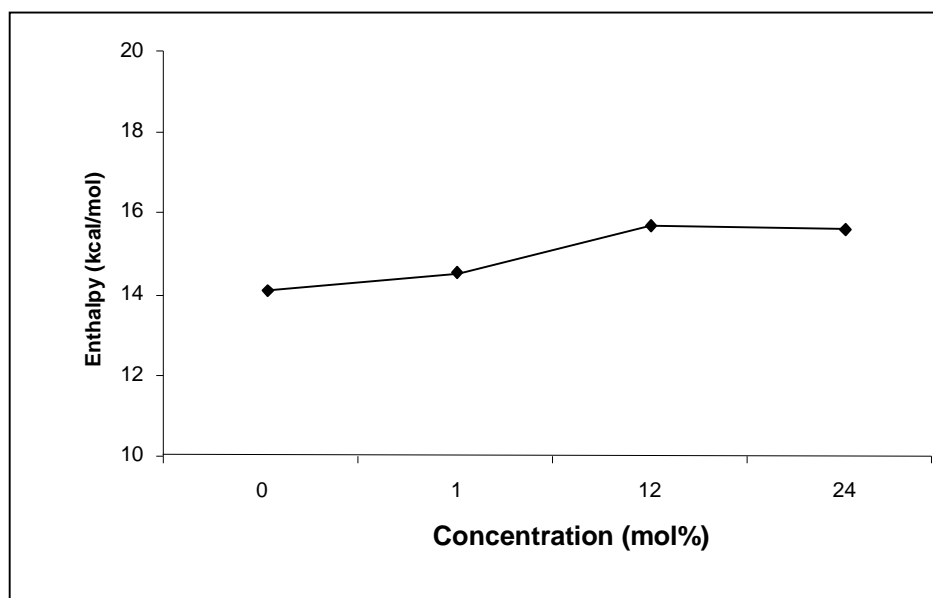
Figure 38. The variation with PTZ concentration of the enthalpy of the gel to liquid crystalline transition for DPPC.
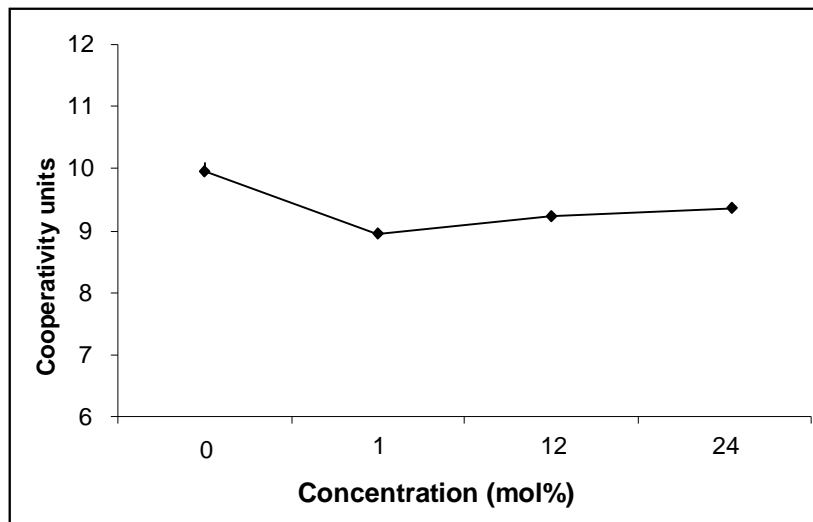
Figure 39. The variation with PTZ concentration of the cooperativity of gel to liquid crystalline transition for DPPC.

The information about the effect of VGB on the phase transition behavior of DPPC MLVs was also obtained using FTIR spectroscopy by the frequency variations of the C-H stretching modes. As can be seen from the figure 28, as the VGB concentration increases in the DPPC MLVs, the main transition temperature shifted to lower values without affecting the general shape of the transition profile, which is in agreement with DSC results.

3.2 Animal Studies

3.2.1 The Effects of PTZ-induced Seizures on Rat Brain Homogenates and Cell Membranes

3.2.1.1 The Investigation of Compositional, Structural and Dynamical Changes of PTZ-induced Seizures on Rat Brain Homogenates

In this part of the study, we aimed to investigate the effects of epileptic seizures induced by subconvulsive (25 mg/kg) and convulsive (60 mg/kg) dose of PTZ on rat brain tissue using FTIR spectroscopy for the evaluation of molecular consequences of epileptic activity. On the basis of the spectral variations, cluster analysis was also performed to differentiate the control, low dose and high dose of PTZ. In addition, the protein secondary structure of each group was estimated by neural network study based on FTIR spectra. The changes in the protein structure were also identified from the intensities of sub-bands in the second derivative of the amide I band. Furthermore, MDA levels, which is the indicator of lipid peroxidation was assayed by TBAR test.

The result of cluster analysis based on the spectral differences between the control and PTZ treated groups and was depicted in Figure 40. As can be seen from the figure, three distinct clusters were produced with a high accuracy with success of (7/8) and (7/8), for low and high dose PTZ-treated samples, respectively.
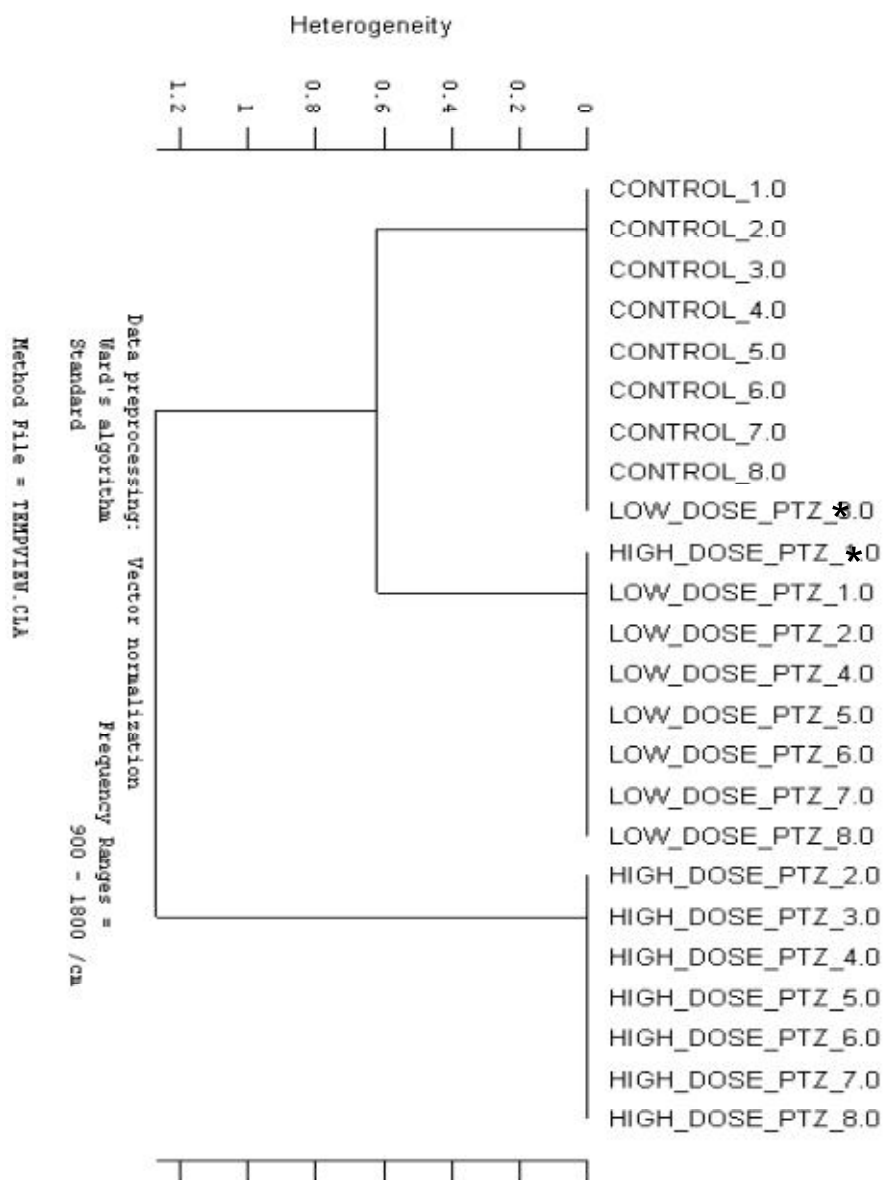
Figure 40. Hierarchial clustering of control, low dose and high dose of PTZ in the 1800-900 cm^{-1} spectral range. The sample labeled with * was not clearly differentiated and not used in the statistical analysis.

Figure 41 and 44 show normalized infrared spectra of control, subconvulsive and convulsive dose of PTZ rat brain homogenate in 3050-2800 cm^{-1} and 2000-900 cm^{-1} region, respectively. As seen from the figures, the brain spectrum is very complex and it contains vibration bands of functional groups present in lipids, proteins, carbohydrates and nucleic acids. The spectral bands were labeled in these figures and detailed band assignments based upon the literature were given in Table 8. In Figure 41, the spectra were normalized with respect to the CH$_2$ asymmetric stretching band at 2925 cm^{-1}, and in Figure 44 the spectra were normalized with respect to the Amide I band at 1645 cm^{-1} for visual demonstration of the spectral variations.

Table 8. General band assignments of average FTIR spectrum of rat brain based on the literature. The peak numbers illustrated in.

No	Frequency (cm^{-1})	Definition of the Spectral Assignments
1	3012	Olefinic =CH stretching: unsaturated lipids
2	2956	CH$_3$ asymmetric stretching: mainly lipids with little contribution from proteins, carbohydrates and nucleic acids
3	2925	CH$_2$ asymmetric stretching: mainly lipids with little contribution from proteins, carbohydrates and nucleic acids
4	2870	CH$_3$ symmetric stretching: mainly protein with the little contribution from lipids, carbohydrates and nucleic acids
5	2852	CH$_2$ symmetric stretching: mainly lipid with the little contribution from proteins, carbohydrates and nucleic acids
6	1736	Saturated ester C=O stretch: phospholipids, cholesterol esters
7	1645	Amide I (protein C=O stretch): proteins
8	1547	Amide II (C=N and N-H stretching): proteins
9	1400	COO$^-$ symmetric stretching: fatty acids
10	1236	PO$_2^-$ asymmetric stretching: phospholipids and nucleic acids
11	1173	C-O asymmetric stretching: glycogen
12	1156	CO-O-C asymmetric stretching: ester bonds in cholesteryl esters
13	1080	PO$_2^-$ symmetric stretching: phospholipids and nucleic acids
14	998	C$^+$-N-C stretching: nucleic acids, ribose phosphate main chain vibrations of RNA

The 3050-2800 cm^{-1} region contains the absorptions arising from the C-H stretching vibrations of olefinic =CH, CH$_2$ and CH$_3$ groups present in membrane lipids and proteins (Mantsch, 1984; Cakmak et al., 2006). In this region, the olefinic band at 3015 cm^{-1} is due to the CH stretching mode of the HC=CH groups in unsaturated lipids (Severcan et al., 2005). According to the empirical rule, the area of IR absorptions arising from a particular species is directly proportional to the concentration of that species (Cakmak et al., 2006; Toyran et al., 2004), therefore; this band can be used to monitor the level of unsaturation in lipids (Melin et al., 2000; Cakmak et al., 2003; Severcan et al., 2005). As can be seen from Fig. 41 and Fig. 42, there was a significant increase (p<0.05*) in the area of

this band for both subconvulsive and convulsive dose of PTZ compared to control group.
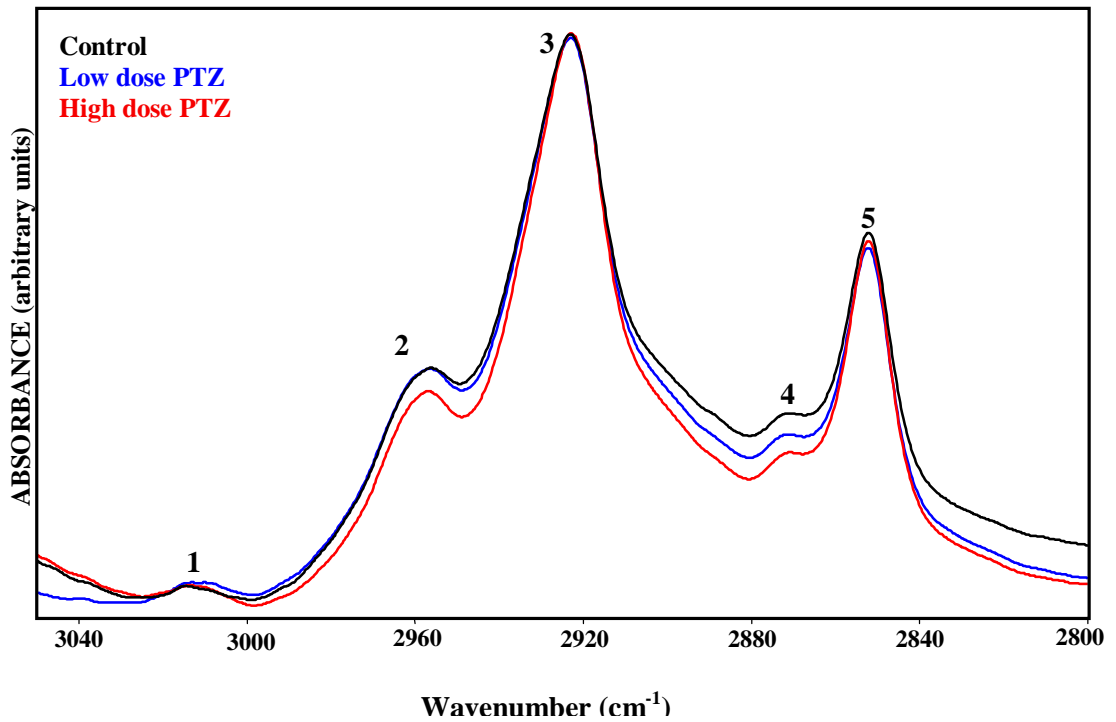
Figure 41. Representative FTIR spectra of control, low dose and high dose of PTZ in the region between 3050-2800 cm^{-1}. The spectra were normalized with respect to the CH_2 asymmetric stretching at 2925 cm^{-1}.
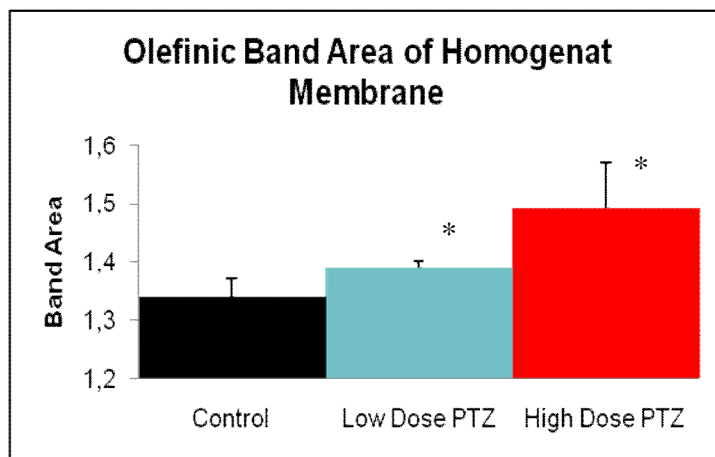
Figure 42. The olefinic band area values of control, low dose and high dose of PTZ.

Alterations in lipid order and fluidity of the cell membrane can be determined by probing the strong bands in the C-H stretching region of the infrared spectra (Akkas et al., 2007b; Toyran et al., 2006). The bandwidth values of the CH_2 asymmetric and the CH_2 symmetric stretching modes for PTZ administrated and control samples were shown in Fig. 43. As can be seen from the figures, both subconvulsive and convulsive dose of PTZ led to a decrease in the bandwidth values of the CH_2 asymmetric and the CH_2 symmetric stretching modes. This reflects PTZ-induced fluidity changes in the cell membrane (Schultz and Naumann, 1991; Lopez-Garcia et al., 1993; Ozek et al., 2009). Besides this, the statistical analysis revealed that the frequency values of the CH_2 asymmetric and symmetric stretching increased slightly but not significantly for low dose and high dose of PTZ (Appendix A).
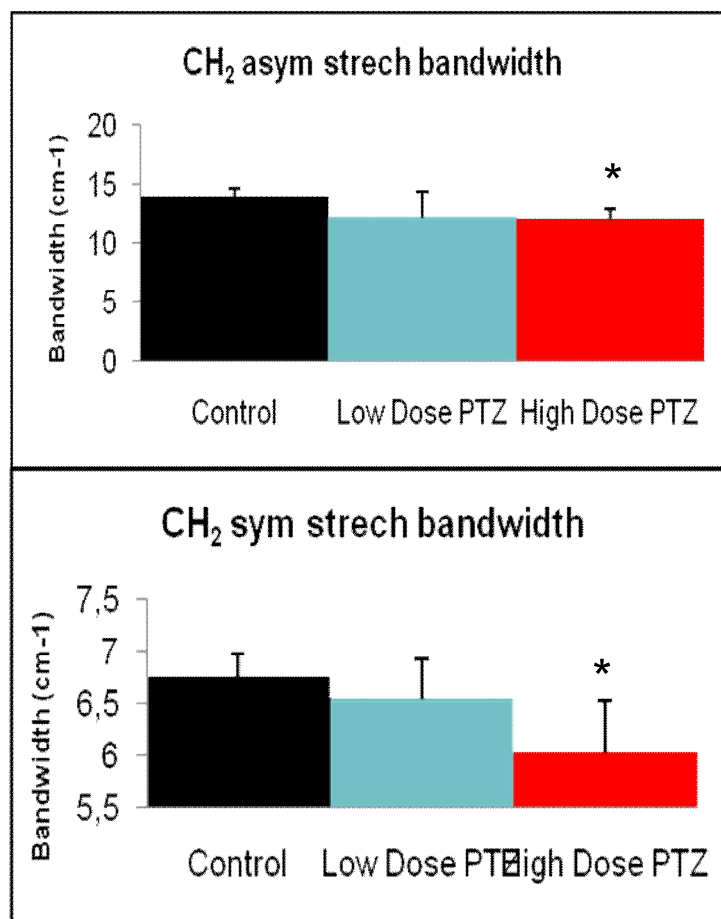
Figure 43. The bandwidth values of CH_2 asymmetric (A) and CH_2 symmetric (B) stretching modes for control, low dose and high dose of PTZ.
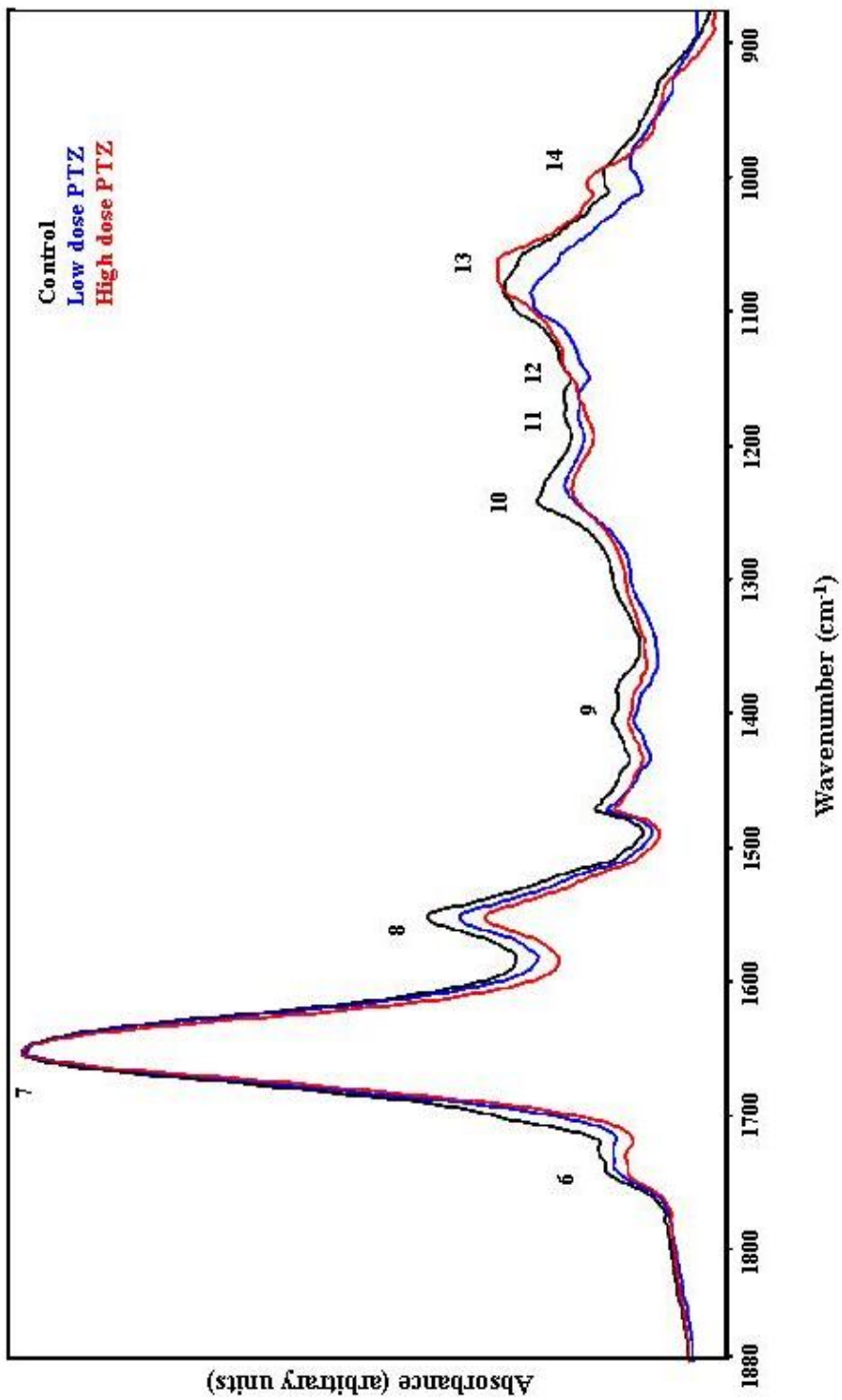
Figure 44. Representative FTIR spectra of control, low dose and high dose of PTZ in the region between 1880-900 cm^{-1} . The spectra were normalized with respect to the Amid I at 1645 cm^{-1} .

85

As seen from Figure 44, the frequency range of 2000-700 cm^{-1}, which corresponds to finger print region, includes several bands that originate from lipids, proteins, carbohydrates and nucleic acids in the samples (Mendelsohn and Mantsch, 1986). Since all bands present in this range are clearly resolved no curve fitting procedure were performed. The band centered at 1736 cm^{-1} is mainly assigned to the C=O stretching vibrations of lipids (Melin et al., 2000; Cakmak et al., 2003). As observed from the Fig. 45, in the spectra of both PTZ treated groups, the frequency of this band significantly shifted to lower values ($p<0.05$*) as well as the area values of the band dramatically reduced for PTZ groups compared to control group ($p<0.05$*).
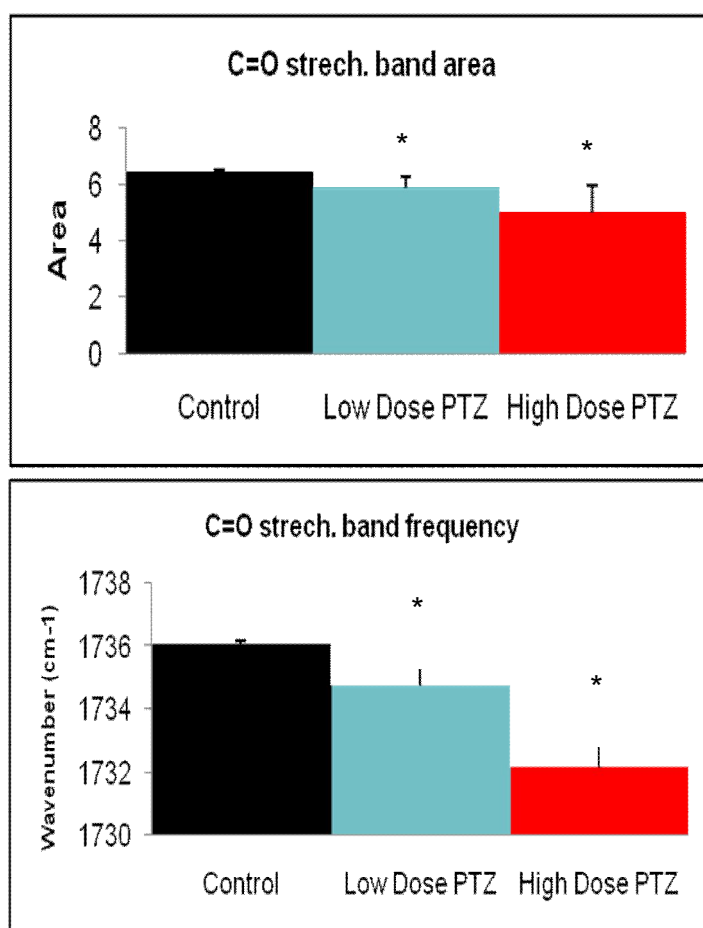
Figure 45. The band area and frequency values of C=O stretching mode for control, low dose and high dose of PTZ.

In the finger print region, the bands at 1645 cm^{-1} and 1540 cm^{-1} are assigned to the amide I and II vibrations of structural proteins. The band centered at 1645 cm^{-1} (amide I) corrresponds to the C=O stretching of proteins (Haris and Severcan, 1999). The band located at 1540 cm^{-1} (amide II) is attributed to the N-H bending and the C-N stretching modes of proteins (Melin et al., 2000; Haris and Severcan 1999). It is seen from Figure 46 that, the areas of these two vibrations significantly decreased in low (p<0.05*) and high dose of PTZ (p<0.05*).
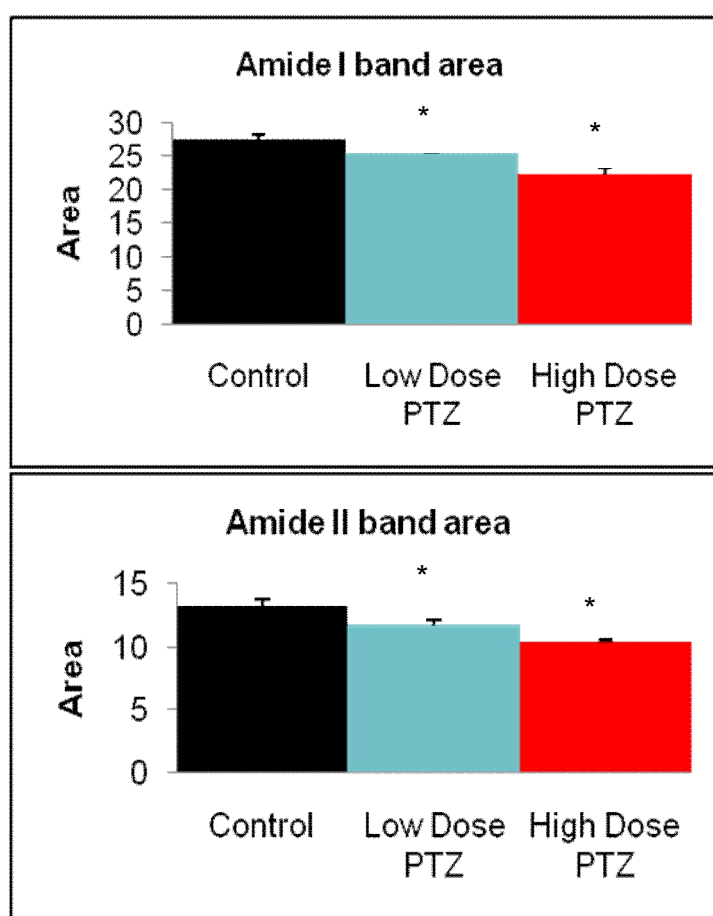
Figure 46. The band area values of Amide I and Amide II for control, low dose and high dose of PTZ.

Lipid to protein ratio of the membrane system can be derived by taking the ratio of the peak areas of the bands belonging to lipids and proteins (Jackson and Mantsch 1996; Toyran et al., 2004). This ratio was calculated from the peak area value of the CH_2 asymmetric (2925 cm^{-1}) to the amide I (1653 cm^{-1}) vibrational modes. This ratio decreased for both two different doses of PTZ but it is significant for convulsive dose of PTZ (p<0.05*).
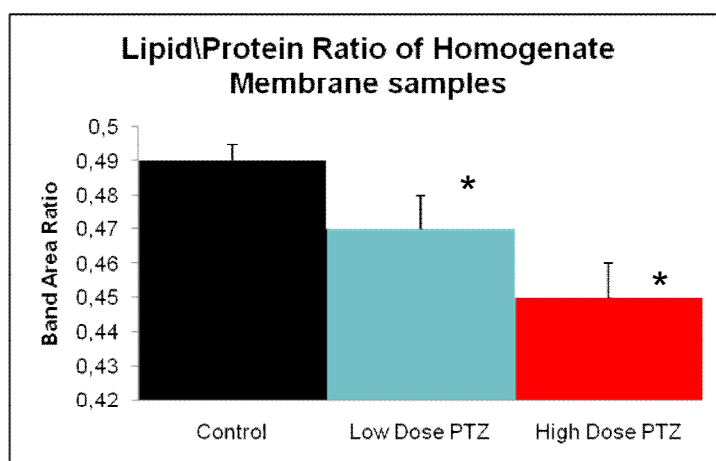
Figure 47. Lipid to protein ratio values for control, low dose and high dose of PTZ.

The vibrational mode located at 1400 cm^{-1} is resulted from the COO^- symmetric stretching vibration of fatty acids (Jackson and Mantsch; Cakmak et al., 2006). A decrease in the area of this band was observed in the spectra of PTZ treated groups, especially significant for convulsive dose of PTZ (p<0.05*) (Appendix B).

In the finger print region, the band centered at 1173 cm^{-1} is originated from the C-O stretching in glycogen and 1156 cm^{-1} is due to the CO-O-C asymmetric stretching in cholesteryl esters. As could be seen from Fig. 44, in the spectrum of convulsive dose of PTZ, these bands diminished.

The bands at 1236 cm^{-1} and 1080 cm^{-1} are mainly originated from the PO_2^- asymmetric and symmetric stretching modes of nucleic acids and phospholipids, respectively (Wong et al., 1991; Wang et al., 1997; Cakmak et al., 2003).

As shown in Fig. 48, the areas of these bands dramatically decreased in both subconvulsive dose (p<0.05*) and convulsive dose of PTZ (p<0.01**). Moreover, the frequency of these vibrational modes significantly shifted to lower values in both PTZ treated groups (p<0.05*) (Fig. 49). In addition, as seen from Fig 44, the shape of the PO_2^- symmetric stretching band was totally different in the spectrum of convulsive dose of PTZ compared to the others.
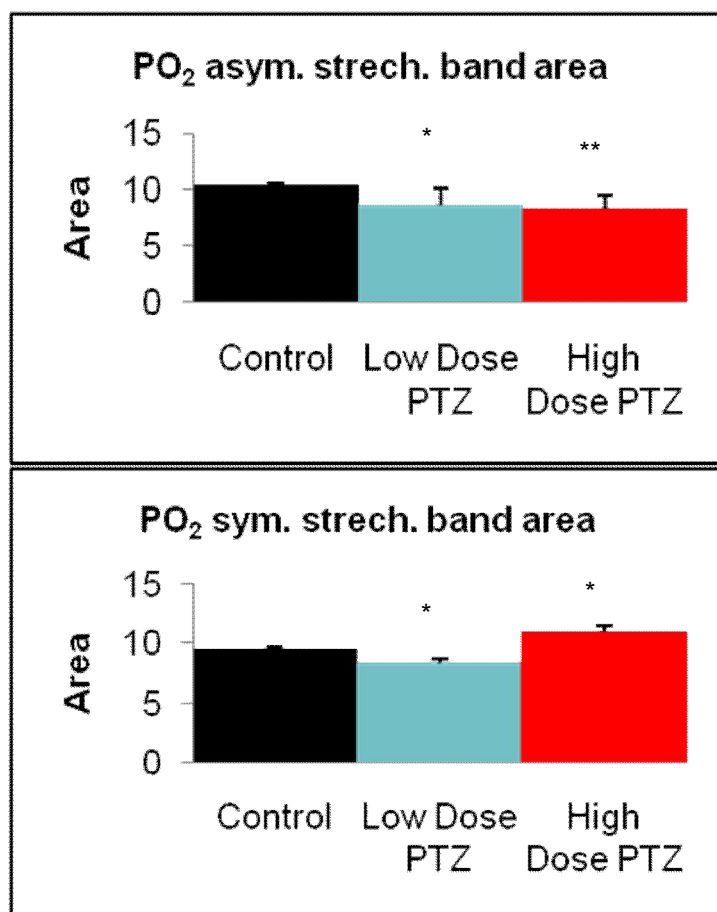
Figure 48. The band area values of PO_2 asymmetric and symmetric sretching modes for control, low dose and high dose of PTZ.
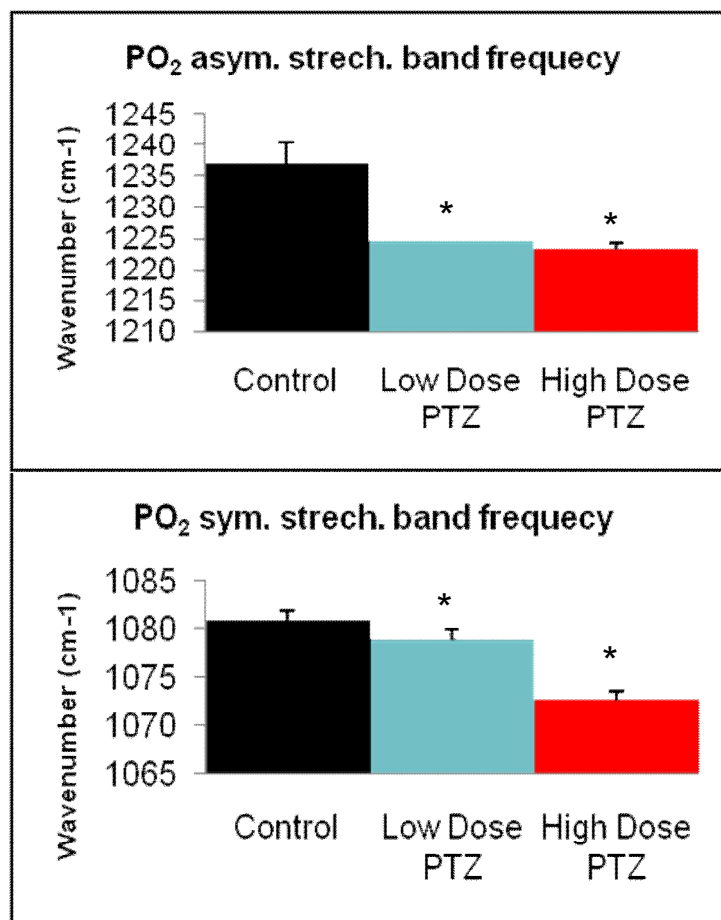
Figure 49. The frequency values of PO_2 asymmetric and symmetric sretching modes for control, low dose and high dose of PTZ.

The mode located at 998 cm^{-1} is generally assigned to symmetric stretching mode of dianionic phosphate monoester of cellular nucleic acids (Ci et al., 1999; Chiriboga et al., 2000) and ribose-phosphate main chain vibrations of the RNA backbone (Banyay et al., 2003). The dramatic shift in the frequency of this band was observed for low dose PTZ group (p<0.05*) and high dose of PTZ (p<0.01**). In addition to that, while the band area decreased in subconvulsive group, it increased in convulsive group compared to the control (Figure 44 and Appendix A).

3.2.1.1.1 FTIR microscopic analysis of rat brain homogenate samples

Figure 50 shows the chemical map of control, low dose PTZ and high dose PTZ homogenate samples. In the figure, the average colored chemical maps of lipid to protein ratio, which was drived from the ratio of the areas of the CH_2 asymmetric stretching to Amide I (A_{2925}/A_{1645}) for each group, was given. The average map was colored according to this ratio, where red color corresponds to the highest and blue color corresponds to the lowest concentrations as shown on a color bars in the figure.
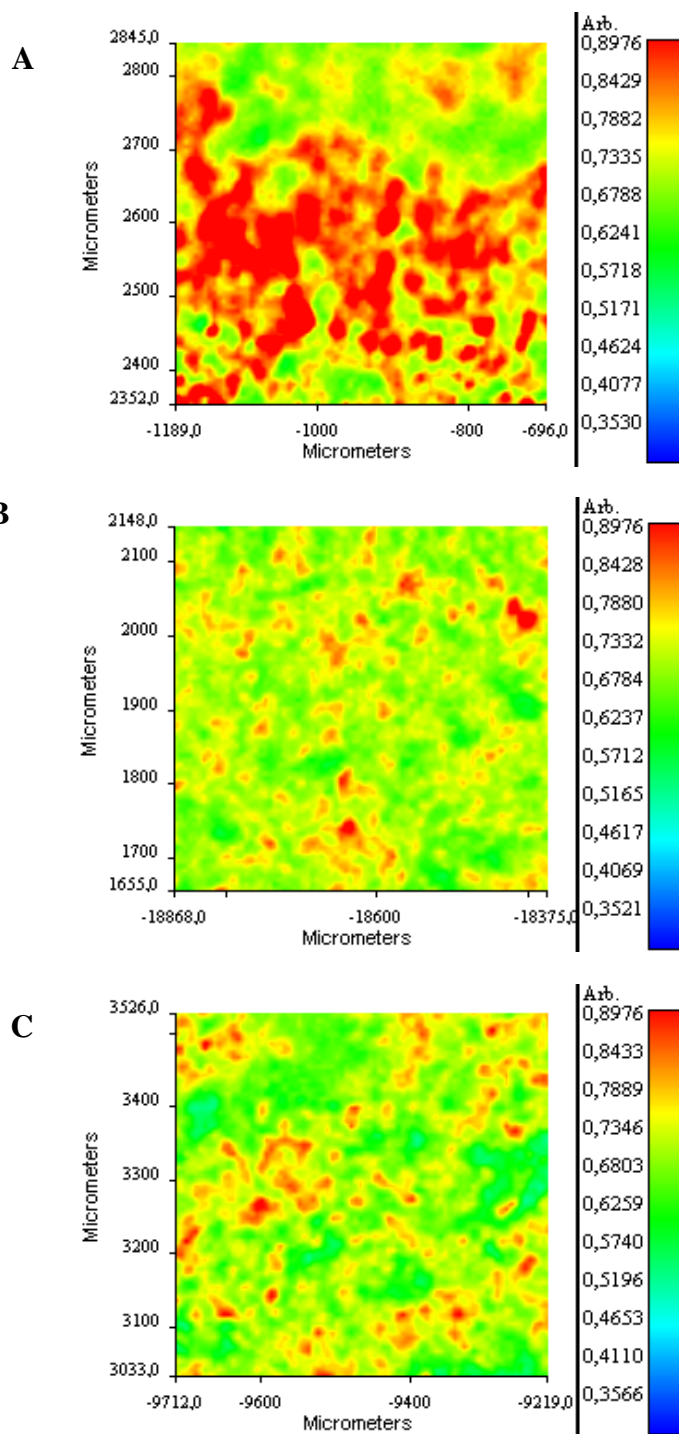
Figure 50. The average chemical map of control (A), low dose (B) and high dose (C) of PTZ for brain homogenate samples

In order to get chemical map for each groups, all spectra were loaded into FTIR microscopy spotlight 400 analysis program. The lipid to protein ratio were calculated and for the comparison of all groups the chemical data were constructed. As seen from the figure, the lipid to protein ratio decreased for PTZ treated groups, which supports FTIR spectroscopic data.

3.2.1.1.2 The secondary structure determination for PTZ-induced seizures on rat brain homogenate

The peak maximum of the amide I band (1700-1600 cm^{-1}) occurs at different frequencies due to the various types of secondary structures present in the proteins (Lopez et al., 2001). For this reason, amid I band was analyzed by taking second derivative of its absorbance spectra for control and PTZ convulsions groups and some peaks were observed (Figure 51). The changes in the intensities of characteristics components of this band were given in Appendix C. The band at 1682 cm^{-1} is from beta turns, the peak at 1652 is due to alpha helix, the peak located at 1643 cm^{-1} are assigned to random coil and the band at 1633 cm^{-1} corresponds to beta sheet (Haris and Severcan, 1999; Lopez et al., 2001). As seen from Figure 51, low and high doses of PTZ led to a significant increase in the intensities of alpha-helix and random coil ($p<0.05*$) and a significant decrease in the intensity of beta sheet of amide I band ($p<0.05*$).
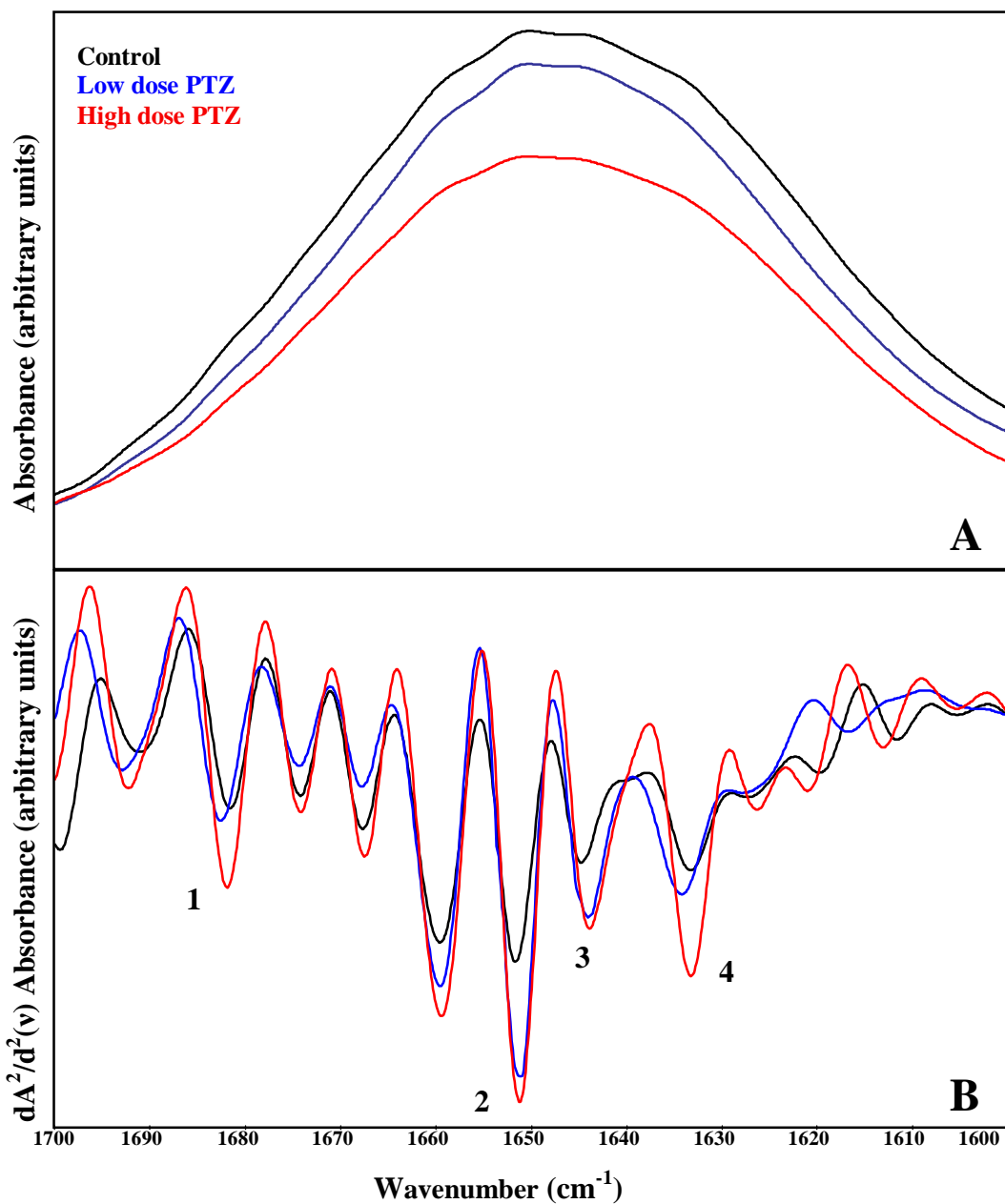
Figure 51. Representative (A) absorbance FTIR spectra and (B) the second derivative spectra of amide I band for control, low dose and high dose of PTZ in the 1700-1600 cm⁻¹. Vector normalization was done in the 1700-1600 cm⁻¹ region. Absorption maxima appear as minima in the second derivatives.

In order to obtain more detail and reliable information about the changes in protein secondary structure, the amide I band between 1700 and 1600 cm^{-1} was also further analyzed using neural network predictions based on FTIR data using the similar approach which was previously applied to protein in solutions (Severcan et al., 2004) and in tissues (Akkas et al., 2007a). As observed from the figure, both low and high doses of PTZ induced significant increase ($p<0.05*$) in alpha helix and random coil and significant decrease ($p<0.05*$) in beta sheet structures. This finding is in accordance with the second derivative analysis of Amid I mode.
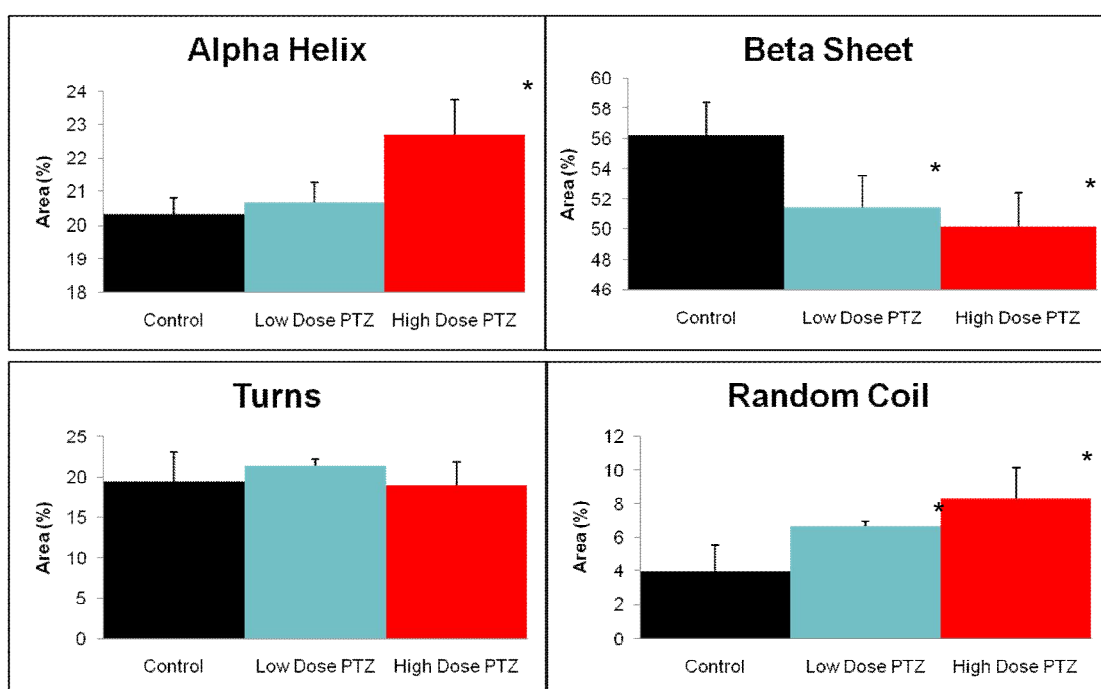
Figure 52. Neural network predictions of control, low dose and high dose of PTZ for homogenate samples.

3.2.1.1.3 The lipid peroxidation determination for PTZ-induced seizures on rat brain homogenate

Beside FTIR study we also performed TBA assay for the determination of lipid peroxidation. MDA levels were found as 7.98 ± 1.28 nmol/mg protein for control samples, 11.32 ± 2.09 nmol/mg protein ($p<0.05*$) for subconvulsive dose PTZ and 14.11 ± 1.07 nmol/mg protein ($p<0.05*$) for convulsive dose of PTZ (Figure 53). The results implied that MDA levels were increased significantly for both PTZ treated groups, which is accordance with our FTIR results.
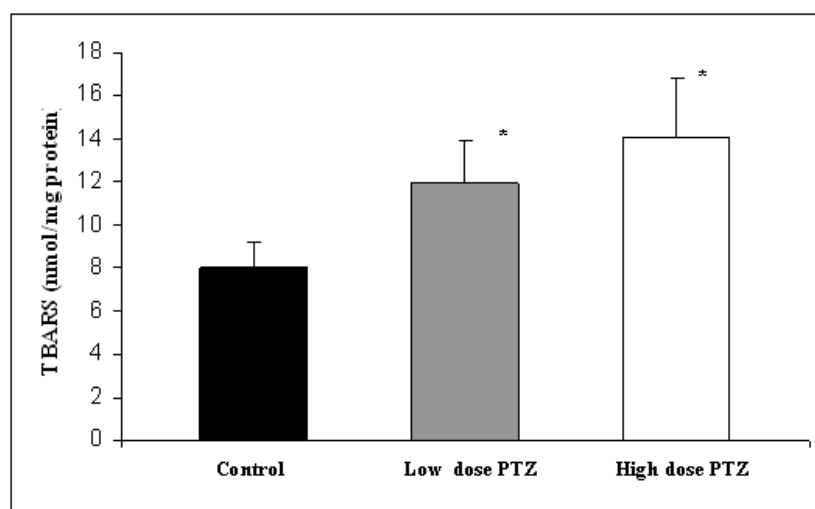
Figure 53. Comparison of MDA levels of control, low dose and high dose of PTZ in the homogenate rat brain.

3.2.1.1 The Investigation of Compositional, Structural and Dynamical Changes of PTZ-induced seizures on rat brain cell membrane

This part of the current study contains the effects of epileptic seizures induced by subconvulsive (25 mg/kg/ml) and convulsive (60 mg/kg/ml) dose of PTZ on rat brain cell membrane tissue using FTIR spectroscopy. Furthermore, in order to elaborate spectral differences among the control, low dose and high dose of PTZ, cluster analysis was also performed. Moreover, the changes in the protein structure were identified by the alterations in the intensities of sub-bands in the second derivative of the amide I band.

The result of cluster analysis in the form of dendrogram based on the spectral differences was shown in Figure 54. As can be seen from the figure, three distinct clusters were produced with a high accuracy with success of (7/8) and (7/8), for low and high dose PTZ-treated samples, respectively.
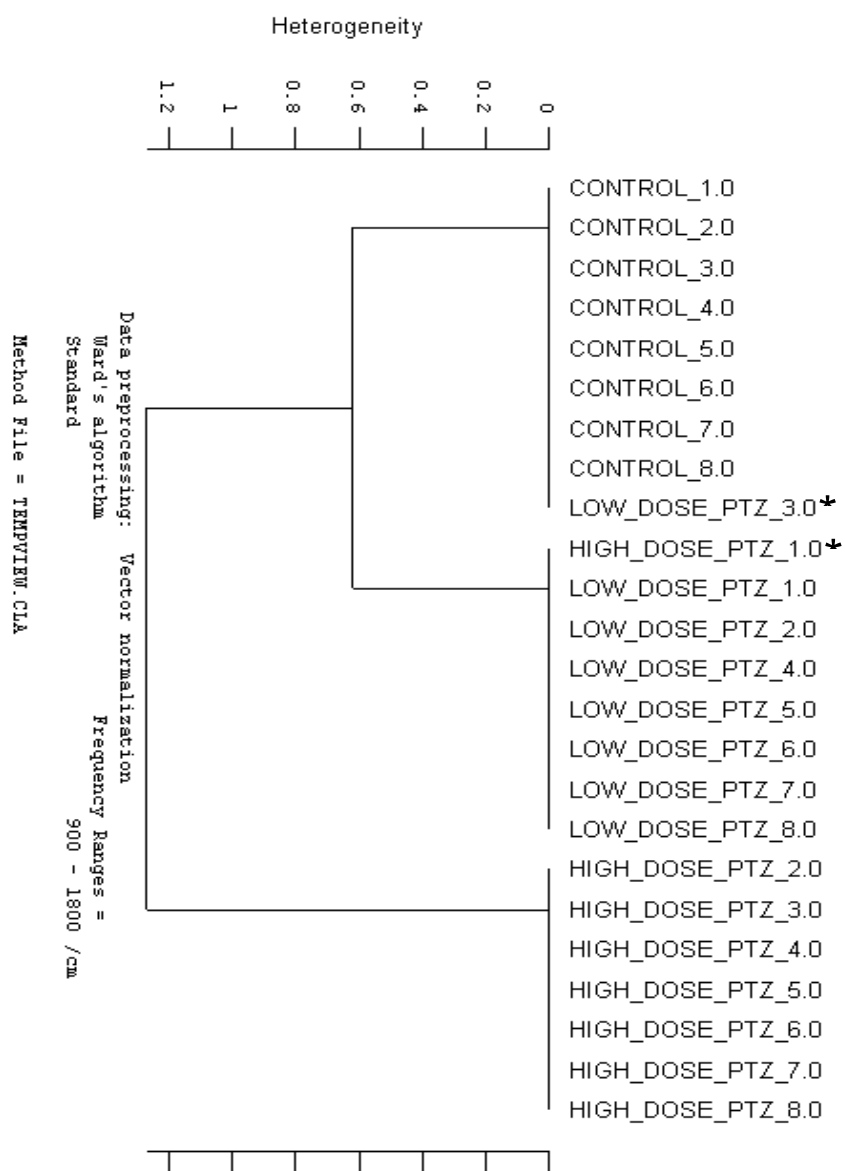
Figure 54. Hierarchial clustering of control, low dose and high dose of PTZ in the 1800-900 cm^{-1} spectral range. The sample labeled with * was not clearly differentiated and not used in the statistical analysis.

Figure 55 show normalized infrared spectra of control, subconvulsive and convulsive dose of PTZ rat brain cell membrane in 3050-2800 cm^{-1} and 2000-900 cm^{-1} region, respectively. The spectral bands were labeled in these figures and detailed band assignments based upon the literature were given Table 9. In Figure 55, the spectra were normalized with respect to the CH$_2$ asymmetric stretching band at 2925 cm^{-1}, and in Figure 48 the spectra were normalized with respect to the Amide I band at 1645 cm^{-1} . The spectral differences in the peak area and frequency values of the control and PTZ treated groups were shown in Appendix D.

Table 9. General band assignments of average FTIR spectrum of rat brain based on the literature. The peak numbers illustrated in Fig. .

No	Frequency (cm^{-1})	Definition of the Spectral Assignments
1	3012	Olefinic =CH stretching: unsaturated lipids
2	2956	CH$_3$ asymmetric stretching: mainly lipids with little contribution from proteins, carbohydrates
3	2925	CH$_2$ asymmetric stretching: mainly lipids with little contribution from proteins, carbohydrates
4	2870	CH$_3$ symmetric stretching: mainly protein with the little contribution from lipids, carbohydrates
5	2852	CH$_2$ symmetric stretching: mainly lipid with the little contribution from proteins, carbohydrates
6	1736	Saturated ester C=O stretch: phospholipids, cholesterol esters
7	1645	Amide I (protein C=O stretch): proteins
8	1547	Amide II (C=N and N-H stretching): proteins
9	1400	COO$^-$ symmetric stretching: fatty acids
10	1236	PO$_2^-$ asymmetric stretching: phospholipids
11	1080	PO$_2^-$ symmetric stretching: phospholipids
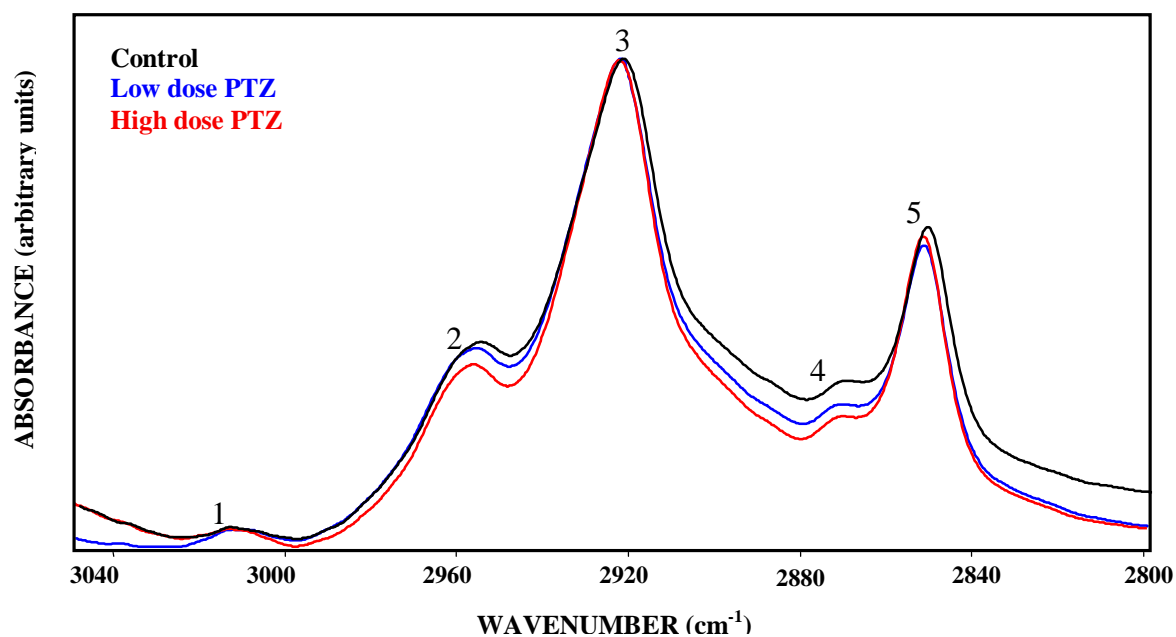
Figure 55. Representative FTIR spectra of control, low dose and high dose of PTZ of brain cell membrane in the region between 3050-2800 cm^{-1}. The spectra were normalized with respect to the CH_2 asymmetric stretching at 2925 cm^{-1}.

In the C-H region, the band (HC=CH mode) at 3015 cm^{-1} gives information about unsaturation of the brain cell membrane lipids (Melin et al., 2000; Cakmak et al., 2003; Severcan et al., 2005). As seen from Figure 55 and 56, the band area of this band significantly decreased in the PTZ-treated groups ($p < 0.05^*$).
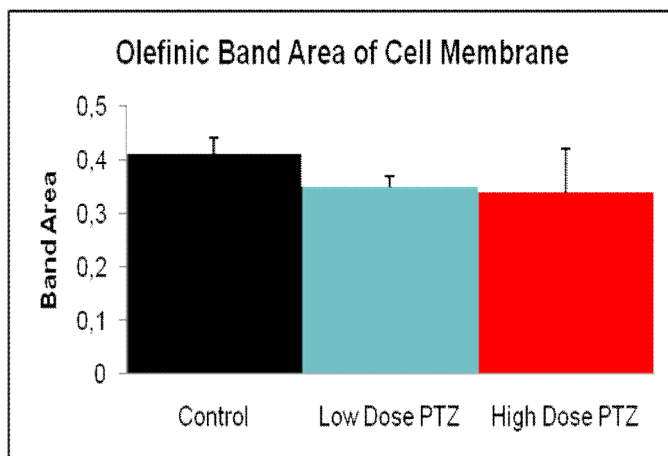
Figure 56. The olefinic band area values of control, low dose and high dose of PTZ.

The CH_2 stretching vibrations depend on the degree of conformational disorder of membrane; hence they can be used to monitor the average trans/gauche isomerization in the system as mentioned before (Mantsch et al., 1984; Bizeau et al., 2000) as reported previously. As can be observed from figure 57, the frequency values of the CH_2 asymmetric stretching mode shifted from 2923.09±0.67 (control) to 2925.14±0.20 (low dose of PTZ) and 2925.88±0.04 (high dose of PTZ) (p<0.05*). In addition, the area of the band significantly decreased for PTZ treated groups as seen from Figure 57.
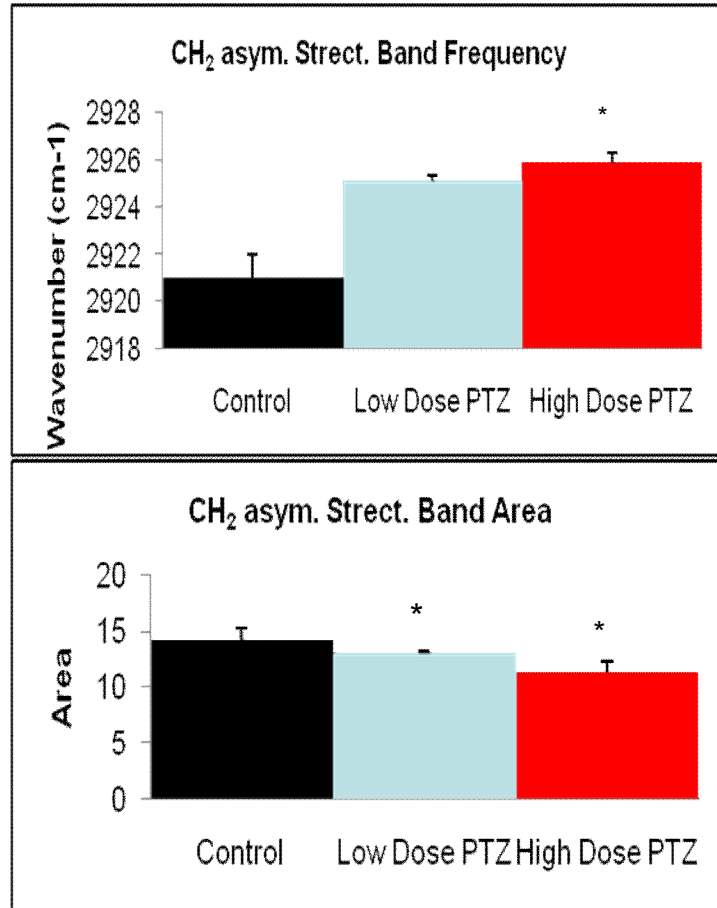
Figure 57. The frequency and band area values of CH_2 asymmetric stretching modes for control, low dose and high dose of PTZ.

The changes in the bandwidth values of the CH₂ asymmetric and symmetric modes were represented in Fig. 58. As seen from table, the bandwidth values of these two bands significanlt decreased for PTZ groups (p<0.05*).
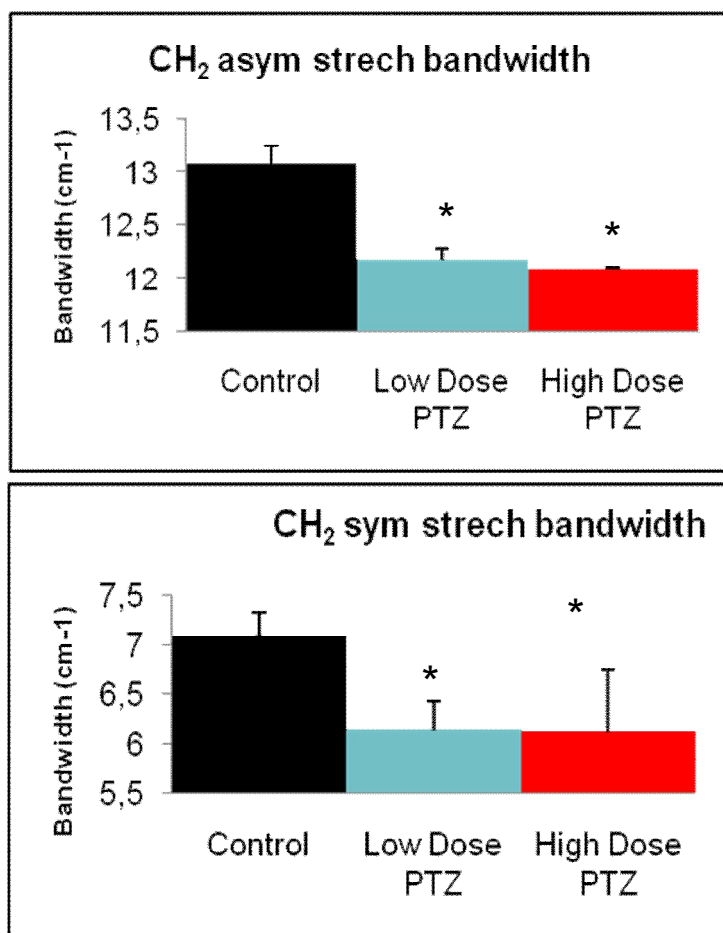
Figure 58. The bandwidth values of CH₂ asymmetric and symmetric stretching modes for control, low dose and high dose of PTZ.

The amounts of proteins and lipids in the membranes is an important factor affecting the membrane structure and dynamics (Szalontai et al., 2000). The changes in the lipid to protein ratio of the membrane system was calculated from the peak area value of the CH₂ asymmetric (2925 cm⁻¹) to the amide I (1653 cm⁻¹)

vibrational modes. The ratio decreased for both two different doses of PTZ but significantly for convulsive dose of PTZ (p<0.05*) (Appendix D).

Figure 59 represents the finger print region covering 1880-900 cm^{-1}range which includes lipids, proteins and carbohydrates in the brain cell membrane samples (Mendelsohn and Mantsch, 1986). The spectra were normalized with respect to the amide I band at 1645 cm^{-1}. Since all bands present in this range are clearly resolved no curve fitting procedure were performed.
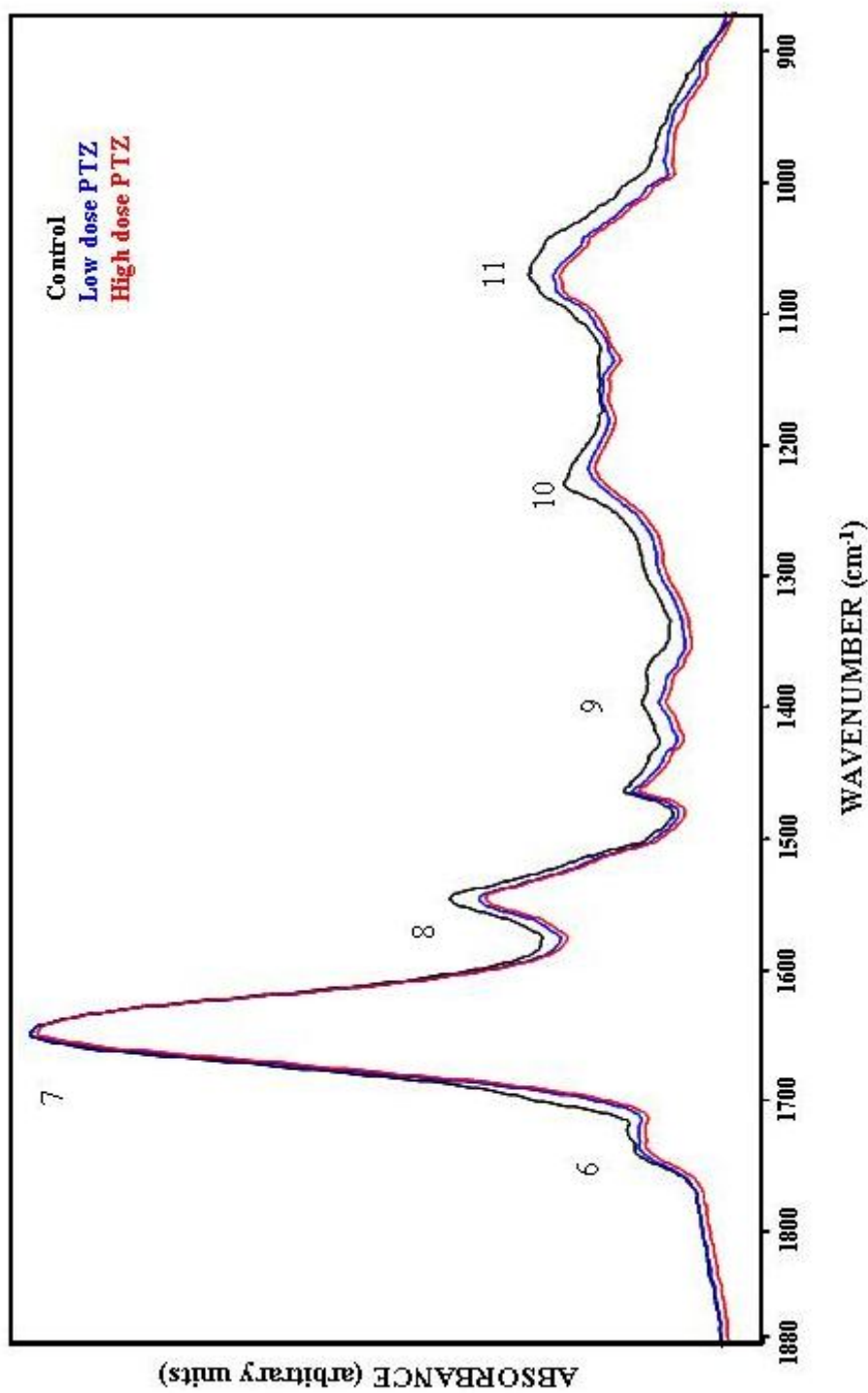
Figure 59. Representative FTIR spectra of control, low dose and high dose of PTZ for rat brain cell membrane in the region between 1880-900 cm^{-1}. The spectra were normalized with respect to the Amid I at 1645 cm^{-1}.
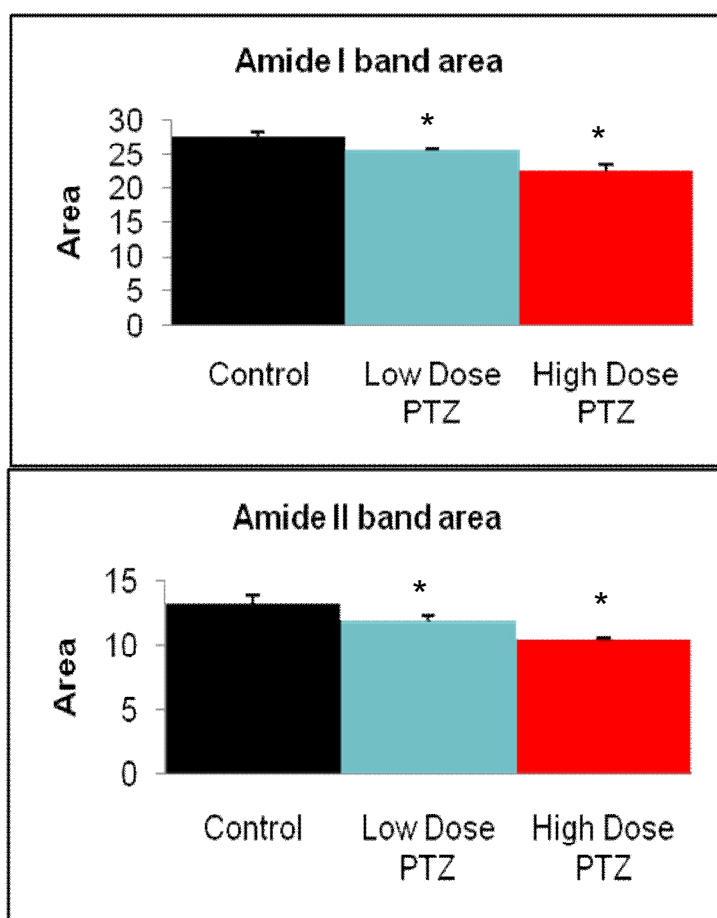
Figure 60. The band area values of Amide II and Amide II for control, low dose and high dose of PTZ.

In the finger print region, the bands at 1645 cm^{-1} and 1540 cm^{-1} are assigned to the amide I and II vibrations of membrane proteins (Melin et al., 2000; Haris and Severcan, 1999). It is seen from Figure 60, the areas of these two modes significantly decreased in low (p<0.05*) and high dose of PTZ (p<0.01*).

The three bands namely the C=O stretching (1736 cm^{-1}), PO_2^- asymmetric sretching (1236 cm^{-1}) and PO_2^- symmetric stretching (1080 cm^{-1}) are resulted from membrane phospholipids (Melin et al., 2000; Cakmak et al., 2003; Severcan et al., 2003). The area of all these bands significantly decreased for both low and high dose of PTZ. On the other hand, as observed from Fig. 62, frequency values of these modes significantly shifted to lower values ($p<0.05*$) in both PTZ-treated groups.
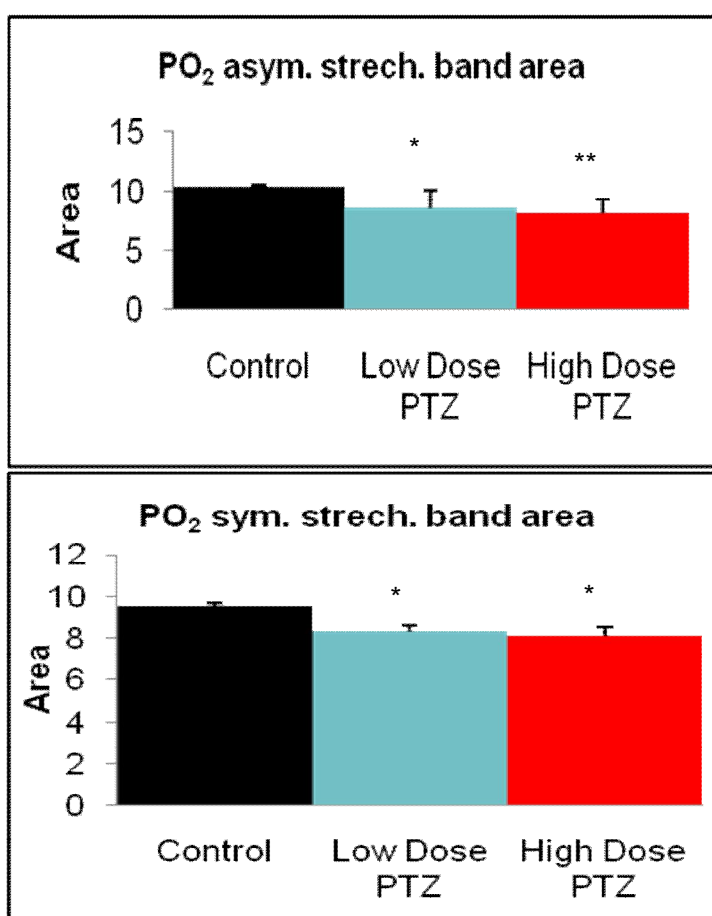
Figure 61. The band area values of PO_2 asymmetric and symmetric stretching for control, low dose and high dose of PTZ.
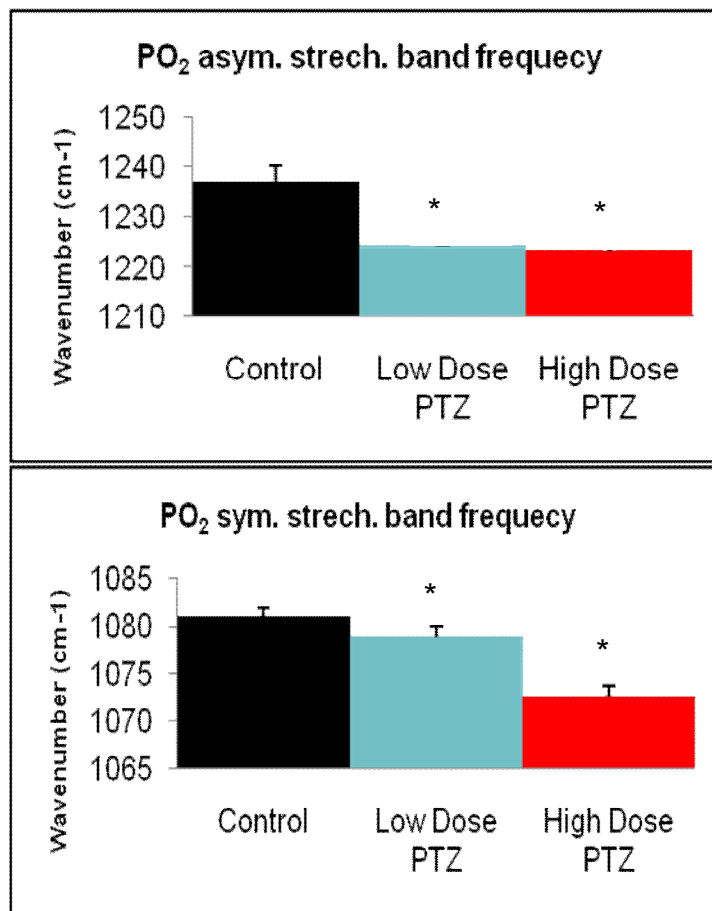
Figure 62. The frequency values of PO_2 asymmetric and symmetric stretching for control, low dose and high dose of PTZ.

3.2.1.1.2 The secondary structure determination for PTZ-induced seizures on rat brain cell membrane

By taking second derivative of amid I mode the various types of secondary structures of membrane proteins were obtained. Figure 63 shows its absorbance spectra for control and PTZ convulsions groups of cell membrane proteins. The changes in the intensities of characteristics components of this band were given in Appendix I. The band at 1682 cm^{-1} is from beta turns, the peak at 1652 is due to alpha helix, the peak located at 1643 cm^{-1} are assigned to random coil and the

band at 1633 cm^{-1} corresponds to beta sheet (Haris and Severcan, 1999; Lopez et al., 2001). As seen from Appendix I, low and high doses of PTZ led to a significant increase in the intensity of random coil ($p<0.05*$) and a significant decrease in the intensity of beta sheet and alpha helix of amide I band ($p<0.05*$) (Appendix F).
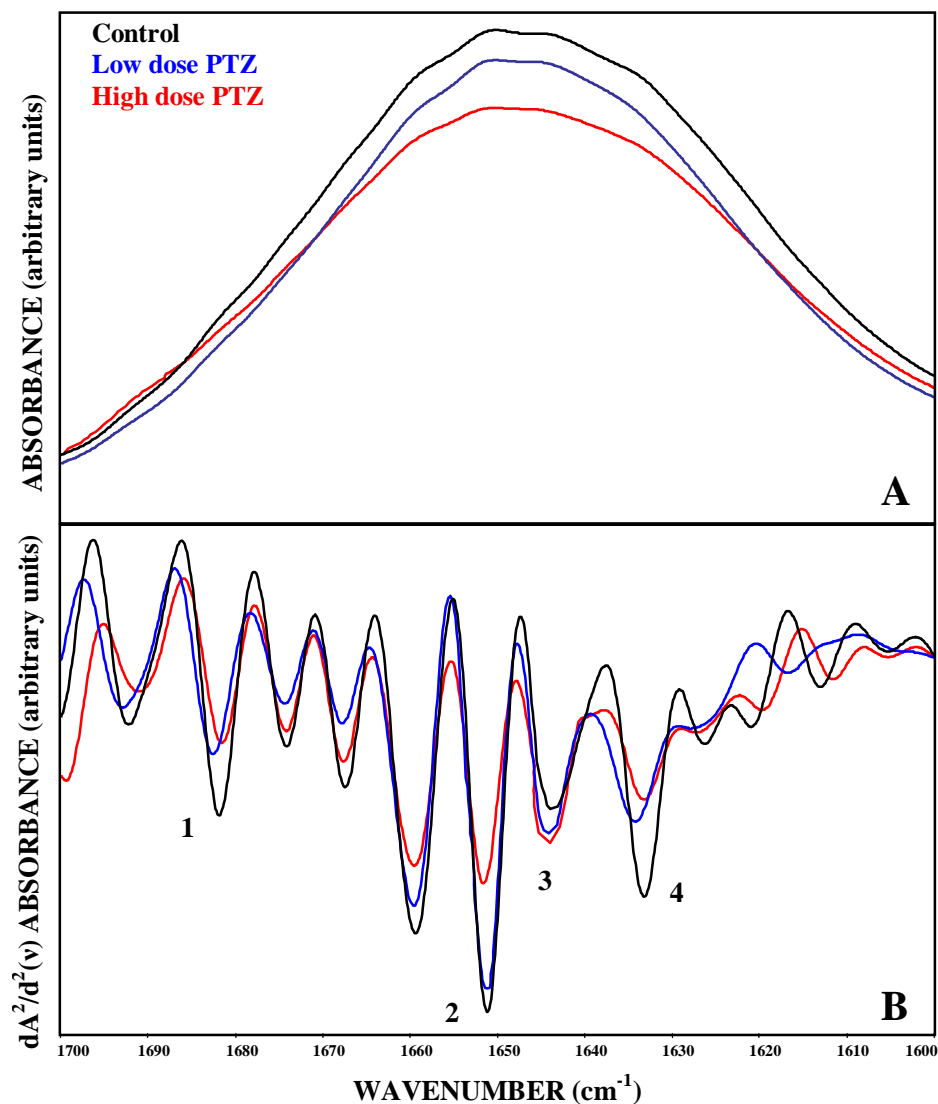
Figure 63. Representative (A) absorbance FTIR spectra and (B) the second derivative spectra of amide I band for control, low dose and high dose of PTZ for rat brain cell membrane in the 1700-1600 cm^{-1}. Vector normalization was done in the 1700-1600 cm^{-1} region. Absorption maxima appear as minima in the second derivatives.
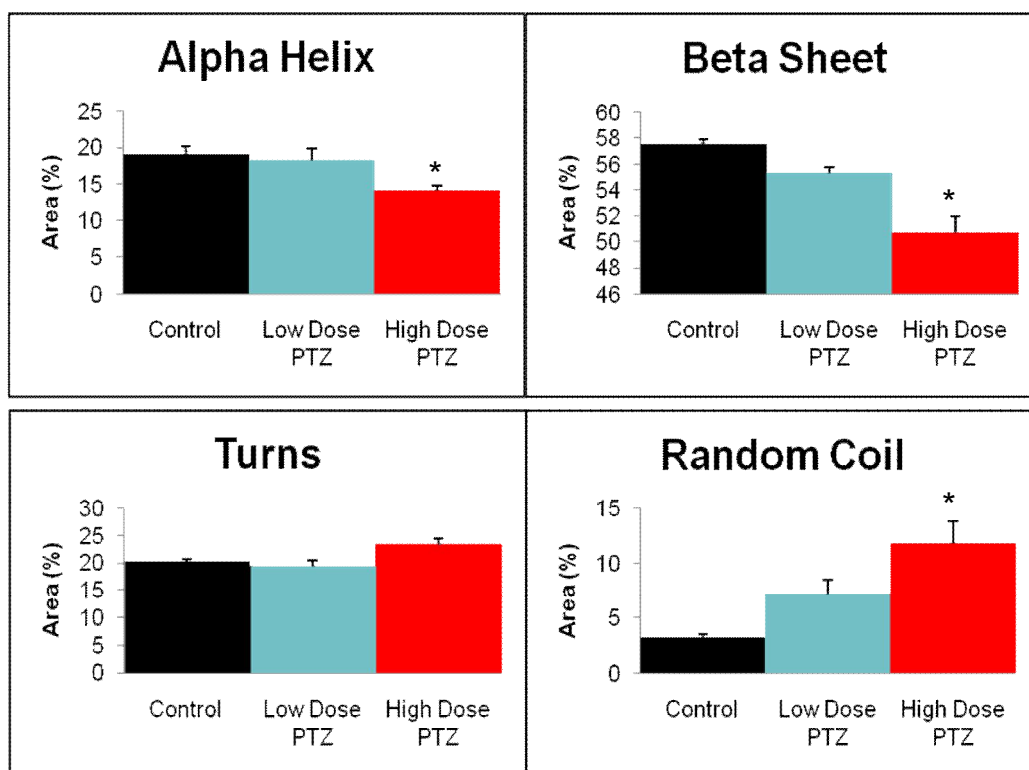
Figure 64. Neural network predictions for control, low dose and high dose of PTZ.

3.2.1.1.3 Atomic Force Microscopic Analysis of Brain cell membrane Samples

In order to obtain the effects of PTZ induced seizures on rat brain cell membrane the topographic imaging were obtained, therefore; morphological changes caused by PTZ induced convulsions on the surface of the brain cell membrane were evaluated. To achieve this, AFM imaging data were collected from all samples and after computitonal comparison the samples that showed the most similarity were obtained and topograhic data was elaborated. As seen from the figure below, there is morphological changes between control and high dose of PTZ samples.

Control

High dose of PTZ

Figure 65. Topography of the AFM image for the surface of the rat brain cell membrane for control and high dose of PTZ. Mean roughness of the surface is less than 0.5 nm over the scan length of 1.0 μm.
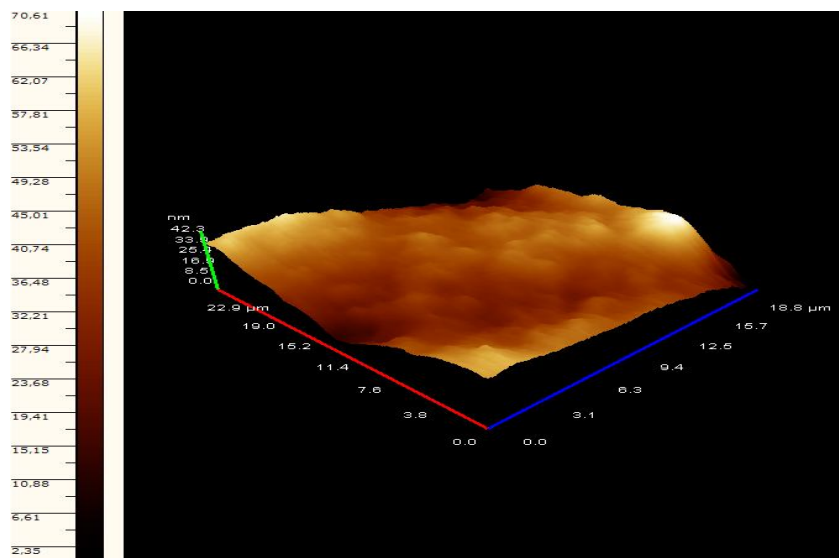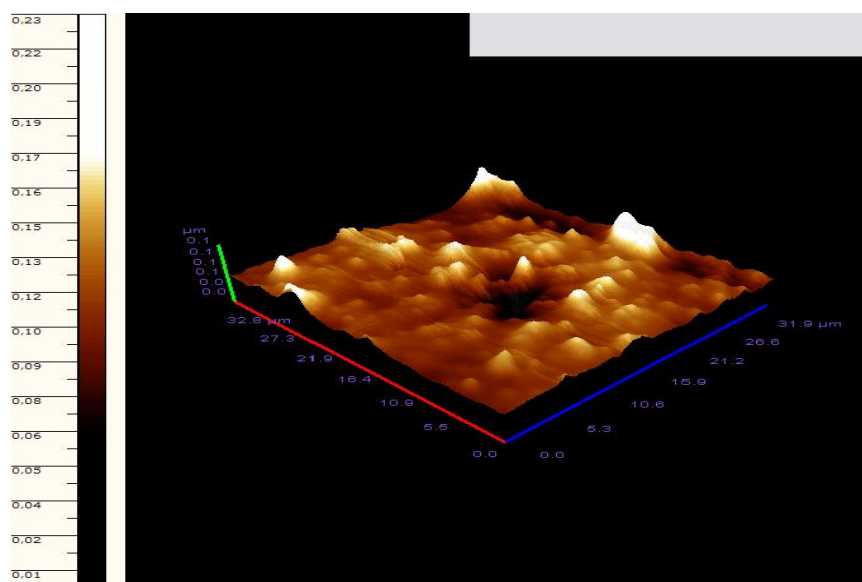
3.2.2 The effects of an antiepileptic agent VGB on epileptic rat brain cell membrane

In this part of the current study the effects of VGB on epileptic rat brain cell membrane have been investigated by using FTIR spectroscopy. To achieve this, three different groups were formed as control, epileptic (induced by 60 mg/kg of PTZ) and epileptic-VGB (100 mg/kg).

In order to elaborate spectral differences among the three different groups cluster analysis was also performed. Moreover, the changes in the protein structure were identified by the alterations in the intensities of sub-bands in the second derivative of the amide I band.

Based on these spectral differences then result of cluster analysis of control and PTZ treated groups was shown in Figure 66. As can be seen from the figure, three distinct clusters were produced with a high accuracy with success of (7/8) and (7/8), for epileptic-VGB and epileptic samples, respectively.
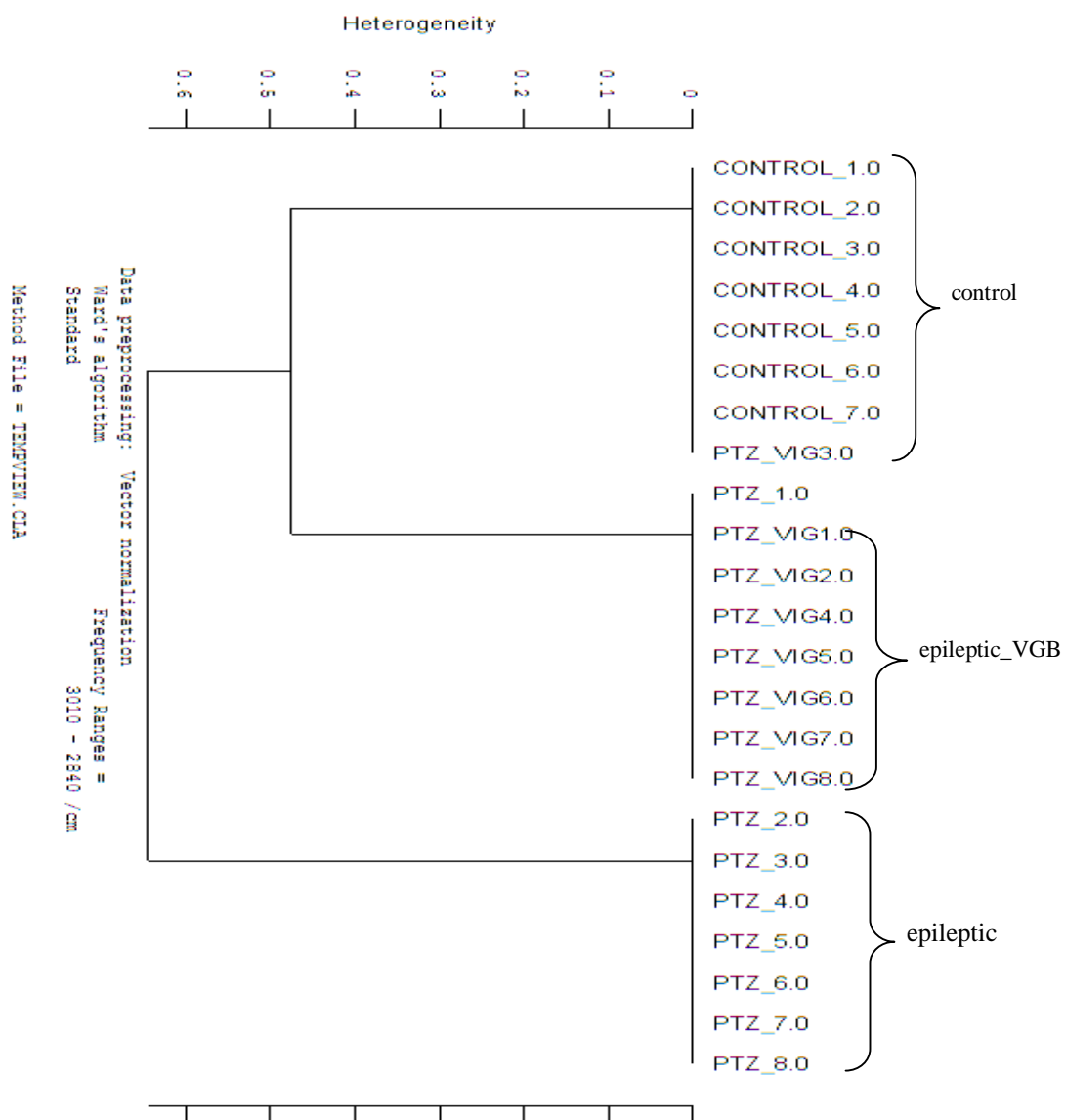
Figure 66. Hierarchial clustering of control, epileptic and epileptic-VGB in the 3010-2840 cm^{-1} spectral range. The sample labeled with * was not clearly differentiated and not used in the statistical analysis.

Figure 67 show normalized infrared spectra of control, epileptic and epileptic-VGB of PTZ rat brain cell membrane in 3050-2800 cm^{-1} region, respectively. The spectral bands were labeled in the figures and for detailed band assignments based upon the literature were used as given before for rat brain cell membrane. In Figure 67, the spectra were normalized with respect to the CH$_2$ asymmetric stretching band at 2925 cm^{-1}
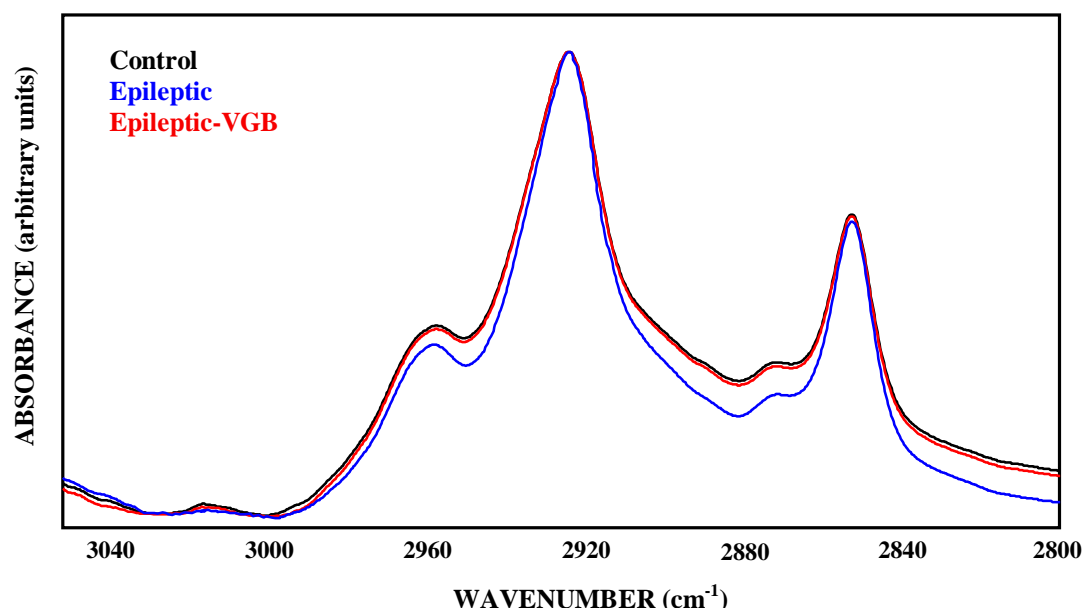

Figure 67. Representative FTIR spectra of control, epileptic and epileptic-VGB of brain cell membrane in the region between 3050-2800 cm^{-1}. The spectra were normalized with respect to the CH$_2$ asymmetric stretching at 2925 cm^{-1}.

As can be observed from Figure 68, the band area value of olefinic band significantly decreased for epileptic (0.34±0.01) (p<0.05*) but no significant variation was observed for epileptic-VGB (0.45±0.04) as compared to control samples (0.41±0.02).
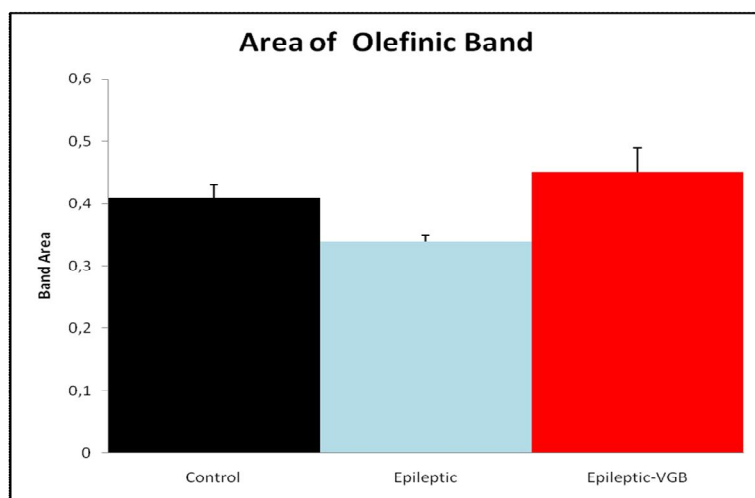
Figure 68. The band area values of control, epileptic and epileptic_VGB.

The CH_2 asymmetric and symmetric band area values also decreased significantly epileptic group, however, for epileptic-VGB group no how significant variation was observed as seen from Figure 69.

The changes in the bandwidth values of the CH_2 asymmetric and symmetric modes and the lipid to protein ratio for each group in were shown in Figure 69 and Figure 70. As seen from table, the bandwidth of the CH_2 asymmetric stretching mode and lipid to protein ratio values got closer to control groups for epileptic-VGB group (Appendix G).
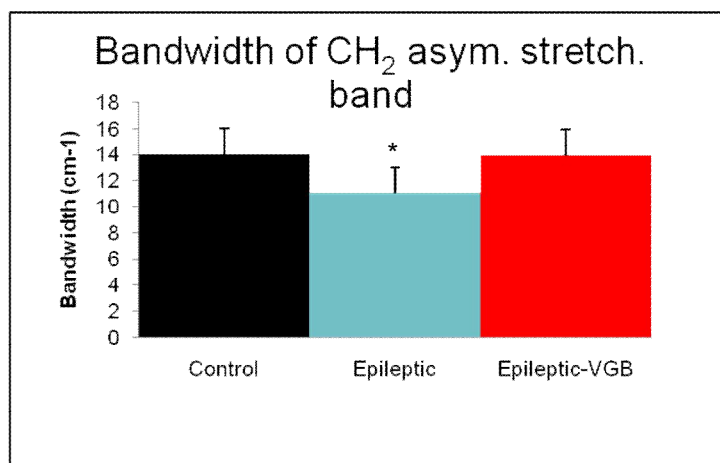
Figure 69. The bandwidth values of CH_2 asymmetric stretching mode for control, epileptic and epileptic_VGB groups.
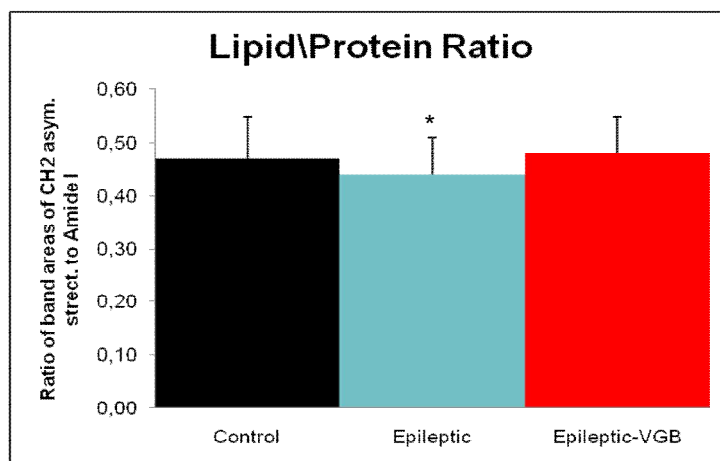
Figure 70. Lipid to protein ratio values for control, epileptic and epileptic_VGB groups.

It is seen from Figure 71 that, the area values of the C=O stretching, PO_2 symmetric and asymmetric stretching modes significantly lowered from control groups. However, after the application of VGB to epileptic these values got closer to the control groups. On the other hand, the frequency values of these bands significantly decreased for epileptic but no significant variation was observed for epileptic-VGB group (Appendix H).
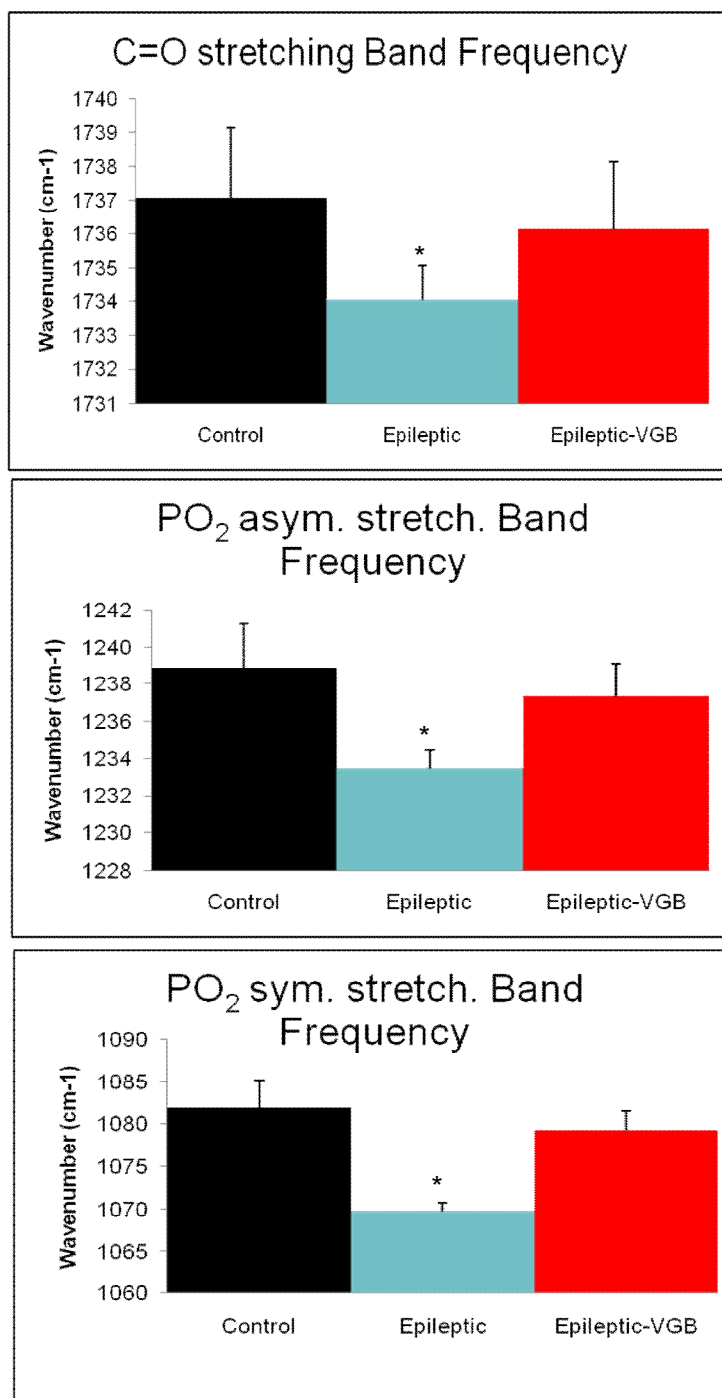
Figure 71. The frequency values of C=O stretching, PO_2 asymmetric and symmetric stretching modes for control, epileptic and epileptic_VGB.
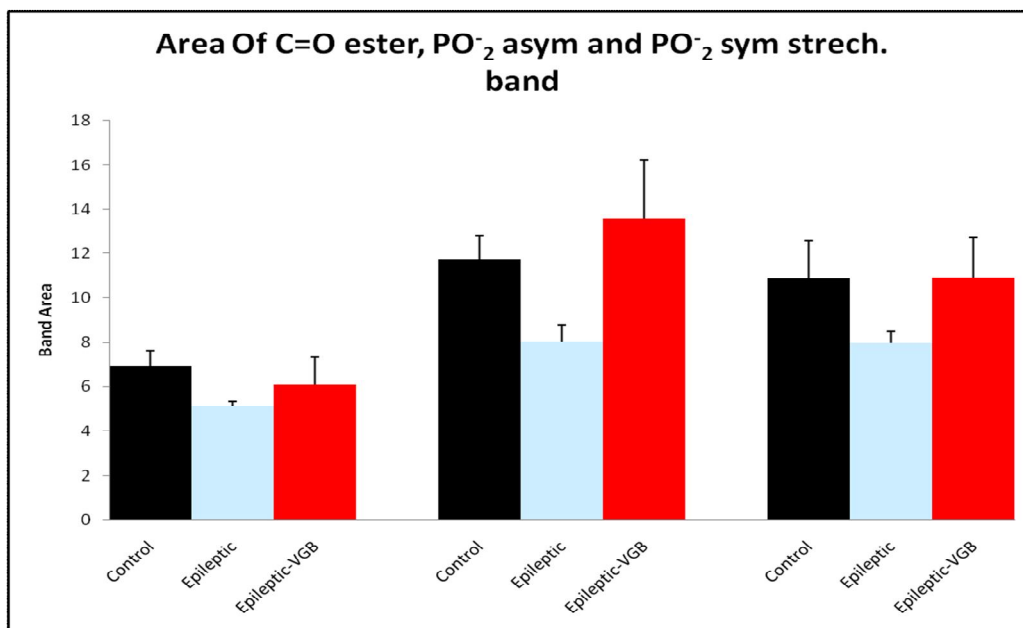
Figure 72. The band area values of C=O stretching, PO_2 asymmetric and symmetric stretching modes for control, epileptic and epileptic_VGB.

3.2.2.1 The secondary structure determination for VGB treatment on epileptic rat brain cell membrane

In order to study, the effects of VGB treatment on epileptic rat brain cell mebrane protein secondary structures, the second derivative spectra of amid I absorbtion mode was usedl . Figure 73 shows its absorbance and second derivative spectra for the control, epileptic and epileptic-VGB groups of cell membrane proteins. The changes in the intensities of characteristics components of this band were given in Appendix I. The band at 1682 cm^{-1} is from beta turns, the peak at 1652 is due to alpha helix, the peak located at 1643 cm^{-1} are assigned to random coil and the band at 1633 cm^{-1} corresponds to beta sheet (Haris and Severcan, 1999; Lopez et al., 2001).

With the treatment of VGB after epileptic condition the intensity of protein secondary structure remain significantly different from control groups, which shows VGB treatment might not affect secondary structure of membrane proteins.
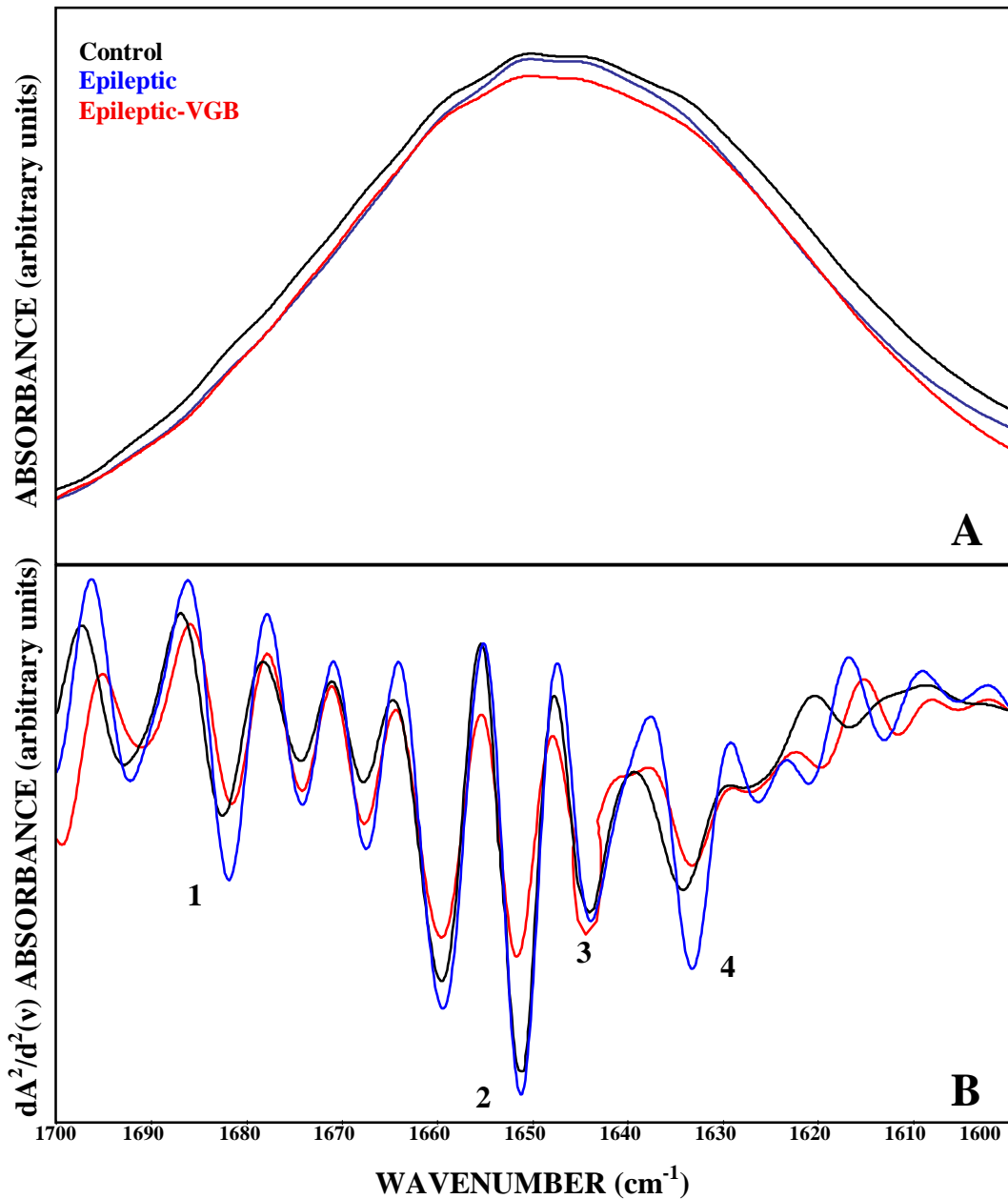
Figure 73. Representative (A) absorbance FTIR spectra and (B) the second derivative spectra of amide I band for control, epileptic and epileptic_VGB for rat brain cell membrane in the 1700-1600 cm^{-1}. Vector normalization was done in the 1700-1600 cm^{-1} region. Absorption maxima appear as minima in the second derivatives.
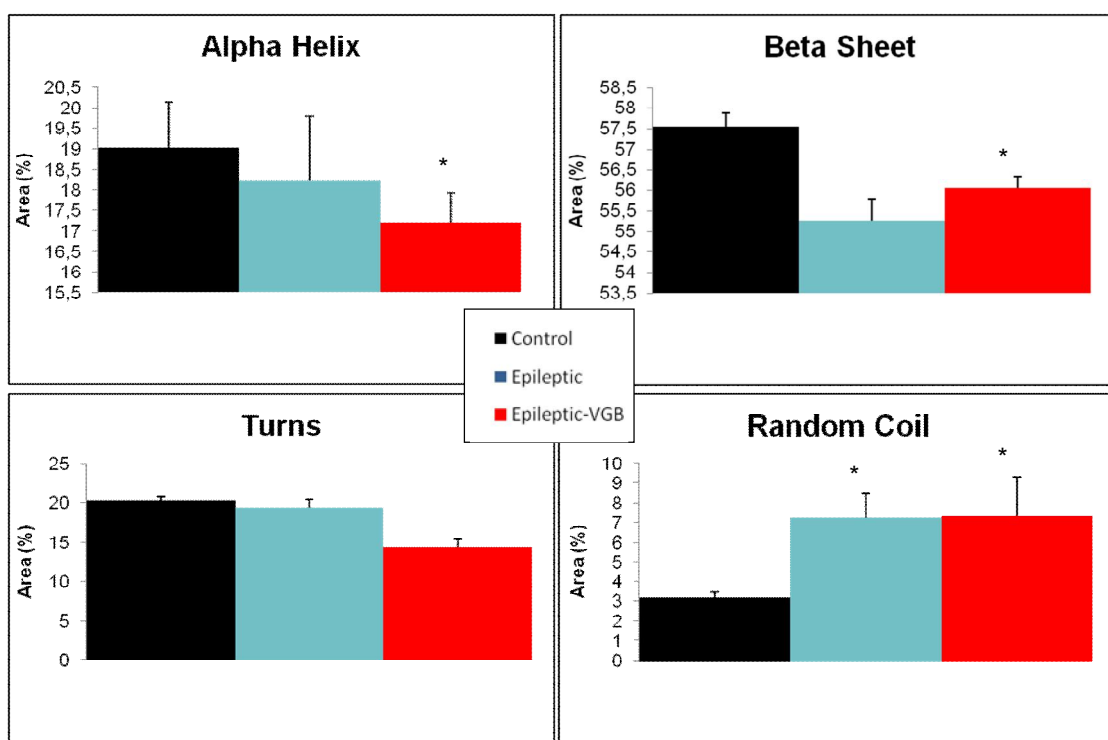
Figure 74. Neural network predictions for control, epileptic and epileptic_VGB.

CHAPTER 4

DISCUSSION

4.1 Model membrane studies

In this part of the study, the interaction of an epileptic agent PTZ and an antiepileptic agent VGB with DPPC MLVs has been investigated. To achieve this, the effetcts of these agents on the phase transition profile, order, dynamics and hydration states of the head and the region near the aqueous region of DPPC MLVs was studied, as a function of temperature and agent concentration. For this part of the study different spectroscopic and calorimetric techniques, namely, DSC, FTIR, ESR and steady-state fluorescence spectroscopy, were used.

In the current study, we were particularly careful in distingusihing between structural parameters describing molecular order and nature of hydrogen bonding and motion parameters, such as bandwidth and correlation time describing molecular dynamics, as suggested by others (Toyran and Severcan, 2003; Severcan et al., 2005; Korkmaz and Severcan, 2005; Severcan and Cannistraro, 1990; Van Ginkel et al., 1989).

4.1.1 Investigation of the interaction of PTZ with DPPC MLVs

PTZ is a convulsant agent widely used in clinical studies, however, it is not clear whether PTZ exerts its function through a direct interaction with membrane proteins or membrane lipids. In the literature, it has been suggested

that most drugs exert their effects through incorporation or penetration into cell membranes by modulating lipid bilayer properties, which in turn, may also affect membrane proteins. This lipid-mediated mechanism includes changing lipid dynamics (Baber et al., 1995), localizing at the membrane interface to modulate dipole potentials and modifying the forces between headgroup and hydrocarbon domains.

In our case, since PTZ is an uncharged, oil-soluble (Merck, Index, 1983) and amphipathic molecule, it was expected to interact with membrane lipids and diffuse into the cell membrane (Altrup et al., 2006). In addition, it has potential to modulate membrane lipids by altering the phase transition, fluidity and order/disorder state (Chalazonitis et al., 1978; Altrup et al., 2006). For this reason, in the current study, we aimed to understand whether or not PTZ interacts with membrane lipids. Cell membrane consists of many different types of lipids; therefore, due to its complexity it is difficult to characterize it (Hauser et al., 1992). For that reason, we used a simplified model membrane system comprised of DPPC MLVs, which are widely used in biological studies (Huang et al., 1999; Severcan et al., 2005; Korkmaz et al., 2005). To the best of our knowledge, we for the first time investigated the effect of PTZ on lipid phase transition profile, lipid order, lipid dynamics and hydration states of the head and the region near the aqueous region of DPPC MLVs, as a function of temperature and PTZ concentration varying from 1-24mol%.

DSC studies revealed that the presence of PTZ caused a pertubation of ripple phase since there was a broadening in the pretransition curve. This suggests that there might be slight influence of PTZ at the surface of the phospholipid vesicles. However, since the pretransition is highly sensitive to the presence of other molecules in the polar region of the phospholipids, the broadening of pretransition with the presence of PTZ cannot be attributed to any specific molecular change as reported by Balasubramanian et al., (1994). On the other hand, no change in the main transition curve was observed at even high concentrations of PTZ. This means that PTZ does not penetrate into the hydrophobic core of the bilayer. However, since the DSC method detects the heat absorbed by the entire bilayer, it gives only bulk information on the thermotropic

properties, but not the detailed dynamic behavior of different regions in the bilayer (Sergio et al., 2005).

In order to corraborate the information about the effect of PTZ on the phase transition behavior of DPPC MLVs, FTIR spectroscopy, which is a a non perturbing technique, was employed by monitoring the frequency variations of the C-H stretching modes. As seen from Figure 19, with the additon of PTZ, at even high concentrations, neither the shape of the phase transition curve nor the main phase transition temperature changed, which are in agreement with the DSC results. Any possible PTZ-induced change in the shape of the main phase transition provides further information on the hydrophobic location of the agent in the bilayer matrix. Any alterations in the shape of the phase transition, such as broadening, would be expected if the agent is localized in the outer hydrophobic cooperative zone of the bilayer, i.e. in the region of the C2-C8 carbon atoms of the acyl chain (Jain et al., 1977; Korkmaz et al., 2005; Sabin et al., 2006; Hendrich et al., 2007;). In short FTIR and DSC studies revealed that PTZ does not penetrate into the bilayer and does not localize in the bilayer.

FTIR spectroscopy was further used to obtain information about lipid order, and dynamics, and the hydration state of the head group and glycerol backbone close to the aqueous interface. Infrared spectral parameters, such as the frequency and bandwidth, are sensitive to the structural and dynamic properties of membrane lipid molecules (Liu et al., 1999; Toyran and Severcan, 2003). The changes in the order-disorder state of DPPC MLVs due to the presence of PTZ were studied by analyzing of the CH_2 asymmetric strecthing mode frequency (Moore et al., 1995; Severcan et al., 2005). The wavenumber values below the main phase transition temperature for DPPC is characteristic of conformationally ordered acyl chains with a high content of trans isomers, whereas, the values at temperatures above the main phase transition is of conformationally disordered acyl chains with a high content of gauche conformers (Severcan, 1997). As observed from the figure, there was no change in the frequency values of this band with the addition of PTZ in either the gel or liquid crystalline phases and this implies that the number of trans/gauche conformers did not change, indicating that PTZ does not cause any alteration in the order/disorder state of DPPC MLVs in

either phase (Korkmaz et al., 2005; Toyran and Severcan, 2003). These results were further supported by ESR spectroscopy using the spin label 5-doxyl stearic acid, which gives information about membrane order in the upper part of the lipid chain (Figure 20, Table 4).

Membrane fluidity is an important parameter for the proper functioning of cell membranes, which in turn, influences cellular processes and disease states (Owen et al., 1982; Chakravarti et al., 1989). Therefore, we investigated the effect of PTZ on the dynamics (fluidity) of DPPC MLVs by FTIR, ESR and steady state fluorescence spectroscopy.

In the FTIR experiments, the variations in the bandwidth of the CH_2 asymmetric stretching band was used to attain information about the dynamics of the system (Severcan et al., 2005; Toyran and Severcan, 2007). As seen from Table 5, PTZ did not exert significant effect on the fluidity of DPPC MLVs in both the gel and crystalline phases.

In the ESR spectroscopic studies, we used the spin label 16-doxyl stearic acid that provides information on the rate of acyl chain motion in the lower portion of the chain towards the center of the membrane (Severcan and Cannistraro, 1990; Wassall et al., 1992). According to the ESR data, which is in agreement with our FTIR results, membrane dynamics was not altered significantly in the presence of PTZ.

The polarization values of DPPC MLVs containing different concentrations of PTZ indicated that PTZ has no significant effect on the fluidity (dynamics) of DPPC MLVs. This also supports the results of ESR and FTIR spectroscopy.

The interaction of PTZ with the glycerol backbone near the head group of phospholipids in the interfacial region and with the head group was studied by monitoring the frequency changes of both the C=O ester stretching (1730 cm^{-1}) mode and the PO$^-_2$ asymmetric double stretching mode (1230 cm^{-1}). According to the empirical rules, a decrease in these frequencies indicates an increase in the strength of hydrogen bonding whereas an increase in the frequency corresponds to dehydration (Lewis et al., 1990; Severcan et al., 2005; Korkmaz et al., 2005). According to the FTIR data, both in the gel and liquid crystalline phases,

the frequency values of these bands were not altered with the presence of PTZ. Although the solubility of PTZ in water suggests a potential to form a hydrogen bond (or hydrogen bonds), the FTIR results revealed that the agent does not form hydrogen bonds with either the glycerol backbone or the head groups of membrane phospholipids.

As a result, our data does not support previous studies, in which membrane lipids were assumed to be the primary site of PTZ action mechanism during the development of epileptic activity (Madeja et al., 1996; Altrup et al, 2006). In these studies, PTZ was suggested to modify membrane lipids and consequently alter membrane protein functions indirectly. In order to affect protein function indirectly, PTZ should interact either with the lipid-water interface or with the hydrophobic core of the phospholipid bilayer. This kind of distribution within the membrane would induce an inhomogeneous increase in the lateral pressure profile, which in turn would specifically affect the activity of membrane proteins. However, it is difficult to accept this model for PTZ action mechanism because the location of PTZ within the membrane is still not known. According to our FTIR and DSC results, PTZ neither penetrates into the cooperativity region (C2-C8) of fatty acyl chains, nor does it disturb the Van der Walls interactions between hydrocarbon chains of phospholipids. Therefore, it could not modify the packing of hydrocarbon acyl chains, since we did not observe any broadening in the phase transition curve. Moreover, although PTZ is expected to be located in the aqueous site, it does not interact with the glycerol backbone and head groups of phospholipids, revealed by FTIR spectroscopy. As suggested by Altrup et al., (2006) in order to influence membrane proteins, PTZ should be incorporated with membrane lipids and thus lead to a disturbance in membrane fluidity. However, according to our ESR, FTIR and steady state fluorescence data, PTZ does not affect membrane fluidity.

According to previous findings, PTZ was suggested to penetrate the cell membrane and affect the GABAa receptor (Bloms-Funke et al., 1996) and $Na^+\backslash K^+$ pump (Dubberke et al., 1998) at the intracellular site of the membrane. Contradictory to these studies, the current study clearly showed that the passage of

PTZ through the cell membrane seems to be nearly impossible, as it does not cause any perturbation in the structural and dynamical properties of DPPC MLVs.

Consequently, although in some earlier studies the findings stated the PTZ interacts with membrane lipids in order to induce epileptic activity, our results showed that there is no interaction between PTZ and membrane lipids. This means that any modulation in the properties of the lipid bilayer might not be due to the action mechanism of PTZ while generating epileptic activity.

4.1.2 Investigation of the interaction of VGB with DPPC MLVs

In pharmacology, drug distribution in the body is very important, which means that the plasma concentration of a drug may not reflect its clinical effect throughout the body. The interaction of VGB with cell membranes is a prerequisite for it to be transfered in the human body because, as a drug consumed orally, it requires the absorption in mouth and intestine, elimination by hepatocytes in the liver, reabsorption through the tubular membranes of the kidney, and the distribution across BBB. Therefore, it is important to evaluate or predict membrane interaction of VGB for its distribution profile in the body. For that reason, we evaluated the capability of VGB to interact with the cell membrane, which is directly related to the degree of incorporation and the distribution of VGB into lipid bilayer (Saija et al., 1995; Castelli et al., 2001). In our case, since VGB is uncharged, has low molecular weight and does not bind to plasma proteins (Richens, 1991; Ben-Menachem, 2002), it was expected to interact with membrane lipids and diffuse into the cell membrane. For this reason, in the present study we investigated, for the first time, the effects of different concentrations of VGB on the hydration state of phospholipids, lipid dynamics (fluidity), lipid acyl chain flexibility (ordering) and phase behavior properties of DPPC MLVs by FTIR, DSC, ESR and steady state fluorescence spectroscopy.

According to the FTIR data, as seen in Figure 27, a decrease in the order of the bilayer in the gel phase, but no effect on the order of DPPC MLVs in the liquid crystalline phase was observed in the presence of VGB. These results in the liquid crystalline phase were further supported by ESR spectroscopy.

The effect of VGB on the dynamics (fluidity) of DPPC MLVs was investigated by means of FTIR, ESR and steady state fluorescence spectroscopy, all of which revealed that VGB induces a fluidifying effect on the membrane.

DSC, which enables the characterization of the thermotropic phase behavior of the lipid bilayer and determination of the interaction of drugs with artificial membranes, was used to investigate the effect of VGB on the phase behavior of DPPC MLVs. The presence of VGB with varied concentrations may cause, depending on their structural features, significant variations in the thermodynamic parameters associated with lipid phase transition, such as transition temperature, enthalpy changes and cooperativity units (Jain and Wu, 1977; Jain, 1988; Castelli et al., 1989). DSC results revealed that in the presence of the VGB, there is perturbation of the ripple phase. This suggests that there might be a slight influence of VGB at the surface of the phospholipid vesicles, which may be due to the strong hydrogen bonding between VGB and phospholipid head groups and the glycerol backbone. On the other hand, although the presence of VGB does not alter the shape of the main transition curve, there is a slight change in the main transition temperature that did not alter the general shape of the transition profile. The detailed analysis of thermograms belonging to VGB-DPPC showed that VGB induced slightly changes on both the enthalpy and the cooperativity of the gel to liquid crystalline transition for DPPC MLVs. This result was supported with FTIR spectroscopic studies on the CH vibrations. As a result, our data revealed that VGB does not penetrate into the bilayer and does not localize in the outer hydrophobic cooperative zone of the bilayer, i.e. in the region of C2-C8 carbon atoms of the acyl chain (Liu et al., 1999; Sabin et al., 2006) since no alteration in the shape of the phase transition, such as broadening, was observed. On the other hand, a slight but not significant change in the cooperativity units in the presence of VGB implies that VGB itself is not enough to lead to the break down of the van der Waals forces between lipid molecules. In other words, VGB does not insert itself into the deep interior of the membrane by disturbing the strong hydrophobic interactions between lipid molecules and does not cause any significant effect on the transition ΔH values of DSC curves.

FTIR spectroscopy enables us to monitor the hydrophilic part of the bilayer, i.e. the head group and the region closer to the polar head group of

phospholipids (Severcan et al., 2000). We observed that VGB strengthens the hydrogen bonding of the C=O groups and PO_2^- head groups of phosholipids in both gel and liquid crystalline phases. In our case, the VGB molecule is defined by a high degree of flexibility and due to the presence of carboxylic (C=O) and amino (N-H) groups, it can give rise to hydrogen bonding (Sadlej-Sosnowska et al., 2002). these bonds can occur in between the C=O groups and PO_2^- groups of DPPC and either with the N-H groups of VGB or water molecules around these functional groups (Casal and Mantsch, 1987; Toyran et al., 2003). As a result, we have found that VGB strongly interacts with the glycerol backbone and head groups of phospholipids and affects order and lipid dynamics. However, in order to attain complete absorption and distribution of VGB throughout the body, not only its lipid-solubility, but also its water-solubility is very important in order for it to reach the intended site of action. In other words, VGB has to partition between the lipid biomembranes and the aqueous biological fluids, although the constituents of membranes vary from one to another (Abraham et al., 1994; von Geldern et al., 1996). VGB has been reported that it reaches the brain with lesser extent. This may be due to lower liposolubility at physiological pH. The pKa of VGB is 9.5 (Jung et al., 2001). Furthermore, it has been also stated that GABA-AT inhibitors, such as VGB in the current study, do not freely cross the BBB and distribute into the brain because they contain hydrophilic functional groups (e.g., a free carboxylic acid group and a free amino group) (Camenisch et al., 1996; Yoon et al., 2001), as revealed by the current study.

As a result, our data is in aggreement with studies, in which VGB was reported to have a potential to interact with membrane lipids in order to transfer itself into the body and to reach its target organ. In these studies, VGB was suggested to completely disperse/diffuse into the cell membrane (Frisk-Holberg et al., 1989; Ben-Menachem et al., 1989; Jung et al, 1977; Nanavati and Silverman, 1991; Tong, 2007). In order to support this conclusion, inhomogenous increase of the lateral profile would be induced, however, our FTIR and DSC revealed that VGB neither penetrates into the cooperativity region (C2-C8) of fatty acyl chains nor does it disturb the Van der Wall's interactions between the hydrocarbon chains of phospholipids. Therefore, it is not possible for VGB to modify the

packing of the hydrocarbon acyl chains, since we did not observe any broadening in the phase transition curve.

Our result reveal that VGB has the potential to interact with membrane lipids but it does not penetrate freely. This might mean that VGB does not show complete distribution and absorption into the body. This could be a plausible explanation for the differences in VGB distribution in different parts of the brain, such as the frontal cortex concentrations being substantially greater than those seen in the hippocampus (Tong et al., 2009).

Consequently, our data support the studies stating that for the complete distribution of VGB into the body, it is highly probable that it also uses specific transporters as routes other than only interacting with membrane lipids to reach its target organ (Abbot et al., 2006; Wu et al., 2004; Berezowski et al., 2004; Eckstein-Ludwig et al., 1999).

4.2 Animal studies

4.2.1 The effects of PTZ-induced convulsions on rat brain homogenate and cell membranes

FTIR spectroscopy monitors the changes in relative concentration, composition, structure and function of macromolecular constituentsin biological samples, rapidly and simultaneously (Dogan et al., 2007; Cakmak et al., 2006). Taking advantages of this property of the technique, the current study is conducted to determine the effects of subconvulsive (25 mg/kg) and convulsive (60 mg/kg) dose of PTZ-treatment on rat brain homogenate and cell membranes by monitoring the variations in the frequencies, bandwidths and peak areas of the vibrational modes of macromolecules. Moreover, we used FTIR microscopy to obtain chemical data of brain homogenate samples based on lipid to protein ratio. In addition, the protein secondary structure was predicted using neural networks based on FTIR data and the level of lipid peroxidation was determined by TBAR assay to support FTIR data. Furthermore, the epileptic convulsions induced morphological changes on brain cell membranes were monitored by AFM.

For homogenate and cell membrane samples, cluster analysis based on the FTIR spectra at the specific regions were performed successfully to differentiate control, convulsive and subconvulsive epileptic groups. This finding revealed that epileptic activities stimulated by low and high doses of PTZ administration both causes important changes in FTIR spectra, which can be effectively determined by the application of cluster analysis (Figure 33 and Figure 39).

Oxidative stress is defined by the excessive production of free radicals (Dal-Pizzol et al., 2000). Free radicals act via peroxidation of membrane lipids, inactivation of enzymes, depolymerization of polysaccharides and disruption of nucleic acids. Brain is highly sensitive to free radical damage due to its high rate of oxidative metabolism and high concentration of lipid content, especially polyunsaturated fatty acids (Reiter et al., 1993). The unsaturated lipids, which are present both in cell and mitochondrial membranes, readily react with free radicals and undergo peroxidation. Lipid peroxidation induces alterations in the structure and function of membranes. Our group has recently shown that the olefinic band located at 3012 cm^{-1} can be used for the rapid monitoring of lipid peroxidation (Severcan et al., 2005). When compared with other spectrophotometric methods, FTIR spectroscopy is more advantageous for the determination of lipid peroxidation, due to its simplicity, speed, and sensitivity (Severcan et al., 2005b). Loss of unsaturation during lipid peroxidation reactions was compensated by the presence of double bonds in the lipid peroxidation products such as MDA,. Therefore, instead of observing a decrease in the intensity of the olefinic band we observed an increase due to the accumulation of end products of lipid peroxidation (Liu et al., 1999; Severcan et al., 2005b). In the present study for the homogenate samples, we observed a significant ($p<0.05*$) increase in the area of the olefinic band in both PTZ-treated groups, which is resulted from the accumulation of lipid peroxidation end-products, such as lipid aldehydes malonydialdehyde (MDA), lipid aldehydes and alkyl radicals (Severcan et al., 2005). This increment in the olefinic band area was accompanied by a decrease in the areas of the CH_2 and the P=O stretching vibrations (Dogan et al., 2007), which reveals that both subconvulsive and convulsive doses PTZ-induced epileptic activity led to lipid peroxidation in rat brain.

130

For cell membrane samples, as can be seen from Figure 35 and Table 14, there is significant decrease in the band area of olefinic band ($p < 0.05*$). However, since lipid peroxidation products are present in cytoplasm, these products are discarded during cell membrane preparation. For that reason, we could not observe any increase in the olefinic band area of PTZ-treated cell membrane samples compared to control. The decrease in the olefinic band area reflects only degree of unsaturation in membrane lipids because of epileptic activities.

In accordance with our FTIR results, the level of lipid peroxidation measured by TBARs assay for homogenate samples. TBAR assay has been well accepted for the measurement of lipid peroxidation and oxidative injury in a variety of biological samples such as liver and brain homogenate (Dawn-Linsley et al., 2005; Meagher and Fitzgerald, 2000). By using this method, MDA level, which is an end product of lipid peroxidation, can be readily determined (Pothiwong et al., 2007). Therefore, the quantity of oxidative stress by PTZ-induced seizures can be estimated by using TBAR assay. According to the results of TBARs test lipid peroxidation level was also increased in PTZ-treated groups. Our data concerning the increase in lipid peroxidation due to PTZ administration correlate with the results of earlier studies that investigate different parts of the brain (Bashkatova et al., 2003; Patsoukis et al., 2005) as well as other models of seizures (Bellissimo et al., 2001; Yamamoto and Tang, 1996). On the other hand, we were not able to apply TBARs assay for cell membrane samples because lipid peroxidation products have been discarded for sample preparation.

Seizure-induced lipid peroxidation might be the outcome of some processes, such as dysfunction of mitochondrial respiratory chain (MRC) and the production of arachinoid acid (AA) during high rate of neuronal activity. Mitochondrial respiratory chain, which is located in the mitochondrial membrane, is the major source of reactive oxygen species (ROS) and nitric oxide (NO) in cells (Cadenas et al., 1997). The attack of ROS to lipids in mitochondrial membrane together with the interaction of NO with cyctochrome c oxidase, complex II and III, leads to defected oxidative phosphorylation; thus, respiration and ATP synthesis are blocked (Brookes et al., 1999. The inhibition of oxidative phosphorylation coupled with increased utilization of energy during epileptic activity interrupts the cell's capability to maintain energy levels, subsequently,

causing mitochondrial damage. Lipid peroxidation induced mitochondrial dysfunction, defected oxidative phosphorylation and reduced energy levels during seizures have been reported by researches (Ueda et al., 1997; Grupta et al., 2001; Archaya and Katyare, 2005) Nevertheless, MRC dysfunction along with elevated free radicals could also trigger the apopototic pathways in the epileptic condition (Cock, 2002).

There is another possible explanation for the source of lipid peroxidation during epileptic convulsions. Throughout high neuronal activity, the release of the excitatory neurotransmitters, such as glutamate, takes place (Adibhatla et al., 2000). With the release of glutamate, glutamate neuronal receptors are initiated, which in turn elevates intracellular Ca^{+2} levels and activates phospholipases, such as phospholipase A_2 (PLA). Activated phospholipases form arachidonic acid by the breakdown of membrane phospholipids, to enhance further glutamate release as well as depolarization-evoked Ca^{+2} accumulations (Adibhatla et al., 2006; Freeman et al., 1990; Ruehr et al., 1997). Afterwards, AA is metabolized to produce prostaglandins, leukrotines and ROS. ROS produced by AA metabolism generate lipid peroxides like MDA, which covalently bind to cellular proteins and alter their function (Nigam, 2000). In addition, AA can also stimulate sphingomyelinase to produce ceramide, inhibiting the mitochondrial electron transport chain and releasing cytochrome c, which also supports mitochondrial dysfunction (Garcia-Ruiz et al., 1997; Ghafourifar et al., 1999). Hence, the over production of ROS causing lipid peroxidation has been related to contribute to membrane malfunction, excitotoxicity, neuronal injury and cell death in both long term (Frantseva et al., 2000; Patel et al., 2001) and short term seizure activity (Akbas et al., 2005; Bashkatova et al., 2003).

Since there is close relationship between lipids and diseases, in recent years, many studies have been devoted to study the changes in lipid metabolism under disease conditions. The evidences have shown that abnormal lipid metabolism is involved in the pathogenesis of epilepsy (Ma et al., 1999). The results of the current study also demonstrated that PTZ-induced seizures altered lipid metabolism, revealed by the observed changes in both the peak areas and frequencies in the lipid bands. The changes in the area of the olefinic band for both homogenate and cell membrane samples might also imply the altered lipid

metabolism induced by epileptic activity (Cakmak et al., 2006). This result was confirmed by the decrease in the areas of the C=O stretching band originating from cholesterol esters, the PO_2^- symmetric and asymmetric stretching bands belonging to phospholipids and the COO^- symmetric stretching band assigned to fatty acids (Jackson et al., 1996; Melin et al., 2000; Cakmak et al., 2003; Cakmak et al., 2006). These alterations may also be the consequences of the breakdown of these groups and damage caused by ROS during epileptic activity. Especially, the reduction in the amount of membrane phospholipids observed in the current study, can also be caused by the activation of phospholipases with a high rate of neuronal activity. During this process, phospholipases use membrane phospholipids as reservoirs to release the second messengers, such as AA, as mentioned above. Besides, it was also demonstrated that AA may also lead to an increase in sphingomyelinase activity, thereby causing demyelination, which is observed in epileptic conditions (Bloom et al., 2002). In addition, Cenedella et al (1984) reported that the administration of U18664, which is the initiator of chronic seizures, decreased the concentration of brain phospholipids through inhibition of phospholipid synthesis. The changes in the synthesis of brain phospholipids could alter both the structure and function of the membranes, which is proposed to be the basis of epileptic activity. As a result, the changes in the lipid content of brain following different doses of PTZ administration might contribute to the generation of epileptic seizures since lipid molecules play several significant roles in the regulation of membrane functions. This alteration in lipid profile was also shown to be present in PTZ-induced kindled seizures (Ma et al., 2007). The presence of these perturbations in lipid content could be a precondition for the development and expression of this disorder (Cenedella et al., 1984) as found in the current study.

As observed in both homogenate and cell membrane samples, the shifting of frequencies of the C=O stretching band, the PO_2^- asymmetric and symmetric modes to lower values, which is more profound for convulsive dose of PTZ, imply that PTZ induced epileptic activity led to an increase in the hydration state of the glycerol backbone near the hydrophilic part and polar head group of the membrane lipids, respectively.

The hydrogen bonding might be between water molecules and the oxygen molecules of both carbonyl and phosphate groups of phospholipids (Akkas et al., 2007a). This may create a difference in packing of phospholipid molecules (Cakmak et al., 2006). In the investigation of the interaction of PTZ and DPPC MLVs we could not observe any potential hydrogen bonding between PTZ and phospholipids. This means that the hydrogen bonding observed in the animal studies is only resulted from epileptic activity not from PTZ itself. The alterations in the packing of phospholipids have been reported to originate from the reaction between free radicals and membrane proteins or lipids, which may increase a cross-linking between these membrane components (Phillis et al., 2006). It has been reported that altered composition of membrane phospholipids results in the changes in the activity and kinetic parameters of membrane proteins, such as synaptic Mg^{+2}, Ca^{+2}-dependent ecto-ATPase, which primarily have an important role in neuronal activity. The decrease in the activity of Ca^{+2} and Mg^{+2} pumps cause a further decrease in neuronal energy, which is suspected to play a particular role in seizure-related neuronal damage (Walton et al., 1999).

The disruption of membrane organization is directly associated with the decrease in membrane fluidity, which is observed by a decrease in the bandwidth values of the CH_2 asymmetric and symmetric stretching modes (Toyran and Severcan, 2003; Korkmaz and Severcan, 2005). Decreased membrane fluidity leads to activity changes or inhibition of membrane-bound enzymes, ion channels, and receptors (Ray et al., 1994). This would make it difficult for the cell to carry out its normal functions and would increase the cell's susceptibility to injuriy and death. In addition, the difference in membrane fluidity together with the changes in packing of membrane phospholipids may explain the dysfunction of glucose transporters in the structure of blood brain barrier (BBB). As a result of the alterations in the activity of glucose transporters, cerebral blood flow does not match the metabolic demand. Thus, apparent net energy impairment occurs in brain. This energy failure can give rise to the loss of ionic homeostasis, which is considered to be one of the important effects generating epileptic activity. It has been reported that especially potassium ion homeostasis plays a crucial role to

initiate the epileptic activity in brain. It is likely that Na/K ATP-ase mechanism other than voltage-dependent potassium uptake provides efficient potassium buffering, which produces an increase in metabolic demand due to the ATP requirement of the pump (Mata et al., 1980; Bruehl et al., 1998). All of the listed events that take place in neuronal activity trigger the uncoupling of metabolic demand and expenditure. This energy impairment may accelerate a variety of mechanisms underlying epileptic activity, such as decreased uptake of excitatory neurotransmitters and decreased inhibition of neuronal depolarization (Janigro et al., 1999).

In homogenate samples, we have found slight but not significant decrease in the frequency values of CH_2 asymmetric stretching and CH_2 symmetric stretching. However, as seen from Figure 40 and Table 15 in cell membrane samples there are significant increases in both CH_2 asymmetric stretching and CH_2 symmetric stretching frequency values for PTZ-treated samples compared to control samples ($p < 0.05^*$). This implies that PTZ cause significant change in the order of the different type membranes structure. Different than cell membranes, homogenate samples contain all crude membrane structure present in brain cells therefore we may observe different behaviour in the order in comparison to cell membranes. The variations in amounts of proteins and lipids in the membranes, which can be monitored by the lipid to protein ratio, have a very important effect on membrane structure and dynamics (Szalontai et al., 2000). A decrease in the lipid to protein ratios in PTZ-treated groups for both homogenate and cell membrane samples suggests a decrease in the lipid content or an increase of proteins in the brain after PTZ-induced epileptic activity, or both (Jackson et al., 1998; Toyran et al., 2004). There was a decrease in both lipid and protein content of PTZ-treated groups but the degree of decrement in lipids was higher than that of lipids. The decrease in the lipid to protein ratio initiates changes in membrane fluidity altering the membrane potential via ion channel kinetics (Akkas et al., 2007b), which may play a fundamental role for the generation of epileptic seizures, as well. Therefore; altered membrane fluidity in PTZ treated groups was further supported by the decrease in the lipid to protein ratio.

All the findings belonging to membrane lipids obtained from animal studies for homogenate and cell membranes samples means are resulted from epileptic activities itself not from PTZ chemical since we could not observe any interaction between PTZ and DPPC MLVs.

FTIR microscopy attached to FTIR spectroscopy gave us opportunity to obtain chemical data of homogenate samples based upon lipid to protein ratio by FTIR microscopy, which support FTIR spectroscopic data. IR spectroscopy in combination with microscopy yielded spatially resolved information on homogenate brain samples that allowed the generation of IR maps with high image contrast.

In the present study, after both low and high dose of PTZ application, the decrease in the protein amount in homogenate and cell membrane samples was supported from the reduction seen in the peak area of amide I and amide II bands (Dogan et al., 2007; Cakmak et al., 2006). This result was also supported by the decrease in the area of the CH_3 symmetric stretching band, which also originates mainly from proteins. The decrease in protein content might be resulted from protein degradation and disruption (Dogan et al., 2007; Gebicki et al., 2000). Damage to proteins might be associated with the effects of free radicals, which may lead to increased susceptibility to proteolysis (Davis et al., 1987) and may result in tissue and membrane damage and neurotoxicity during PTZ-induced convulsions. The convulsive dose of PTZ, which corresponds to the tonic-clonic seizure, was more effective for the decrement of proteins compared to subconvulsive dose, as there was a more profound decrease in the protein amount in this group. Thus, the decrease in protein content could be observed as an early consequence of PTZ-induced epileptic activity by using FTIR spectroscopy. Our finding contradicts with a previous study reporting the increase in some intracellular proteins during PTZ-induced bursting activity in snail neurons (Sugaya et al., 1982).

Alterations in secondary structures of proteins in different disease states have been reported in literature (Toyran et al., 2007; Sadqi et al., 2002; Moore et al., 2009; Liao et al., 2007). The secondary structural changes has been also reported for neurodegenerative diseases (Lin and Chu, 2003; Apetri et al., 2006; Ronga et al., 2007).

In this context, we firstly, investigated epileptic induced changes in protein conformation of brain homogenate and cell membrane by second derivative analyses of Amid I band. In brain homogenate samples, the results of this study showing the alterations in the amount of alpha helix and beta sheet structures such as increase in alpha helix and random coil and a decrease in beta sheet structures were demonstrated in Table 13. For more precise determination of the changes in protein conformation a detailed analysis using neural network predictions based on FTIR data was carried out. Neural network method of prediction of secondary structure contents of proteins has been proven to be an alternative powerful tool for the analysis of protein structure using FTIR data. The method is based on the optimization of a neural network trained by the FTIR data of proteins whose secondary structure are available from X-ray crystallography. In recent years, this method has been effectively applied to determine protein secondary structure (Ceylan et al., 2009, Toyran et al., 2007, Akkas et al., 2007a; Severcan et al., 2004). The results of neural network predictions are presented in Table 13. On the contrary, in cell membrane samples, the second derivative analysis of Amid I band revealed that there is a decrease in both the amount of alpha helix and beta sheet structures, however, an increase in random coil structure (Table 17). It is clearly seen from the table that both low and high dose of PTZ administration caused significant changes in protein structure for homogenate and cell membrane, which might be due to the attack of free radicals, as mentioned before (Davies et al., 1987). Moreover, Adler et al. (1999) have reported that the changes in protein conformation might be also due to the altered redox potential, which is observed in epileptic activity. In the present study, we obtained significant insights into the changes in protein secondary structure of rat brain tissue and cell membrane, which might be important in understanding the molecular mechanism underlying epileptic conditions. By using FTIR spectroscopy, PTZ-induced changes in the secondary structure of proteins in rat brain tissue and cell membrane could be determined, without the need for the application of isolation procedures. PTZ-induced structural changes in proteins may possibly alter the phospholipid behavior in membranes, such as membrane dynamics.

These changes may probably have importance for the regulation of membrane functions of the brain in epileptic conditions.

We have also found that two different doses (25 mg/kg and 60 mg/kg) of PTZ administration have both caused a reduction in glycogen content in homogenate samples. We could not observe any glycogen band in the FTIR spectra of cell membrane samples. This result is directly related to the energy requirement during epileptic activity (Petroff et al., 2002). During neuronal activity, apart from the maintenance of ionic homeostatis, some of the required energy is used for glutamate/GABA metabolism, including release and uptake of neurotransmitters. Under normal conditions, the resting awake brain depends on ATP that is generated from oxidation of glucose (oxidative glycolysis), which cause low lactate level. However, stimulated neuronal activity, as seen in seizures, requires energy produced by nonoxidative glycolysis, which leads to accumulation of lactate. Stimulated neuronal epileptic activity creates an uncoupling of glucose consumption and oxidation mainly caused by the altered activity of glucose transporters in the structure of BBB (Petroff et al., 2002). This uncoupling appears to be compensated by glycogen (Magistretti et al., 1999). The increase in nonoxidative glycolysis is a normal metabolic process used to support glutamate/GABA metabolism during enhanced neuronal activity. The majority of glucose required to fuel the pumping of glutamate from synaptic cleft during intense bursts of activity is provided by the glycogen in brain. There is in vivo evidence that brain glycogen may be rapidly mobilized to support in the physiologic brain activation (Rothman et al., 1999). Taking this into consideration, the disappearance of glycogen band located at 1170 cm^{-1} in the convulsive group can be explained by the high rate of utilization of glycogen during epileptic activity. Thus, this metabolic changes induced by PTZ, seizures might be indicative of cell stress in epileptic rat brain.

In brain homogenate samples the administration of PTZ at different doses led to the shifting of the frequencies to lower values and characteristic changes of all the nucleic acid bands (1236 cm^{-1}, 1080 cm^{-1}, 998 cm^{-1}). These observed changes might be due to the structural and functional alterations of nucleic acids, which are susceptible to seizure-induced oxidative stress (Lopez et al., 2001).

In the current study area of the band assigned to ribose phosphate main chain of RNA significantly increased in the PTZ convulsive dose, in comparison to control and subconvulsive groups, indicating high RNA content. This further suggests the increase in RNA production, reflecting the increment in the protein synthesis. These findings are in accordance with the results of a previous study, in which gene transcriptions for three immediate early genes, c-fos, c-jun and NGFI-A, and three neuropeptide genes, enkephalin, dynorphin and neuropeptide Y have been increased following a single injection of the convulsant PTZ (Yount et al., 1994). Among these genes, especially c-fos has been reported to be induced in neurons following the increase in intracellular calcium levels. Therefore, this gene is responsible for molecular events leading to the permanent changes in brain underlying epilepsy and neural plasticity (Kohmura et al., 1995). Hence, these results reveal dose dependent effects of PTZ-induced seizures on the level of gene expression, which can be detected by FTIR spectroscopy. We did not observed these bands in cell membranes since cell membranes do not contain nucleic acid bands.

Figure 43 shows topographic image of brain cell membrane for epileptic and control samples. As seen from the figure, all the molecular changes obtained from FTIR spectroscopic and FTIR microscopic data in biomolecules present in cell membrane structure resulted from PTZ-induced convulsions cause some morphological alterations on cell membrane structure.

We could not observe PTZ-induced alteration in dynamics, order, phase transition profile, the hydrogen bonding capacity of the glycerol backbone near the hydrophilic part and polar head group of DPPC MLVs. This results revealed that in animal studies PTZ itself do not cause any effects on brain tissue and cell membrane. All observed changes are consequences of PTZ-induced convulsions.

4.2.2 The effects of an antiepileptic agent VGB on epileptic rat brain cell membrane

This part of the study was undertaken to investigate theurapeutic effects of VGB treatment on epileptic rat brain cell membrane. To achieve this, we studied the administration of VGB on lipid dynamics, lipid order, quantity of biomolecules, the hydrogen bonding capacity of the glycerol backbone near the hydrophilic part and polar head group of cell membrane lipids by FTIR spectroscopy. We have also determined VGB treatment-induced changes in the protein secondary structure by second derivative analysis of Amid I band. Moreover, all the spectral data obtained from FTIR spectroscopy have been used to apply cluster analysis to discriminate vigabatrin, epileptic and control samples.

In the literature it was shown that VGB treatment has an anticonvulsant affect against PTZ in mice and rat in terms of reducing the severity of seizures and in delaying the onset of first myoclonic twitches, however, the theurapeutic effect of VGB on PTZ induced convulsions lying molecular mechanism is not known very well.

The results given in table 18 and figure 45 reveal that PTZ induced convulsions increase significantly membrane lipid peroxidation. VGB treatment restored this parameter near to control values, tended to normalize the content of unsaturated membrane lipids. This implies that VGB treatment caused the decrease in lipid peroxidation. This might be resulted from reduction in high neuronal activity. Since VGB itself causes the increase GABA level in both presynaptic terminal and synaptic cleft, high neuronal activity can be prevented, therefore; the release of glutamate and synthesis of phospholipases which in turn the production of AA can be reduced. With this reduction the metabolism of AA, AA could not be metabolized efficiently and, therefore; the production of ROS attacking to membrane lipids were lowered. Moreover, since the high rate of neuronal activity was decreased, somehow MRC dysfunction could be prevented, which is the major source of free radicals and reactive oxygen species. As a result, lipid peroxidation can be reduced upon VGB treatment. This may lead to prevent

membrane malfunction, excitotoxicity, neuronal injury and cell death in both long term (Frantseva et al., 2000; Patel et al., 2001) and short term seizure activity (Akbas et al., 2005; Bashkatova et al., 2003) induced by the over production of ROS.

We see a remarkable significant decrease in the area of all membrane lipid bands namely, the CH_3 asymmetric, the CH_2 asymmetric, the CH_2 symmetric, the C=O stretching, the PO_2 asymmetric and symmetric stretching in epileptic group. As reported previously, epileptic convulsions cause some alterations in lipid metabolism. Our results reveal that VGB treatment tends to normalize these changes to control values. These might be resulted from the prevention of high production of ROS, which attacks to membrane lipids. Especially we should point out that the reductions in the amount of membrane phospholipids that is caused by the activation of phospholipases was lowered in VGB treatment. In addition, the frequency values of the bands belonging to membrane phospholipids tended to normalize once, which might imply the prevention of membrane disorganization. Moreover, the decrease in the production of AA might also lead to lower sphingomyelinase activity, therefore; demyelination might be prevented (Bane et al., 2002). As a result, since lipid molecules have important roles in the regulation of membrane functions as reported previously, it can be concluded that VGB treatment has major effect on lipid metabolism in order to prevent epileptic activity.

The restoring effect of VGB for membrane disorganization can be resulted from the potential of VGB for hydrogen bonding to membrane phospholipids, which is obtained from model membrane studies.

It is clearly seen in Table 19 the lipid to protein ration and the bandwidth value of the CH_2 asymmetric stretching decrease significantly in epileptic group, however, when VGB treatment was applied these differences become no more statistically significant. This shows the restoring effect of VGB treatment on membrane fluidity and lipid to protein ratio. In the model membrane study of VGB with DPPC MLVs also revealed an increase in the membrane fluidity, which show the potential of VGB to restore decreased membrane fluidity in epileptic group.

These effects together with the prevention of membrane disorganization may lead to the cell to to carry out its normal functions and would decrease the cell's susceptibility to injuriy and death. For example, some ion channels, membrane bound enzymes and some transporters in BBB such as glucose transporters act properly. With normal function of these transporters and ion channels present on membrane structure cerebral blood flow matches the metabolic demand. Thus, energy impairment, which is seen in epileptic activity does not occur in brain.

As seen from Table 20, with the treatment of VGB the intensity of protein secondary structure remain significantly different from control groups, which shows VGB treatment might not have restoring affect on secondary structure of membrane proteins.

Consequently, according to our result, the VGB treatment has major effect in lipid metabolism to supress seizure activity rather than to affect protein structure.

CHAPTER 5

CONCLUSION

- In the first part of the study, we have tested the possible interaction of PTZ with DPPC MLVs by studying its effect on phase behavior, lipid order, nature of hydrogen bonding and lipid dynamics. Our results revealed that in the presence of PTZ these structural and dynamical properties of DPPC model membrane were not altered. DPPC MLVs are simplified form of biological membrane and show similar properties with biological membranes, therefore; our results can be attributed to biological membranes. Even though some earlier findings stated PTZ has the ability to interact with membrane lipids, our results clearly showed that there is no interaction between PTZ and membrane lipids. This means that modulation of the properties of the lipid bilayer is not the action meachanim of PTZ to generate epileptic activity. Our results may provide a better understanding of PTZ action mechanism and its role in epilepsy. As a result, insight in the pathophysiology of epilepsy this study will contribute to development of new anti-epileptic drugs and will offer more promising approaches for the treatment of this disorder. This result also revealed that the effects of epilepsy on rat brain tissue and cell membranes are resulted from epileptic activity or PTZ itself.

- The current study for the first time demonstrated the molecular alterations resulted from both subconvulsive and convulsive doses of PTZ-induced epileptic activity on rat brain tissue and cell membranes at molecular level by investigating the FTIR spectral parameters in detail. Our findings suggest that PTZ-induced convulsions cause some alterations in the macromolecular content, structure and function that may contribute to the development of epileptic activity. For example a decrease in lipid and protein concentration, a decrease in membrane fluidity, the difference in membrane packing by changing the nature of hydrogen bonding, an increase in lipid peroxidation and the transcription of early genes were observed. Additionally, it has been shown an altered protein profile with an increase in alpha helix and a decrease in beta sheet, in both PTZ-treated groups. In previously published papers, the long term effects of epileptic seizures on brain of animals and/or humans had been investigated. The present study demonstrates that even a relatively short term of PTZ-induced epileptic activity induces significant effects on rat brain and cell membrane. It has been found that convulsive dose of PTZ induced seizures caused more significant molecular changes on rat brain and cell membrane compared to subconvulsive dose. Hence, FTIR spectroscopy could be effective tool to investigate PTZ induced seizures alterations, which obviously appears to improve the understanding of epilepsy and new strategies in treatment of this disorder.

- In order to investigate theurapeutic effect of VGB in epilepsy treatment we first evaluated biopharmaceutic property of this drug, which is based on the degree of incorporation and uniform distribution into lipid bilayer. According to our data, VGB strongly interact with glycerol backbone and phosphate head groups of membrane phospholipids, however, it does not penetrate freely into lipid bilayer. This might mean that VGB does not show complete distribution and absorption into the body.

Consequently, it is highly probable that VGB also uses specific transporters as routes other than only interacting with membrane lipids to reach its target organ. This information will further support that designing AEDs with its biological profile, therefore; it will contribute to development of new anti-epileptic drugs and will offer more promising approaches for the treatment of epilepsy.

- The next section of the study was undertaken to show the effects of VGB on PTZ-induced epileptic activity on brain cell membrane. The findings of our study revealed that VGB treatment restored some of the changes caused by epileptic activity such as decreased membrane fluidity, increased lipid peroxidation and alterations in membrane organization. On the other hand, it was found that VGB has no significant effects on changes in protein secondary structure. Thus, this study revealed the partial protecting action mechanism of VGB on epileptic rat brain cell membranes.

REFERENCES

Adibhatla, R.M., Hatcher, J.F., Dempsey, R.J., (2000). Lipid alterations in transient fore brain ischemia: Possible new mechanisms of CDP–choline neuroprotection, J. Neurochem., 75:2528–2535.

Adibhatla, R.M., Hatcher, J.F., Dempsey, R.J., (2006). Lipids and lipidomics in brain injury and diseases, The AAPS National Biot. Conf. Symp. on Lipidomics, 8:36.

Adler, V., Yin, Z., Tew, K.D., Ronai, Z., (1999). Role of redox potential and reactive oxygen species in stress signaling, 45: 6104-6111.

Akbas, S.H., Yegin, A., Ozben, T., (2005). Effect of pentylenetetrazole-induced epileptic seizure on the antioxidant enzyme activities, glutathione and lipid peroxidation levels in rat erythrocytes and liver tissues, Clinical Biochemistry, 38:1009-1014.

Akkas, S.B., Severcan, M., Yilmaz, O., Severcan, F., (2007). Effects of lipoic acid supplementation on rat brain tissue: An FTIR spectroscopic and neural network study, Food Chemistry, 105: 1281-1288.

Akkas, S.B., Inci, S., Zorlu, F., Severcan, F., (2007). Melatonin affects the order, dynamics and hydration of brain membrane lipids, J Mol Struct, 834: 207-215.

Ali, A., Ahmad, F.J., Pillai, K.K., Vohora, D., (2004). Evidence of the antiepileptic potential of amiloride with neuropharmacological benefits in rodent models of epilepsy and behavior, Epilepsy Behav., 5:322-8.

Altrup, U., Hader, M., Caceres, J.L.H., Malcharek S., Meyer, M., Galla, H., (2006). Epileptogenic drugs in a nervous system: Electrophysiological effects and incorporation into a phospholipid layer, Brain Res., 1122: 65-77.

Apetri, M.M., Maiti, N.C., Zagorski, M.G., Carey, P.R., Anderson, V.E., (2006). Secondary structure of alpha-synuclein oligomers: Characterization by Raman and atomic force microscopy, J Mol Biol., 355(1):63-71.

Archaya, M.M., Katyare, S.S., (2005). Structural and functional alterations in mitochondrial membrane in picrotoxin-induced epileptic rat brain, Experimental Neurology, 192: 79-88.

Avanzini, G., Franceschetti, S., (2003). Cellular biology of epileptogenesis, Lancet Neurology, 2: 33–42.

Ayyildiz, M., Yildirim, M., Agar, E., Baltaci, A.K., (2006). The effects of leptin on penicillin-induced epileptiform activity in rats, Brain Res. Bull., 68: 374-378.

Baber, J., Ellena, J.F., Cafiso, D.S., (1995). Distribution of general-anesthetics in phospholipid-bilayers determined using H-2 NMR and H-1-H-1 Noe spectroscopy, Biochemistry, 19: 6533-6539.

Balasubramanian, S.V., Straubinger, R.M., (1994). Taxol-lipid interactions-Taxol dependent effects on the physical properties model membranes, Biochemistry, 33: 8941-8947.

Banyay, M., Sarkar, M., Gräslund, A., (2003). A library of IR bands of nucleic acids in solution, Biophysical Chemistry, 104: 477–488.

Bashkatova, V., Narkevich, V., Viskova, G., Vanin, A., (2003). The influence of anticonvulsant and antioxidant drugs on nitric oxide level and lipid peroxidation in the rat brain during pentylenetetrazole-induced epileptiform model seizures, Progress in Neuro-Psychopharmacology & Biological Psychiatry, 27: 487-492.

Bazil, C.W., Pedley, T.A., (1998). Advances in the medical treatment of epilepsy, Annu. Rev. Med., 49: 135–162.

Beaumont, D., Olive, G., (1990). Pharmacokinetics of the individual enantiomers of vigabatrin (gamma-vinyl gaba) in epileptic children, Br. J. Clin. Pharmacol., 30(2): 253-257.

Bellissimo, M.I., Amado, D., Abdalla, D.S.P., Ferreira, E.C., Cavalheiro, E.A., (2001). Superoxide dismutase, glutathione peroxidase activities and the hydroperoxide concentration are modified in the hippocampus of epileptic rats, Epilepsy Res., 46: 121-128.

Berliner, L.J., (1976). Spin Labeling Theory and Applications, Vol. 1, Academic Press, New York.

Bloms, P., MuBhoff, U., Madeja, M., Müsch-Nittel, K., Kuhlmann, D., Spencer, F., Speckmann, E.J., (1992). Supression of a ligand operated membrane currents by the epileptogenic agent pentylenetetrazol in oocytes of *Xenopus laevis* after injection of rat brain RNA, Neuroscience Letters, 147: 155-158.

Bloms-Funke, P., Madeja, M., MuBhoff, U., Speckmann, E.J., (1996). Effects of pentylenetetrazol on GABA receptors expressed in oocytes of *Xenopus laevis*: extra- and intracellular sites of action, Neuroscience Letters, 205: 115-118.

Bloom, C.M., Anch, A.M., Dyche, J.S., (2002). Behavioral effects of chronic melatonin and pregnenolone injections in a myelin mutant rat (taiep), J. Gen. Psych., 129:226-237.

Bozkurt, O., Bilgin, M.D., Severcan, F., (2007). The effect of diabetes mellitus on rat skeletal Extensor digitorum longus muscle tissue: An FTIR study, Spectroscopy - Int. J., 21: 151-160.

Brookes, P.S., Bolanos, J.B., Heales, S.J., (1999). The assumption that nitric oxide inhibits mitochondrial ATP synthesis is correct, FEBS Lett., 446: 261-263.

Browne, T.R., Holmes, G.L., (2001). Primary care: Epilepsy, New England Journal of Medicine, 344(15): 1145-1151.

Bruce, A.J., Baudry, M., (1995). Oxygen free radicals in rat limbic structures after kainate-induced seizures, Free Radic. Biol. Med., 18: 993-1002.

Bruckner, H., Wittner, R., Godel, H., (1989). Automated enantioseparation of amino-acids by derivatization with ortho-phthaldialdehyde and n-acylated cysteines, J. Chromatogr., 476: 73-82.

Bruehl, C., Hagemann, G., Witte, O.W., (1998). Uncoupling of blood flow and metabolism and epilepsy, Epilepsia, 39: 1235-1242.

Buege, J.A., Aust, S.D., (1978). Microsomal lipid peroxidation, Methods in Enzymology, 52: 302-310.

Cadenas, E., Boveris, A., Ragan, C.I., Stoppani, A.O.M., (1997). Production of superoxide radicals and hydrogen peroxide by NADH-ubiquinone reductase and ubiquinol-cytochrome c reductase from beef heart mitochondria, Arch. Biochem. Biophys., 180: 248-257.

Chakravarti, A., Slaugenhaupt, S.A., Zubenko, G.S., (1989). Inheritance pattern of platelet membrane fluidity in Alzheimer disease, Am. J. Hum. Genet., 44: 799-805.

Cakmak, G., Togan, I., Severcan, F., (2003). FT-IR spectroscopic analysis of rainbow trout liver exposed to nonylphenol, Applied Spectroscopy, 57: 835-841.

Cakmak, G., Togan, I., Severcan, F., (2006). 17β-Estradiol induced compositional, structural and functional changes in rainbow trout liver, revealed by FT-IR spectroscopy: A comparative study with nonylphenol, Aquat. Toxicol, 77: 53–63.

Casal, H.L., Mantsch, H.H., Hauser,H., (1989). Infrared and 31 P-NMR studies of the interaction of Mg with phosphatidylserines: effect of hydrocarbon chain unsaturation, Biochim. Biophys. Acta, 982: 228-236.

Cenedella, R.J., Sarkar, C.P., (1984). Mechanism of depression of brain phospholipid levels by an epileptogenic drug, Biochemical Pharmacology, 33:591-598.

Ceylan, C., Severcan, M., Bozoglu, F., Severcan, F., (2009). Effect of hydrostatic pressure on bovine blood protein and lipid constituents revealed by Fourier transform infrared spectroscopy, High Pressure Research, 29(2): 358-368.

Ceyhan, M., Kayir, H., Uzbay, I.T., (2005). Investigation of the effects of tianeptine and fluoxetine on pentylenetetrazole-induced seizures in rats, J. Psychiatric. Res., 39:191-6

Chalazonitis, N., Boisson, M., (1978). Abnormal Neuronal Discharges, Raven Press, New York.

Chen, H.C., Mendelsohn, R., Rerek, M.E., Moore, D.J., (2000). Fourier transform infrared spectroscopy and differential scanning calorimetry studies of fatty acid homogenous ceramide, Biochimica et Biophysica Acta, 1468: 293-303.

Chiriboga, L., Yee, H., Diem, M., (2000). Infrared spectroscopy of human cells and tissues. Part VII. FT-IR Microspectroscopy of DNAase- and RNAase-treated normal, cirrhotic, and neoplastic liver tissue, Appl. Spectrosc., 54: 480–485.

Chollet, D.F., (2002). Determination of antiepileptic drugs in biological material, Journal of Chromatography B, 767:191–233.

Chollet, D.F., Goumaz, L., Juliano, C., Anderegg, G., (2000). Fast isocratic high-performance liquid chromatographic assay method for the simultaneous determination of gabapentin and vigabatrin in human serum, J. Chromatogr. B, 746(2):311-314.

Ci, Y.C., Gao, T.Y., Feng, J., Guo, Z.Q., (1999). FTIR spectroscopic characterization of human breast tissue: implications for breast cancer diagnosis, Appl. Spectrosc., 53: 312-315.

Cock, H.R., (2002). The role of mitochondria and oxidative stress in neuronal damage after brief and prolonged seizures, Prog. Brain Res., 135: 187-196.

Commission on Classification and Terminology of Epilepsy of the International League Against Epilepsy (1989). Proposal for revised classification of epilepsies and epileptic syndromes, Epilepsia, 30:389-399.

Commission on Classification and Terminology of the International League Against Epilepsy, (1981). Proposal for revised clinical and electroencephalographic classification of epileptic seizures, Epilepsia, 22:489-501

Contreras, D., (2000). Experimental models in epilepsy, Rev. Neurol., 30 (4):370-376.

Dalby, N.O., Mody, I., (2001). The process of epileptogenesis: a pathophysiological approach, Curr. Opin. Neurol., 14:187–192.

Dal-Pizzol, F., Klamt, F., Vianna, M.M.R., Schroder, N., Quevedo, J., Benfato, M.S., Moreira, J.C.F., Walz, R., (2000). Lipid peroxidation in hippocampus early and late after status epilepticus induced by pilocarpine or kainic acid in Wistar rats, Neuroscience Letters, 291: 179-182.

Dalton, L.R., (1984). EPR and Advanced EPR Study of Biological Sytems, CRC Press, Boca Raton.

Dawn-Linsley, M., Ekinci, F.J., Ortiz, D., Rogers, E., Shea, T.B., (2005). Monitoring thiobarbituric acid-reactive substances (TBARs) as an assay for oxidative damage in neuronal cultures and central nervous system, Journal of Neurosience Methods, 141: 219-222.

Davies, K.J., (1987). Protein damage and degradation by oxygen radicals. I. General aspects, Journal of Biological Chemistry, 262: 9895-9901.

De Lorenzo, R.J., (1989). The epilepsies. In Bradley WG, Daroff RB, Fenichel GM, Marsden CD (Eds.), Neurology in Clinical Practice, Butterworth Publishers, Stoneham, MA.

De Lorenzo, R.J., (1991). The challenging genetics of epilepsy, Epilepsy Res. Suppl., 4: 3-17.

De Lorenzo, R.J., Sun, D.A., Deshpande, L.S., (2005). Cellular mechanisms underlying acquired epilepsy: the calcium hypothesis of the induction and maintenance of epilepsy, Pharmacol. Ther., 105: 229-266.

DeToledo, C.J., Ramsay, R.E., Lowe, M.R., (2003). Editorial: Epilepsy: disease, illness, or disorder?, Epilepsy and Behaviour, 4:455-456.

De Sousa, D.P., Gocalves, J.C.R., Quintans, L., (2006). Study of anticonvulsant effect of citronellol, a monoterpene alcohol, in rodents, Neuroscience Letters, 401: 231-235.

Dicko, A., Morissette, M., Ben Ameur, S., Pezolet, M., Di Paolo, T., (1999). Effect of estradiol and tamoxifen on brain membranes: investigation by infrared and fluorescence spectroscopy, Brain Res. Bull., 49: 401-405.

Dichter, M.A., (1997). Basic mechanisms of epilepsy: targets for therapeutic intervention, Epilepsia, 38 (Suppl. 9): S2– S6.

Dogan, A., Ergen, K., Budak, F., Severcan, F., (2007). Evaluation of disseminated candidiasis on an experimental animal model: a Fourier Transform Infrared study, Applied Spectroscopy, 61: 199-203.

Dubberke, R., Vasilets, L.A., Schwarz, W., (1998). Inhibition of the Na^+, K^+ pump by the epileptogenic pentylenetetrazole, Pflügers Arch-Eur. J. Physiol., 437: 79-85.

Ekonomou, A., Smith, A. L., Angelatou F., (2001). Changes in AMPA receptor binding and subunit messenger RNA expression in hippocampus and cortex in the pentylenetetrazole-induced kindling model of epilepsy, Molecular Brain Research, 95: 27-35.

Eloqayli, H., Dahl, C.B., Gotesman, K.G., Unsgard, G., Hadidi, H., Sonnewald, U., (2003). Pentylenetetrazole decreases metabolic glutamate turnover in rat brain, Journal of Neurochemistry, 85: 1200-107.

Engel Jr., J., Pedley, T.A., (1998). Epilepsy A Comprehensive Textbook, Lippincott-Raven, Philadelphia.

Erakovic, V., Zupan, G., Varljen, J., Laginja, J., Simonic, A., (2001). Altered activities of rat brain metabolic enzymes caused by pentylenetetrazol kindling and pentylenetetrazol-induced seizures, Epilepsy Resarch, 43: 165-173.

Erakovic, V., Zupan, G., Varlijen, J., Simonic, A., (2003). Pentylenetetrazol-induced seizures and kindling: changes in free fatty acids, superoxide dismutase and glutathione peroxidase activity, Neurochemistry Int., 42: 173-178.

Fa, N., Ronkart, S., Schanck, A., Deleu, M., Gaigneaux, A., Goormaghtigh, E., Minqeot-Leclercq, M.P., (2006). Effect of the antibiotic azithromycin on thermotropic behavior of DOPC and DPPC bilayers, Chemistry and Physics of Lipids, 144: 108-116.

Fisher, R.S., (1989). Animal models of the epilepsies, Brain Res., 14: 245-278.

Follesa, P, Tarantino, A., Floris, S., Mallei, A., Porta, S., Tuligi, G., Cagetti, E., Caddeo, M., Mura, A., Serra, M., Biggio, G., (1999). Changes in the gene expression of $GABA_A$ receptor subunit mRNAs in the septum of rats subjected to pentylenetetrazol-induced kindling, Molecular Brain Research, 70: 1-8.

Foot, M., Wallace, J., (1991). New Antiepileptic Drugs, Pisani, F., Avanzio, G., Richens, A., (Eds.), Elsevier, Amsterdam.

Forrest, G., Sills, G., Leach, J.P., Brodie, M.J., (1996). Determination of gabapentin in plasma by high-performance liquid chromatography, J. Chromatogr. B, 681(2):421425.

Frantseva, M.V., Velazquez, J.L., Hwang, P.A., Carlen, P.L., (2000). Free radical production correlates with cell death in an in vitro model of epilepsy, Eur. J. Neurosci., 12:1431-1439.

Frazen, N., (2000). Seizures and Epilepsy: Hope Through Research, Bethesda, MD7 NINDS.

Freeman, E.J., Terrian, D.M., Dorman, R.V., (1990). Presynaptic facilitation of glutamate release from isolated hippocampal mossy fiber nerve endings by arachidonic acid, Neurochem Res., 15:743-750.

Garcia-Ruiz, C., Colell, A., Mari, M., Morales, A., Fernandezcheca, J.C., (1997). Direct effect of ceramide on the mitochondiral electron transport chain leads to generation of reactive oxygen species-role of mitochondrial glutathione, J Biol Chem., 272: 11369-11377.

Garip, S., Bozoglu, F., Severcan, F., (2007). Differentiation of mesophilic and thermophilic bacteria with FTIR spectroscopy, Applied Spectroscopy, 61: 186-192.

Gebicki, J.M., Du, J., Collins, J., Tweeddale, H., (2000). Peroxidation of proteins and lipids in suspensions of liposomes in blood serum and in mouse myeloma cells, Acta Biochimica Polonica, 47: 901-911.

Getova, D., Froestl, W., Bowery, N.G., (1998). Effects of GABA(B) receptor antagonism on the development of Pentylenetetrazol-induced kindling in mice, Brain Resarch, 809: 182-188.

Ghafourifar, P., Klein, S.D., Schucht, O., (1999). Ceramide induces cytochrome c release from isolated mitochondria. Importance of mitochondrial redox state, J Biol. Chem., 274: 6080-6084.

Goldensohn, E.S., Porter, R.J., Schwartzkroin, P.A., (1997). The American Epilepsy Society: An historic perspective on 50 years of advances in research, Epilepsia, 38(1): 124-150 .

Grant, S.M., Heel, R.C., (1991). Vigabatrin - A review of its pharmacodynamic and pharmacokinetic properties, and therapeutic potential in epilepsy and disorders of motor control, Drugs 41(6): 889-926.

Grove, J., Alken, R.G., Schechter, P.J., (1984). Assay of gamma-vinyl-gamma-aminobutyric acid (4-amino-hex-5-enoic acid) in plasma and urine by automatic amino-acid-analysis - application to human pharmacokinetics, J. Chromatogr., 306: 383-387.

Gross, G.J., Woodbury, D.M., (1972). Effects of pentylenetetrazol on ion transport in the isolated to bladder. Journal of Pharmacology And Experimental Therapeutics, 181: 257-272.

Grupta, R.C., Milatovic, D., Dettbarn, W.D., (2001). Nitric oxide modulates high-energy phosphates in brain regions of rats intoxicated with diisopropylphosphofluoridate or carbofuran by N-tert-butyl-alpha-phenylnitrone or vitamin E, Arch. Toxicol., 75: 346-356.

Haegele, K.D., Schoun, J., Alken, R.G., Huebert, N.D., (1983). Determination of the r(-)-enantiomers and s(+)-enantiomers of gamma-vinyl-gamma-aminobutyric acid in human-body fluids by gas-chromatography mass-spectrometry, J. Chromatogr., 274:103-110.

Hansen, S.L., Sperling, B.B., Sanchez, C., (2004). Anticonvulsant and antiepileptogenic effects of GABAa receptor ligands in pentylenetetrazole-kindled mice, Progress in Neuro-Psychopharmacology & Biological Psychiatry, 28: 105-113.

Haris, P.I., Severcan, F., (1999). FTIR spectroscopic characterization of protein structure in aqueous and non-aqueous media, J. Mol. Catal., 7: 207–221.

Harrison, J.E., Groundwater, P.W., Brain, K.R., Hadgraft, J., (1996). Azone induced fluidity in human stratum corneum. A Fourier transform infrared spectroscopy investigation using the perdeuterated analogue, J. Controll. Rel., 41: 283-290.

Hartung, K., Hermann, A., (1987). Differential effects of pentylenetetrazole on ion currents of *Aplysia* neurones, Brain Res., 419: 55-64.

Hauser, W.A., Hesdorffer, D.C., (1990). Epilepsy: Frequency, Causes and Consequences, New York: Demos.

Hauser, H., Poupart, G., (1992). The structure of biological membranes, P.L. Yeagle (Ed.), CRC Press, Boca Raton, FL.

Hauser, W.A., (1997). Insidence and prevelance. In: Engel, J., Pedley, T.A., (Eds.), Epilepsy: A comprehensive textbook, Lippincott-Raven Publishers, Philadelphia.

Hendrich, A.B., Michalak, K., Wesolowska, O., (2007). Phase separation is induced by phenothiazine derivatives in phospholipid/sphingomyelin/cholesterol mixtures containing low levels of cholesterol and sphingomyelin, Biophysical Chemistry, 130: 32-40.

Hernandez, T.D., (1997). Preventing post-traumatic epilepsy after brain injury: weighing the costs and benefits of anticonvulsant prophylaxis, Trends Pharmacol. Sci., 18: 59–62.

Hippocrates, (1839-1861). On the sacred disease in oeuvres completes d'Hippocrate par E. Litre, Paris.

Holmes, G.L., (1991). Do seizures cause brain damage? Epilepsia, 32(Suppl 5):S14-28.

Huang, J., Buboltz, J.T., Feigenson, G.W., (1999). Maximum solubility of cholesterol in phosphatidylcholine and phosphatidylethanolamine bilayers, Biochimica Biophysica Acta, 1417: 89-100.

Hubbard, A. L., Wall, D. A., Ma, A., (1983). Isolation of rat hepatocyte plasma membranes. I. Presence of the three major domains, J. Cell Biol., 96: 217-229.

Jackson, M., Mantsch, H.H., (1996). Biomedical infrared spectroscopy, in: Mantsch, H. H. and Chapman, D. (Eds.) Infrared Spectroscopy of Biomolecules, Wiley-Liss Inc., USA.

Jackson, M., Ramjiawan, B., Hewko, M., Mantsch, H.H., (1998). Infrared microscopic functional group mapping and spectral clustering analysis of hypercholesterolemic rabbit liver, Cellular and Molecular Biology, 44: 89-98.

Jain, M.K., Wu, N.M., (1977). Effect of small molecules on dipalmitoyl lecithin liposomal bilayer 3 phase transition in lipid bilayer, Journal of membrane biology, 34: 157-201.

Janigro, D., (1999). Blood brain barrier, ion homeostasis and epilepsy: possible implications towards the understanding of ketogenic diet mechanisms, Epilepsy Research, 37: 223-232.

Jones, O.T., (2002). Ca2+ channels and epilepsy, European Journal of Pharmacology, 447: 211 – 225.

Juergens, U.H., May, T.W., Rambeck, B., (1996). Simultaneous HPLC determination of vigabatrin and gabapentin in serum with automated pre-injection derivatization, J. Liq. Chromatogr. Rel. Technol., 19(9): 1459-1471.

Kajiwara, K., Sugaya, E., Kimura, M., Katsuki, M., Nagasawa, H., Yuyama, N., Tsuda, T, (1995). Cloning and characterization of pentylenetetrazole-related cDNA, PTZ-17, Brain Research, 671: 170-174.

Kelso, A.R.C. and Cock, H.R., (2004). Advances in epilepsy, British Medical Bulletin, 72: 135–148.

Kiviranta, T., Tuomisto, L., Airaksine, E.M., (1996). Osmolarity and electrolytes in cerebrospinal fluid and serum of febrile children with and without seizures, Eur. J. Pediatr.,155:120-5.

Kotloski, R., Lynch, M., Lauersdorf, S., Sutula, T., (2002). Repeated brief seizures induce progressive hippocampal neuron loss and memory deficits, Prog Brain Res., 135: 95–110.

Kneipp, J., Lasch, P., Baldauf, F., Beekes, M., Naumann, D., (2000). Detection of pathological molecular alterations in scrapie-infected hamster brain by Fourier transform infrared (FT-IR) spectroscopy, Biochim. Biophsy. Acta, 1501: 189-199.

Kohlschütter, A., Hübner, C., Gärtner, J., Reynolds, J.F., Pullarkat, R.K., (1987). Decreased membrane fluidity of lymphycotes from patients with juvenile neuronal ceroid-lipofuscinosis, Am. J. Med. Genet., 31: 203-207.

Kohmura, E., Yuguchi, T., Yamada, K., Sakaguchi, T., Wanaka, A., Hayakawa, T., (1995). Expression of c-*fos* mRNA after cortical ablation in rat brain is

modulated by basic fibroblast growth factor (bFGF) and the NMDA receptor is involved in c-*fos* expression, Molecular Brain Res., 28: 117-121.

Korkmaz, F., Severcan, F., (2005). Effect of progesterone on DPPC membrane: Evidence for lateral phase separation and inverse action in lipid Dynamics, Archives of Biochem. Biophys,. 440: 141-147.

Korkmaz, F., Kirbiyik, H., Severcan, F., (2005). Concentration dependent different action of progesterone on the order, dynamics and hydration states of the head group of dipalmitoyl-phosphatidylcholine membrane, Spectroscopy-an International Journal, 19: 213-219.

Lewis, R.N., Mannok, D.A., McElhaney, N., (1990). Physical properties of glycosyldiacylglycerols: an infrared spectroscopic study of the gel-phase polymorphisms of 1,2-di-O-acyl-3-O-(b-D-glucopyranosyl)-sn-glycerols, Biochemistry, 29:8933-8943.

Liao, M.Q., Tzeng, Y.J., Chang, L.Y.X., (2007). The correlation between neurotoxicity, aggregative ability and secondary structure studied by sequence truncated A beta peptides, FEBS Letters, 581: 1161-1165.

Liu, K., Jackson, M., Sowa, M.G., Ju, H., Dixon, I.M.C., Mantsch, H.H., (1996). Modification of the extracellular matrix following myocardial infarction monitored by FTIR spectroscopy, Biochim Biophys Acta, 1315: 73–77.

Lin, S.Y., Chu, H.L., (2003). Fourier transform infrared spectroscopy used to evidence the prevention of beta-sheet formation of amyloid beta(1-40) peptide by a short amyloid fragment, Int. J. Biol. Macromol., 32:173-7.

Liu, K.Z., Schultz, C.P., Johnston, J.B., Beck, F.W., Al-katib, A.M., Mohammad, R.M., Mantsch, H.H., (1999). Infrared spectroscopic study of bryostatin I-induced membrane alterations in a B-CLL cell line, Leukemia, 13: 1273-1280.

Lopez, G., Martinez, R., Gallego, J., Tarancon, M.J., Carmona, P., Fraile, M.V., (2001). Dietary fats affect rat plasma lipoprotein secondary structure as assessed by fourier transform infrared spectroscopy, J. Nutr., 131: 1898–1902.

Loscher, W., Honack, D., (1991). Responses to NMDA receptor antagonists altered by epileptogenesis, Trends Pharmacol. Sci., 12: 52.

Loscher, W., (1998). New visions in the pharmacology of anticonvulsion, Eur. J. Pharmacol., 342: 1–13.

Loscher, W., Schmidt, D., (2002). New horizons in the development of antiepileptic drugs, Epilepsy Research, 50: 3-16.

Loscher W., Honack D., Fassenber C.P., Nolting B., (1991). The role of technical, biological and pharmacological factors in the laboratory evaluation of

anticonvulsant drugs: III. Pentylenetetrazole seizure models, Epilepsy Res., 8: 171-189.

Lothman, E.W., Bertram, E.H., Stringer, J.L., (1991). Functional anatomy of hippocampal seizures, Prog Neurobiol, 37(1): 1-82

Lowry, O.H., Rosebrough, N.J., Farr, A.L., Randall, R.J., (1951). Protein measurements with folin phenol reagent, Biol. Chem., 193: 265-275.

Ma, X., Liu, G., Wang, S., Chen, Z., Lai, M., Liu, Z., Yang, J., (2007). Evauation of sphingolipids changes in brain tissues of rats with pentylenetetrazol-induced kindled seizures using MALDI-TOF-MS, Journal of Chromatography B, 859: 170-177.

Madeja, M., Stocker, M., MuBhoff, U., Pongs, O., Speckmann, E.J., (1994). Potassium currents in epilepsy: effects of the epileptogenic agent pentylenetetrazol on a cloned potassium channel, Brain Res., 656: 287-294.

Madeja, M., MuBhoff, U., Lorra, C., Pongs, O., Speckmann, E.J., (1996). Mechanism of action of the epileptogenic drug pentylenetetrazol on a cloned neuronal potassium channel, Brain Res., 722: 59-70.

Magistretti, P.J., Pellerin, L., Rothman, D.L., (1999). Energy on demand, Science, 283: 496-497.

Mallick, B.N., Thakkar M., Gangabhagirathi, R., (1995). Rapid eye movement sleep deprivation decreases membrane fluidity in the rat brain, Neurosci Res., 22: 117-22.

Mantsch, H.H., (1984). Biological applications of Fourier-transform infrared-spectroscopy - a study of phase-transitions in biomembranes, Journal of Molecular Structure, 113: 201-212.

Marangoz, C., Ayyildiz, M., Agar, E., (1994). Evidence that sodium nitroprusside possesses anticonvulsant effects mediated through nitric oxide, Neuro. Report, 5:2454-2456.

Mata, M., Fink, D.J., Gainer, H., (1980). Activity dependent energy metabolism in rat posterior pituitary primarily reflects sodium pump activity, J. Neurochem., 34: 213-215.

McCabe, P.H., (2000). New anti-epileptic drugs for the 21st century, Expert Opin. Pharmacother., 1: 633–674.

McCorry, D., Chadwick, D., Marson, A., (2004). Current drug treatment of epilepsy in adults, Lancet Neurol., 3: 729–35

Mc Namara, J.O., (1994). Cellular and molecular basis of epilepsy, J Neurosci., 14(6): 3413-3425.

Mc Namara, J.O., (1999). Emerging insights into the genesis of epilepsy, Nature, 399: A15-A22.

Meagher, E.A., Fitzgerald, G.A., (2000). Indices of lipid peroxidation in vivo: strengths and limitations, Free Radicals in Biology and Medicine, 28: 1745-1750.

Melin, A., Perromat, A., Deleris, G., (2000). Pharmacological application of Fourier transform IR spectroscopy: in vivo toxicity of carbontetrachloride on rat liver, Biopolymers (Biospectroscopy), 57: 160–168.

Mendelsohn, R., Mantsch, H.H., (1986). Fourier transform infrared studies of lipid-protein interaction, in: Watts, A and De Pont, J. J. H. H. M. (Eds.) Progress in Protein-Lipid Interactions, Volume 2, Elsevier Science Publishers, Netherlands.

Merck Index, (1983). Tenth edn., Merck, Rahmay, NJ.

Moore, R.A., Taubner, L.M., Priola, S.A., (2009). Prion protein misfolding and disease, Current Opinion in Structural Biology, 19: 14-22.

Moore, D.J., Sills, R.H., Patel, N., Mendelsohn, R., (1996). Conformational order of phospholipids incorporated into human erythrocytes: an FTIR spectroscopy study, Biochemistry, 35: 229-235.

Moore, D.J., Sills, R. H., Mendelsohn, R., (1995). Peroxidation of erythrocytes: FTIR spectroscopy studies of extracted lipids, isolated membranes, and intact cells, Biospectroscopy, 1: 133-140.

Morimoto, K., Fahnestock, M., Racine, R.J., (2004). Kindling and status epilepticus models of epilepsy: rewiring the brain, Progress in Neurobiology, 73:1-60.

Nigam, S., Schewe, T., (2000). Phospholipase As and lipid peroxidation, Biochim. Biophys. Acta, 1488: 167-181.
Norden, A.D., Blumenfeld, H., (2002). The role of subcortical structures in human epilepsy, Epilepsy and Behavior, 3:219–231.

Olsen, R.W., Delorey, T.M., Gordey, M., Kang, M.H., (1999). GABA receptor function and epilepsy, Adv. Neurol., 79:499–510.

Onozuka, M., Watanabe, K., (1996). Intracellularly applied anti-P70 antibody blocks the induction of abnormal membrane properties by pentylenetetrazole in identified *Euhadra* neurons, Brain Res., 716: 187-191.

Owen, J.S., Bruckdorfer, K. R., Day, R.C., McIntyre, N., (1982). Decreased erythrocyte membrane fluidity and altered lipid composition in human liver disease, Journal of Lipid Research, 23: 124-132.

Ozek, N.S., Sara, Y., Onur, R., Severcan, F., (2009). Low dose simvastatin induces compositional structural and dynamical changes in rat skeletal extensor

digitorum longus muscle tissue, Bioscience Report (in press) (doi 10.1042/BSR20080150).

Patel, M., Liang, L.P., Roberts, L.J., (2001). Enhanced hippocampal F2-isoprostane formation following kainate-induced seizures, J. Neurochem., 79:1065-1069.

Patel, M., (2004). Mitochondrial dysfunction and oxidative stress: cause and consequence of epileptic seizures, Free Radical Biology & Medicine, 3: 1951-1962.

Patsoukis, N., Zervoudakis, G., Georgiou, C.D., (2005). Thiol redox state and lipid and protein oxidation in the mouse striatum after PTZ-induced epileptic seizure, Epilepsia, 46: 1205-1211.

Pavlova, T., Stepanichev, M., Gulyaeva, N., (2006). Pentylenetetrazole kindling induces neuronal cyclin B1expression in rat hippocampus, Neuroscience Letters, 392: 154–158.

Petibois, C., Deleris, G., (2006). Chemical mapping of tumor progression by FT-IR imaging: towards molecular histopathology, Trends in Biotechnology, 24: 455-462.

Petroff, O.A.C., Pan, J.W., Rothman, D.L., (2002). Magnetic resonance spectroscopic studies of neurotransmitters and energy metablism in epilepsy, Epilepsia, 43: 40-50.

Phillis, J.W., Horrocks, L.A., Farooqui, A.A., (2006). Cyclooxygenases, lipoxygenases and epoxygenases in CNS: their role and involvement in neurological disorders, Brain Res., 52: 201-243.

Pothiwong, W., Laorpaksa, A., Pirarat, N., Sirisawadi, S., Intarapanya, J., Jianmongkol, S., (2007). Autoxidation of brain homogenates from various animals as measured by thiobarbituric acid assay, Journal of Pharmacological and Toxicological Methods, 56: 336-338.

Racine, R.J., (1972). Modification of seizure activity by electrical stimulation. II Motor seizure, Electroenceph. Clin. Neurophysiol., 32: 1039-1049.

Ramanjaneyulu, R., Ticku, M., (1984). Interactions of pentamethylene-tetrazole and tetrazole analogues with the picrotoxin site of the benzodiazepine-GABA receptor-ionophore complex, European Journal of Pharmacology, 98: 337-345.

Ray, P., Ray, R., Broomfield, C.A., Berman, J.D., (1994). Inhibition of bioenergetics alters intracellulat calcium, membrane composition and fluiditiy in a neuronal cell line, Neurochem. Res., 19: 57-63.

Regesta, G., Tanganelli, P., (1999). Clinical aspects and biological bases of drug-resistant epilepsies, Epilepsy Res., 34: 109–122.

Reiter, R.J., Poeggeler, B., Tan, D.X., Chen, L.D., Manchester, L.C., Guerrero, J.M., (1993). Antioxidant capacity of melatonin: A novel action not requiring a receptor, Neuroendocrinol., 15: 103-116.

Rocha, L.., Ackermann, R.F., Engel, J.Jr., (1996). Chronic and single administration of pentylenetetrazol modifies benzodiazepine receptor binding: an autoradiography study, Epilepsy Res., 24: 65-72.

Ronga, L., Palladino, P., Costantini, S., Facchiano, A., Ruvo, M., Benedetti, E., Ragone, R., Rossi, F., (2007). Conformational diseases and structure-toxicity relationships: lessons from prion-derived peptides, Curr Protein Pept Sci., 8(1):83-90.

Rothman, D.L., Sibson, N.R., Hyder, F., (1999). In vivo nuclear magnetic resonance spectroscopy studies of the relationship between the glutamate-glutamine neurotransmitter cycle and functional neurogenesis, Trans R Soc London (Biol Sci), 354: 1165-1177.

Ruehr, M.L., Zhang, L., Dogman, R.V., (1997). Lipid-dependent modulation of Ca availability in isolated mossy fiber nerve endins, Neurochem Res., 22: 1215-1222.

Saunders, D.C., O'Malley, C.D., (1950). Veselius, World Publishing, Cleveland, OH.
Schramm, T.M., McKinnon, G.E., Eadie, M.J., (1993). Gas-chromatographic assay of vigabatrin enantiomers in plasma, J. Chromatogr., 616(1):39-44.

Scott, D.F., (1993). The history of epileptic theraphy: Account of how medications was discovered, Parthenon Publishing Group, Pearl River, NY.

Sabin, J., Prieto, G., Sennato, S., (2006). Effect of Gd^{+3} on the collodial stability of liposomes, Physical Review E., 74: 194-198.

Sadqi, M., Hernandez, F., Pan, U., Perez, M., Schaeberle, M.D., Avila, J., Munoz, V., (2002). alpha helix strucutre in alzheimer's disease aggregates of tau-protein, Biochemistry, 41: 7150-7155.
Sarkisian, M.R., (2001). Overview of the current animal models for human seizure and epileptic disorders, Epilepsy Behav. 2: 201-216.

Scheuer, M.L., Pedley, T.A., (1990). The evaluation and treatment of seizures, N. Engl. J. Med., 323:1468-1474.

Schreier, S., Polnaszek C.F., Smith, I.C.P., (1978). Spin Labels in membranes problems in practice, Biochim. Biophys. Acta, 515: 375-436 .

Schultz, C.P., Liu, K.Z., Kerr, P.D., Mantsch, H.H., (1998). In situ infrared histopathology of keratinization in human oral/oropharyngeal squamous cell carcinoma, Oncol. Res., 10: 277-286.

Schultz, C., Naumann, D., (1991). In vivo study of the state of order of the membranes of Gram-negative bacteria by Fourier-transform infrared spectroscopy (FT-IR), FEBS Letters, 294: 43-46.

Scott, L., Schell, M. J., Hubbard, A. L., (1993). Methods in Molecular Biology, Vol. 19, Humana Press, Totowa, NJ, USA.

Sechi, G.P., Rosati, G., Deiana, G.A., Petruzzi, V., Deriu, F., De Riu, P.L., Correddu, P., (1997). Short communication, Co-variation of free aminoacids in brain interstitial fluid during pentylenetetrazole-induced convulsive status epilepticus, Brain Res., 764: 230-236.

Sejima, H., Ito, M., Kishi, K., Tsuda, H., Shiraiski, H., (1997). Regional excitatory and inhibitory amino acid concentrations in pentylenetetrazol kindling and kindled rat brain, Brain & Development, 19: 171-175.

Sergio, F.A., Mesa J.L., Pizarro J.L., Chung, C., Arriortua M.I., Rojo, T., (2005). Two new two-dimensional organically templated phosphite compounds: $(C_6H_{16}N_2)_{0.5}[M(HPO_3)F]$, M=Fe(II) and Co(II): Solvothermal synthesis, crystal structures, thermal, spectroscopic, and magnetic properties, Journal of Solid State Chemistry,178:3554-3562.

Severcan F., (1997). Vitamin E decreases the order of the phospholipid model membranes in the gel phase: An FTIR study, Bioscience Reports, 17: 231-235.

Severcan, F., Sahin, I., Kazancı, N., (2005). Melatonin strongly interacts with zwitterionic model membranes-evidence from Fourier transform infrared spectroscopy and differential scanning calorimetry, Biochimica et Biophysica Acta, 1668: 215-222.

Severcan, F., Toyran, N., Kaptan, N., Turan, B., (2000). Foruier transform infrared study of the effect of diabetes on rat liver and heart tissues in the C-H region, Talanta, 53: 55-59.

Severcan, M., Severcan, F., Haris, I.P., (2004). Using artificially generated spectral data to improve protein secondary structure prediction from FTIR spectra of proteins, Analytical Biochemistry, 332: 238-244.

Severcan, F., Gorgulu, G., Gorgulu, S.T., Guray, T., (2005). Rapid monitoring of diabetes-induced lipid peroxidation by Fourier transform infrared spectroscopy: Evidence from rat liver microsomal membranes, Anal. Biochem, 339: 36-40.

Severcan F., Cannistraro, S., (1990). A Spin Label ESR and Saturation Transfer ESR Study of a-tocopherol containing model membranes, Chemistry and Physics of lipids, 53: 17-26.

Shaefi, S., Harkness, W., (2004). Current status of surgery in the management of epilepsy, Epilepsia, 44:43-47.

Silva, L., Coutinho, A., Fedorov, A., Prieto, M., (2006). Nystatin-induced lipid vesicels permeabilization is strongly dependent on sterol structure, BBA-Biomembranes, 1758: 452-459.

Singh, A., Kumar, G., Naidu, P.S., Kulkami, S.K., (2003). Protective effect of FK506 (Tacrolimus) in pentylenetetrazol-induced kindling in mice, Pharmacology, Biochemistry and Behavior, 75: 853-860.

Smithers, J.A., Lang, J.F., Okerholm, R.A., (1985). Quantitative-analysis of vigabatrin in plasma and urine by reversed-phase high-performance liquid-chromatography, J. Chromatogr., 341(1): 232-238.

Szalontai, B., Nishiyama, Y., Gombos, Z., Murata, N., (2000). Membrane dynamics as seen by Fourier transform infrared spectroscopy in a cyanobacterium, Synechocysis PCC 6803 the effects of lipid unsaturation and protein to lipid ratio, Biochimica et Biophysica Acta, 1509: 409-419.

Sugaya, E., Onozuka, M., Kishii, K., Sugaya, A., Tsuda, T., (1982). Intracellular protein changes during pentylenetetrazole induced bursting activity in snail neurons, Brain Res., 253(1-2):271-279.

Szczerbowska-Boruchowska, M., Dumas, P., Kastyak, M.Z., Chwiej, J., Lankosz, M., Adamek, D., Krygowska-Wajs, A., (2007). Biomolecular investigation of human substantia nigra in Parkinson's disease by synchrotron radiation Fourier transform infrared microspectroscopy, Archives of Biochemistry and Biophysics, 459: 241-248.

Tang, P.H., Miles, M.V., Glauser, T.A., DeGrauw, T., (1999). Automated microanalysis of gabapentin in human serum by high-performance liquid chromatography with fluorometric detection, J. Chromatogr. B, 727(1-2):125-129.

Tempkins, O., (1971). The falling sickness, 2nd ed., John Hopkins Press, Baltimore, MD.

Tsanaclis, L.M., Wicks, J., Williams, J., Richens, A., (1991). Determination of vigabatrin in plasma by reversed-phase high-performance liquid-chromatography, Ther. Drug Monit., 13(3):251-253.

Tejada, S., Sureda, A., Roca, C., Gamundi, A., Esteban, S., (2007). Antioxidant response and oxidative damage in brain cortex after high dose of pilocarpine, Brain Res. Bull., 71: 372-375.

Temkin, N.R., Jarell, A.D., Anderson, G.D., (2001). Antiepileptogenic agents: how close are we?, Drugs, 61:1045–1055.

Thom, M., (2004). Neuropathological findings in epilepsy, Current Diagnostic Pathology, 10:93-105.

Toyran, N., Severcan, F., (2003). Competitive effect of vitamin D_2 and Ca^{2+} on phospholipid model membranes: An FTIR study, Chemistry and Physics of Lipids, 123:165-176.

Toyran N., Severcan F., (2007). Interaction between vitamin D2 and magnesium in liposomes: Differential scanning calorimetry and FTIR spectroscopy studies, Journal of Molecular Structure, 839: 19-27.

Toyran, N., Zorlu, F., Donmez, G., Oge, K., Severcan, F., (2004). Chronic hypoperfusion alters the content and structure of proteins and lipids of rat brain homogenates: a Fourier Transform Infrared Spectroscopic study, Eur Biophy J , 33: 549-554.

Toyran, N., Lasch, P., Naumann, D., Turan, B., Severcan, F., (2006). Early alterations in myocardia and vessels of the diabetic rat heart :An FTIR microspectroscopic study, Biochemical Journal, 397: 427-436.

Toyran, N., Severcan, F., Severcan, M., Turan, B., (2007). Investigation of diabetes-induced effect on apex of rat heart myocardium by using cluster analysis and neural network approach: An FTIR study, Spectroscopy-An International Journal, 21: 269-278

Ueda, Y., Yokoyama, H., Niwa, R., (1997). Generation of lipid radicals in the hippocampal extracellular space during kainic acid induced seizures rats, Epilepsy Res., 26: 329-333.

Uribe-Escamilla, R., Mota-Rojas, D., Sanchez-Aparicio, P., Alonso-Spilsbury, M., Gonzalez-Pina, R., Alfaro-Rodri´guez, A., (2007). Effect of pentobarbital on pHandelectrolyte Levels after induced seizure in rats, Seizure, 16: 397-401.

Vermeij, T.A.C., Edelbroek, P.M., (1998). High-performance liquid chromatographic analysis of vigabatrin enantiomers in human serum by precolumn derivatization with o-phthaldialdehyde-N-acetyl-L-cysteine and fluorescence detection, J. Chromatogr. B, 716(1-2): 233-238.

Wad, N., Kramer, G., (1998). Sensitive high-performance liquid chromatographic method with fluorometric detection for the simultaneous determination of gabapentin and vigabatrin in serum and urine, J. Chromatogr. B, 705(1):154-158.

Wagner, J., Wolf, E., Hemtzelmann, B., Gaget, C., (1987). Chiral separation of enantiomers of substituted alpha-alanine and beta-alanine and gamma-aminobutyric-acid analogs by gas-chromatography and high-performance liquid-chromatography, J. Chromatogr., 392:211-214.

Walsh, L.A., Li, M., Zhao, T.J. (1998). Acute pentylenetetrazol injection reduces rat GABA(A) receptor mRNA levels and GABA stimulation of benzodiazepine binding with no effect on benzodiazepine binding site density, Journal of Pharmacology and Experimental Therapeutics, 289: 1626-1633.

Walton, N.Y., Nagy, A.K., Treiman, D.M., (1999). Altered residual ATP content in rat brain cortex subcellular fractions following status epilepticus induced by lithium and pilocarpine, J. Mol. Neurosci., 11: 233-242.

Wang, J., Chi, C., Lin, S., Chern, Y., (1997). Conformational changes in gastric carcinoma cell membrane protein correlated to cell viability after treatment with adamantyl maleimide, Anticancer Res., 17: 3473–3478.

Wassall, S.R., McCabe, R.C.Y., Ehringer, D.W., Stillwell, W., (1992). Effects of Dietary Fish Oil on Plasma High Density Lipoprotein, The Journal of Biological Chemistry, 267: 8168-8174.

Wassall, S.R., Stillwell, W., (1990). Interactions of retinoids with phospholipid-membranes-Electron spin resonance spectroscopy, Methods in Enzymology, 189: 383-394.

Webster's encyclopedic unabriged dictionary of the English language (1989). Gramercy Books, New York.

Wong, P.T.T., Papavassiliou, E.D., Rigas, B., (1991). Phosphodiester stretching bands in the infrared spectra of human tissues and cultured cells, Appl. Spectrosc., 45: 1563–1567.

Woodbury, D.M., (1980). Convulsant Drugs: Mechanism of Action. Advances in Neurology, Raven Press, NewYork

Yahyavi-Firouz-Abadi, N., Tahsili-Fahadan, P., Riazi, K., Hossein, M., Reza, A., (2006). Involvement of nitric oxide pathway in the acute anticonvulsant effect of melatonin in mice, Epilepsy Res., 68:103-13.

Yamamoto, H., Tang, H., (1996). Melatonin attenuates L-cysteine-induced seizures and lipid peroxidation in the brain of mice, J. Pineal Res., 21: 108-113.

Yano, K., Ohoshima, S., Shimmizu, Y., Moriguchi, T., Katayama, H., (1996). Evaluation of glycogen level in human lung carcinoma tissues by an infrared spectroscopic method, Cancer Lett., 110: 29-34.

Yatin, S.M., Varadarajan, S., Butterfield, D.A., (2000). Vitamin E prevents Alzheimer's amyloid beta-peptide (1-42)-induced neuronal protein oxidation and reactive oxidation and reactive oxygen species production, J. Alzheimers Dis., 2: 123-131.

Yount, G.L., Ponsalle, P., White, J.D., (1994). Pentylenetetrazole-induced seizures stimulate transcription of early and late response genes, Molecular Brain Research, 21:219-224.

APPENDICES

APPENDIX A

The frequency and band area values of FTIR bands for control, low dose and high dose of PTZ for rat brain homogenate. The values are the mean ± standart deviation for each sample. The degree of significance was denoted as (p<0.05*), (p<0.01**) and (p<0.001***).

No	**Frequency and Band area (upper one is the frequency and the lower one in the area values of the same band)**		
	Control (n = 8)	**Low dose PTZ (25 mg/kg) (n = 7)**	**High dose PTZ (60 mg/kg) (n=7)**
1	3012.93±1.25	3011.89±0.24	3010.36±2.04
	1.34±0.03	1.39±0.01*	1.49±0.08*
2	2956.32±0.52	2954.23±0.86	2956.27±0.28
	6.56±0.52	6.69±1.52	6.70±1.23
3	2923.09±0.67	2922.14±0.20	2921.88±0.84
	13.59±0.76	12.08±0.14	10.20±0.48*
4	2870.22±1.24	2871.34±1.51	2871.78±0.91
	3.89±0.04	3.77±0.16	3.65±0.03*
5	2852.27±0.53	2852.14±0.91	2852.17±0.04
	9.20±1.53	9.19±0.91	9.14±1.18
6	1736.09±0.07	1734.72±1.37*	1732.17±1.39*
	6.41±0.07	5.87±0.37*	4.98±0.99*
7	1646.96±0.78	1646.21±1.23	1646.08±0.93
	27.47±1.78	25.37±2.23*	22.45±1.93*
8	1547.15±0.14	1547.70±0.98	1548.15±0.14
	13.27±2.14	11.85±0.98*	10.47±0.14*
9	1400.38±1.66	1400.76±2.67	1400.96±0.78
	3.79±0.06	3.72±0.34	3.71±0.17*
10	1236.88±3.45	1225.40±1.15*	1223.32±0.87*
	10.41±0.14	8.56±1.54*	8.18±1.17**
11	1171.88±1.02	1171.85±0.29	NOT OBSERVED
	5.78±0.11	4.27±0.37*	NOT OBSERVED
12	1156.95±0.18	1155.80±0.18	NOT OBSERVED
	5.18±0.03	4.32±1.70*	NOT OBSERVED
13	1080.92±0.58	1077.92±2.76*	1062.58±2.12*
	9.56±0.14	8.36±0.28*	10.98±0.46*
14	998.91±0.12	992.21±0.65*	1001.98±0.51*
	3.79±0.26	3.12±0.34	5.72±0.79*

APPENDIX B

Changes in the bandwidth values and the area ratios of control, low dose and high dose of PTZ for rat brain homogenate. The values are the mean $\pm$ standart deviation for each sample. The degree of significance was denoted as (p<0.05*), (p<0.01**) and (p<0.001***).

	Bandwidth value or area ratio		
Functional group	**Control** **n = 8**	**Low dose PTZ** **n = 7**	**High dose PTZ** **n = 7**
Bandwidth of CH_2 asymmetric stretching	13.98±0.67	12.18±2.13	12.01±0.83*
Bandwidth of CH_2 symmetric stretching	6.75±0.23	6.55±0.38	6.03±0.50*
Ratio of areas of CH_2 asymmetric stretching to Amide I (A_{2925}/A_{1645})	0.49±0.02	0.47±0.09*	0.45±0.01*

APPENDIX C

The changes in value of protein secondary structure estimation by NN predictions (A) and the intensities of amide I sub-bands (B) (second derivative) for control, low dose and high dose of PTZ for rat brain homogenate. The values are the mean ± standart deviation for each sample. The degree of significance was denoted as (p<0.05*), (p<0.01**) and (p<0.001***).

A - Neural network predictions			
Functional groups	Control (n = 8)	Low dose PTZ (25 mg/kg) (n = 7)	High dose PTZ (60 mg/kg) (n=7)
Alpha-helix	20.32 ±0.49	20.69±0.58	22.69±1.04*
Beta sheet	56.23 ±2.18	51.47±2.05*	50.16±2.28*
Turns	19.51±3.64	21.41±0.79	18.97±2.84
Random coil	3.95 ±1.53	6.64±0.32*	8.27±1.91*

B- Secondary structure intensities			
1-Beta turn (1682 m^{-1})	-0.13± 0.02	- 0.15±0.03	- 0.20±0.03*
2-Alpha helix (1652 cm^{-1})	- 0.22±0.03	- 0.29±0.03*	- 0.31±0.02*
3-Random coil (1645 cm^{-1})	- 0.17±0.01	- 0.21±0.02*	- 0. 22±0.04*
4-Beta sheet (1633 cm^{-1})	- 0.16±0.07	-0.17± 0.06	- 0.26±0.04*

APPENDIX D

The frequency and band area values of FTIR bands for control, low dose and high dose of PTZ for rat brain cell membrane. The values are the mean ± standart deviation for each sample. The degree of significance was denoted as (p<0.05*), (p<0.01**) and (p<0.001***).

No	Frequency and Band area(the upper one denotes the frequency, the lower one denotes to area values)		
	Control (n = 8)	Low dose PTZ (25 mg/kg) (n = 6)	High dose PTZ (60 mg/kg) (n=6)
1	3012.93±1.05	3011.19±0.24	3012.37±2.05
	0.41±0.03	0.35±0.02*	0.34±0.08*
2	2957.22±0.59	2956.33±0.16	2956.27±0.28
	8.06±0.52	8.69±1.52	8.70±2.23
3	2921.07±0.97	2925.14±0.20	2925.88±0.43*
	14.19±1.06	13.01±0.11*	11.29±1.04*
4	2870.21±1.49	2870.34±1.51	2870.78±0.91
	3.99±0.04	3.72±0.16	3.65±0.03*
5	2852.27±0.53	2854.14±0.91	2854.17±0.45
	9.20±1.53	8.99±0.91	8.77±0.18*
6	1736.09±0.07	1733.72±1.37*	1732.07±1.39*
	6.41±0.07	5.97±2.37*	5.98±0.09*
7	1646.96±0.78	1646.21±1.23	1646.08±0.93
	27.47±1.78	25.77±2.23*	23.05±1.93*
8	1547.15±0.14	1547.70±0.98	1548.15±0.14
	13.27±2.14	11.85±0.98*	10.47±0.14*
9	1400.38±1.66	1400.76±2.67	1400.96±0.78
	3.79±0.06	3.72±0.34	3.71±0.17*
10	1236.88±3.45	1224.40±0.15*	1223.32±0.87*
	10.41±0.14	8.56±1.54*	8.18±1.17**
11	1080.92±0.58	1078.92±1.76*	1072.58±2.12*
	9.56±0.14	8.36±0.28*	8.08±0.46*

APPENDIX E

Changes in the bandwidth values and the area ratios of control, low dose and high dose of PTZ for rat brain cell membrane. The values are the mean ± standart deviation for each sample. The degree of significance was denoted as (p<0.05*), (p<0.01**) and (p<0.001***).

Functional group	Bandwidth value or area ratio		
	Control n = 8	Low dose PTZ (25 mg/kg) n = 7	High dose PTZ (60 mg/kg) n = 7
Bandwidth of CH_2 asymmetric stretching	13.08±0.17	12.18±0.10*	12.09±0.01*
Bandwidth of CH_2 symmetric stretching	7.09±0.23	6.51±0.87*	6.12±0.92*
Ratio of areas of CH_2 symmetric stretching to Amide I (A_{2925}/A_{1645})	0.52±0.08	0.50±0.02	0.48±0.07*

APPENDIX F

The changes in value of protein secondary structure estimation by second derivative for control, low dose and high dose of PTZ for rat brain cell membrane. The values are the mean ± standart deviation for each sample. The degree of significance was denoted as (p<0.05*), (p<0.01**) and (p<0.001***).

Functional groups	Control (n = 8)	Low dose PTZ (25 mg/kg) (n = 7)	High dose PTZ (60 mg/kg) (n=7)
A - Neural network predictions			
Alpha-helix	19.02 ±1.11	18.21±1.58	14.09±0.07*
Beta sheet	57.55 ±0.33	55.27±0.51	50.65±1.28*
Turns	20.26±0.44	19.32±1.09	23.40±1.04
Random coil	3.17 ±0.31	7.24±1.22*	11.86±1.91*
B- Second derivative analysis			
1-Beta turn (1682 m^{-1})	-0.21± 0.02	- 0.16±0.03*	- 0.15±0.04*
2-Alpha helix (1652 cm^{-1})	- 0.34±0.03	- 0.31±0.03*	- 0.21±0.02*
3-Random coil (1645 cm^{-1})	- 0.17±0.01	- 0.22±0.02*	- 0. 23±0.04*
4-Beta sheet (1633 cm^{-1})	- 0.26±0.07	-0.17± 0.06	- 0.16±0.04*

APPENDIX G

Changes in the bandwidth values and the area ratios of control, epileptic and epileptic-VGB for rat brain cell membrane. The values are the mean ± standart deviation for each sample. The degree of significance was denoted as (p<0.05*), (p<0.01**) and (p<0.001***).

	Bandwidth value or area ratio		
Functional group	**Control** **n = 7**	**Epileptic** **n = 7**	**Epileptic-VGB** **n = 7**
Bandwidth of CH_2 asymmetric stretching	13.98±0.67	11.01±1.03*	13.95±1.10
Bandwidth of CH_2 symmetric stretching	6.75±0.23	6.03±1.01	6.66±0.32
Ratio of areas of CH_2 symmetric stretching to Amide I (A_{2925}/A_{1645})	0.47±0.08	0.44±0.07*	0.48±0.07

APPENDIX H

Changes in frequency values of C=O stretching, PO_2 asymmetric and symmetric stretching modes of control, epileptic and epileptic-VGB for rat brain cell membrane. The values are the mean ± standart deviation for each sample. The degree of significance was denoted as (p<0.05*), (p<0.01**) and (p<0.001***).

	Frequency values		
Functional group	**Control** **n = 7**	**Epileptic** **n = 7**	**Epileptic-VGB** **n = 7**
C=O stretching	1737.09±2.07	1734.05±1.01*	1736.15±1.98
PO_2 asymmetric stretching	1238.88±2.42	1233.49±0.98*	1237.32±1.78
PO_2 symmetric stretching	1081.92±3.21	1069.77±1.02*	1079.31±2.22

APPENDIX I

The changes in value of protein secondary structure estimation by second derivative for control, epileptic and epileptic-VGB for rat brain cell membrane. The values are the mean ± standart deviation for each sample. The degree of significance was denoted as ($p < 0.05$*), ($p < 0.01$**) and ($p < 0.001$***).

A - Neural network predictions			
Functional groups	**Control (n = 8)**	**Epileptic n = 7**	**Epileptic-VGB n = 7**
Alpha-helix	19.02 ±1.11	18.21±1.58	17.19±0.72*
Beta sheet	57.55 ±0.33	55.27±0.51	56.05±0.28*
Turns	20.26±0.44	19.32±1.09	14.40±1.04
Random coil	3.17 ±0.31	7.24±1.22*	7.36±1.91*
B- Second derivative analysis			
1-Beta turn (1682 m^{-1})	-0.21± 0.02	- 0.16±0.03*	- 0.15±0.04*
2-Alpha helix (1652 cm^{-1})	- 0.34±0.03	- 0.31±0.03*	- 0.21±0.02*
3-Random coil (1645 cm^{-1})	- 0.17±0.01	- 0.22±0.02*	- 0. 23±0.04*
4-Beta sheet (1633 cm^{-1})	- 0.26±0.07	-0.17± 0.06	- 0.16±0.04*

CURRICULUM VITAE

PERSONEL INFORMATION

Surname, Name:	Görgülü Türker, Sevgi
Nationality:	Turkish (TC)
Date and Place of Birth:	30 October 1976, Kocaeli
Phone:	+90 312 210 51 57
E-mail:	sevgiss@yahoo.com
Foreign Languages:	English

EDUCATION

Degree	Institution	Graduation
Ph.D.	METU Biology Dept.	
M.Sc.	METU Biology Dept.	2003
B.Sc.	Hacettepe Uni. Biology Dept.	1998
High School	İzmit Lisesi, Kocaeli	1993

WORK EXPERIENCE

Year	Place	Enrollment
2002-Present	METU Biology Dept.	Teaching Assistant
2004-2005	IUPUI, USA	Invited Researcher

TEACHING EXPERIENCE

Coordination of assistant's activities
BIO 475 "Molecular Biology Laboratory" Assistantship
BIO 101-102 "General Biology I-II Laboratory" Assistantship
BIO 112, BIO 501 and BIO 601 "Seminars in Biology for Freshman and Graduate Students" Assistantship
GENE 103 "Molecular and Cellular Biology I Laboratory" Assistantship
GENE 270 "Experimental Techniques in Molecular Biology Laboratory" Assistantship

ACADEMIC ACTIVITIES

Academic Publications

Görgülü ST., Dogan M., Severcan F., `The characterization and differentiation of higher plants by FTIR spectroscopy. `*Applied Spectroscopy*`, 61 (3), (2007), 310-316.

Severcan F., Görgülü G., **Görgülü ST.**, Guray T., `Rapid monitoring of diabetes-induced lipid peroxidation by Fourier transform infrared spectroscopy:evidence from rat liver microsomal membranes. *"Analytical Biochemistry"*, 339, (2005), p.36-40.

Görgülü ST., Wassall S., Stilwell W., Severcan F., "Convulsant agent penthyleneterazol does not alter the structural and dynamical properties of dipalmitoylphosphatidylcholine model membranes" *Manuscript submitted to Bioscience Reports*

Görgülü ST., Ilbay Gul, Severcan M., Severcan F., "The Investigation of Compositional, Structural and Dynamical Changes of PTZ-induced seizures on rat brain homogenate: Evidences for early molecular consequences of epilepsy" *Manuscript submitted to Epilepsia*

Görgülü ST., Wassall S., Stilwell W., Severcan F., "Antiepileptic agent vigabatrin interacts with membrane phospholipids" *Manuscript in preparation*

Academic Research Projects

"The investigation of the role of new antiepileptic agents in epilepsy treatment by molecular and biotechnological techniques"
Funded by: DPT / BAP - 01 - 08 DPT 2003 K120920/790
Principal Investigator: Prof. Dr. Sezer Komsuoğlu
Status: Completed (3 years)

"The investigation of molecular mechanism of epilepsy and the role of antiepileptics vigabatrin and topiramate in epilepsy treatment"

Abstract in referred Journals

Görgülü ST., İlbay G., Ateş N., Güneş Z., Kara N., Severcan F., An FTIR Approach to Investigate Molecular Changes Induced by Epilepsy *"WSEAS Transactions on Biology and Biomedicine"*, 2, (2005), p.351-354. Greece (**oral presentation**)

Erar H., **Görgülü ST.,** Akkaş B., Yılmaz O., Severcan F., `The Effect of STZ-Induced Diabetes on Lipid Structure, Function and Composition of Rat Skeletal Muscle: An FTIR Study. *"WSEAS Transactions on Biology and Biomedicine"*, 2, (2005), p.351-354. Greece (**oral presentation**)

Görgülü ST., Deniz O., Komsuoğlu S., Severcan F., Antiepileptic agent vigabatrin - Model membrane interaction. *"Biophysical Journal"*, 88, (2005), p.418A-419A. (**poster**)

Görgülü ST., Wassall S., Stillwell W., Severcan F., `The investigation of the interaction of pentyleneterazol with model membranes` *Biophysical Journal,* 92 (2006), p212A-212A. USA (**poster**)

Görgülü ST., Wassall S., Stillwell W., Severcan F., `The interaction of Picrotoxin with DPPC Model Membrane` *Epilepsia*, Suppl. 4. 47, (2006) 348-348. USA (**poster**)

Görgülü ST., Kara N., Güneş Z., Ateş N., İlbay G., Severcan F., `The investigation of early molecular consequences of chemically induced epileptic activity ` *Epilepsia*, Suppl. 4. 47, (2006) 234-234. USA (**poster**)

Abstracts in Congress Proceedings

Turker S., Doğan M., ve **Severcan F**., "The identification of different plant genera by FTIR spectroscopy" XIV. National Biophysics Congress, September, 4-6 2002, Turkey (**poster**).

Görgülü G., **Türker S**., Güray T., Yılmaz Ö., **Severcan F**, "Microsomal lipid peroxidation: the investigation of the effects of STZ-induced diabetes on rat liver tissue by FTIR spectroscopy" XIV. National Biophysics Congress, September, 4-6 2002, Turkey (**poster**).

Görgülü ST., Deniz Ö, Komsuoglu S, Severcan F., "The effects of antiepileptic agents on membranes" XVI. National Biophysics Congress, 2004, (**poster**)

Görgülü ST., İlbay G., Ateş N., Severcan F., "The investigation of molecular alterations induced by PTZ by using FTIR spectroscopy" IX. National Spectroscopy Congress June 09-11, 2005, Turkey (**1st poster award**)

Görgülü ST., Doğan M., Severcan F, "The usage of infared spectroscopy in plant taxonomy" IX. National Spectroscopy Congress, June 09-11, 2005, Turkey (**oral presentation**)

Erar H., **Görgülü ST.**, Akkaş B.,Yılmaz Ö., Severcan F. " The analysis of the effects of Tip I diabetes on rat skeletal muscle" IX. National Spectroscopy Congress, June 09-11, 2005, Turkey (**poster**)

Görgülü ST., Wassall S., Stillwell W., **Severcan F.**, "DPPC model and PTZ interaction" IIX. National Biophysics Congress, September, 6-9 2006, Turkey, (**3rd poster award**)

Görgülü ST., İlbay G., Ateş N., Severcan F., "The effects of epilepsy on cell membranes" IV. National Neuroscience Congress, 2007**, (oral presentation**)

Görgülü ST., İlbay G., Severcan F., "The investigation of the molecular alterations of genetically induced epilepsy by FTIR spectroscopy" XX. National Biophysics Congress, 2008, Turkey, ((**3rd poster award**)

Görgülü ST., Akkaş, SB., Cakmak G., Severcan M., Severcan F., "Prediction of protein secondary structure using neural networks in biological systems" HIBIT, 2009, Turkey (**poster**)